NTNU – Trondheim
Norwegian University of
Science and Technology

Analysis of Hull Structure Response for a Sevan Arctic Mobile Drilling Unit in Arctic Areas subjected to Ice Loading

Ine Haugen

Analysis of Hull Structure Response for a Sevan Arctic Mobile Offshore Drilling Unit in Arctic Areas subjected to Ice Loading

by Ine Haugen

Marine Technology
Submission date: 10.06.2014
Supervisor: Bernt Johan Leira, IMT

Master Thesis, Spring 2014
for
Master Student Ine Haugen

ANALYSIS OF HULL STRUCTURE RESPONSE FOR A SEVAN ARCTIC MOBILE OFFSHORE DRILLING UNIT IN ARCTIC AREAS SUBJECTED TO ICE LOADING

Responsanalyse av Skrogkonstruksjon for en Mobil Sevan Boreplattform i Arktiske Farvann Utsatt for Isbelastning

As the oil and gas industry moves into Arctic areas the need for considerations towards safe operations in ice infested environments arises. With the entry of floating drilling and production units into ice infested environments on a more long term basis, adequate design criteria are required. The structural capability to withstand ice actions needs to be assessed in the light of hull geometry and design features of local details. The applicability of existing rules applied for ship hulls then needs to be assessed. This also needs to be considered in the light of added risks related to such long term engagements.

The candidate shall address the following topics:

1. A summary of ice properties, ice mechanics and ice load formulations. In particular, the ice-load formulations in ISO 19906 and the IACS Polar Class rules are to be summarized.

2. Application of relevant load formulations is to be investigated in relation to the Sevan Arctic Mobile Offshore Drilling Unit (MODU). Basic information related to the hull geometry is to be provided by Sevan. Ice loading represented in terms of global and local ice action is to be established by the candidate.

3. Two different hull geometries for the drilling platform. The two alternative geometries differ with respect to up-slope versus down-slope ice-breaking functionality. Displacements and stresses for two corresponding parts of the two hulls are to be analysed by means of the computer program Abaqus. A non-linear incremental static analysis option is to be applied.

4. Parametric studies are to be performed to the extent that time allows and based on discussion with the supervisor. In particular, the sensitivity of the computed displacements and stresses to the selection of mesh layout should be investigated.

The work scope may prove to be larger than initially anticipated. Subject to approval from the supervisor, topics may be deleted from the list above or reduced in extent. In the thesis the candidate shall present her personal contribution to the resolution of problems within the scope of the thesis work. Theories and conclusions should be based on mathematical derivations and/or logic reasoning identifying the various steps in the deduction.

PREFACE

The candidate should utilise the existing possibilities for obtaining relevant literature.

The thesis should be organised in a rational manner to give a clear exposition of results, assessments, and conclusions. The text should be brief and to the point, with a clear language. Telegraphic language should be avoided.

The thesis shall contain the following elements: A text defining the scope, preface, list of contents, summary, main body of thesis, conclusions with recommendations for further work, list of symbols and acronyms, references and (optional) appendices. All figures, tables and equations shall be numbered.

The supervisor may require that the candidate, in an early stage of the work, presents a written plan for the completion of the work. The plan should include a budget for the use of computer and laboratory resources which will be charged to the department. Overruns shall be reported to the supervisor.

The original contribution of the candidate and material taken from other sources shall be clearly defined. Work from other sources shall be properly referenced using an acknowledged referencing system.

The thesis shall be submitted in electronic form:

- Signed by the candidate
- The text defining the scope included
- Drawings and/or computer prints which cannot be bound should be organised in a separate folder.

Supervisor: Professor Bernt J. Leira   Contact person at Sevan Marine: Hans Olav Sele

Deadline: June 10th 2014

Trondheim, January 16th, 2014

Bernt J. Leira

PREFACE

The following report is an individual Master's thesis in the field of marine structural engineering undertaken during the spring semester of 2014. The thesis's work has mainly been carried out at the Department of Marine Technology, Norwegian University of Technology and Science in Trondheim with the exception of two trips to Sevan Marine's office in Oslo to undertake necessary work in respect to the partnership.

Throughout the semester the scope of work has changed, but in the end the results has come out satisfactorily with respect to the final scope. The work of the thesis has been more time consuming than anticipated, and the work load has been large near the submission date. Especially establishing a finite element model in the software ABAQUS has been time consuming. Overall, the work has been a highly educational experience, especially knowledge regarding engineering in ice-infested waters.

I wish to extend my gratitude towards thesis advisor Professor Bernt Johan Leira for his helpful guidance and discussions. Further, I would like to thank Hans Olav Sele and Audun Arnesen Nyhus at Sevan Marine for general support and guidance to the Sevan Arctic Mobile Offshore Drilling design and help regarding modelling in ABAQUS.

Ine Haugen
Trondheim, 10th of June 2014

_____

PREFACE

ABSTRACT

The interest for Arctic deep water development intensifies as the worldwide demand for oil and gas continues to grow. As much as 25 % of the world's remaining hydrocarbons are assumed to be located in the Arctic area. However, the Arctic environment represents engineering challenges due to sea ice, temperature, darkness and environmental impact requirements. To meet these challenges for Arctic deep water developments to have a possibility for year-round operations, particularly for ice loading, a combination of traditional and innovative technology is the key. A buoy shaped floater with a single point detachment is suggested. The hull shape of a buoy has the advantage to reduce loading from ice features and to be loaded in all directions. The geometry of the hull in the ice action area has a significant effect on the magnitude of ice action. In this thesis, the main scope of work is to investigate and analyze ice actions subjected to a floating offshore structure with sloping hull in the ice action water line.

The first section is a literature review of the different aspect of sea ice to get a better knowledge of sea ice's properties and behavior such that the Arctic engineering becomes more comprehensible. Further, a study of the Arctic areas of interest with focus on the Barents Sea has been carried out, followed by an assessment of the industry's experiences with floating platforms in ice infested waters.

An assessment of ice actions, both global ice action and local ice pressure, has been performed using a Sevan Arctic Mobile Offshore Drilling Unit design as reference structure. Theoretical formulations to determine global ice action from level ice and ridge has been examined, as well as an assessment of ice actions from managed ice due to full scale experience from an identical design, the Kulluk Drilling unit. A comparative study of upward and downward sloping structure has been conducted towards geometrical parameters for the ice features, such as level ice thickness, rubble height, consolidated layer thickness and keel height. It is found that increasing level ice thickness is more severe than increasing geometrical sizes of ridges if the slope is bending ice upwards, but opposite if the slope is bending ice downwards. Local ice pressure on sloping structures has been difficult to determine due to lack of literature available. Hence, several approaches have been assessed and the most suited approach for sloping structures has been used further in the thesis to examine structural hull capacity.

ABSTRACT

As a final assessment, a nonlinear static analysis has been performed in ABAQUS of a local model extracted from a Sevan Arctic Mobile Offshore Drilling Unit design which is a buoy shaped floater. ABAQUS solves the finite element method numerically. Hence, a theory part targeting ABAQUS and the element theory relevant for this thesis has been presented. Further, the footsteps necessary to perform in ABAQUS to submit a nonlinear static analysis has been presented. A study has been done with regards to the selection of element size and type by a convergence test which establishes that linear quadrilateral elements with reduced integration and global size 200mm provide conservative results. The local model was check with regards to structural capacity for uniformly distributed ice pressure. In this thesis, the structural capability has been examined for stiffeners and plates and limited by the yielding criterion given by von Mises stress. Based on the results, it has been suggested to design the scantling with higher capability in the stiffeners and reduce the capability in the hull plate to decrease this scattering in structural capability between stiffener and plate. It has also been suggested that the operational ice draft should be designed such that ice actions are loaded on the elevation of a stringer.

SAMMENDRAG

Interessen for Arktisk dypvanns utvikling intensifiserers ettersom den globale etterspørselen for olje og gass fortsetter å vokse. Så mye som 25 % av verdens gjenværende hydrokarboner antas å være i det arktiske området. Det arktiske miljøet representerer tekniske utfordringer på grunn av havis, temperatur, mørke og miljøpåvirknings krav. For å møte disse utfordringene for arktiske dypvanns utviklinger til å ha helårs drift, særlig for islast, er nøkkelen å kombinere tradisjonell og nyskapende teknologi. En bøye formet flyter med enkelt punkts løsgjøring er foreslått. Skrog formen til en bøye har en fordel å kunne redusere laster fra is i alle retninger. Geometrien til skroget i islast regionen har en betydelig effekt på omfanget av den totale islasten. I denne Masteren er den viktigste oppgaven av arbeidet å undersøke og analysere islaster på en flytende offshore struktur med skrått skrog i islastens vannlinjen.

Det første kapitlet er en litteraturgjennomgang av ulike aspekter av havis for å få bedre forståelse om havisens egenskaper og atferd slik at Arktisk prosjektering blir letter gjennomførbart. Videre har et studie av de mest interessante arktiske områdene med fokus på Barentshavet blitt gjennomført, etterfulgt av en vurdering av bransjens erfaringer med flytende plattformer i isfarvann.

En vurdering av islaste, både global islast og lokalt istrykk, har blitt utført med hensyn på et Sevan Arctic Mobile Offshore Drilling Unit konsept. Teoretiske formuleringer for å avgjøre global islast fra level-is og is-rygg har blitt undersøkt, samt en vurdering av islast fra oppdelt is med hensyn på fullskala erfaring fra et identisk design, Kulluk drilleren. En sammenligningsstudie av oppover og nedover skrånende struktur har blitt utført med hensyn på geometriske parametere for istyper, for eksempel level-istykkelse, knust is høyde, konsolidert istykkelse og kjøl høyde. Det er funnet at å øke istykkelsen er mer belastende enn å øke geometriske størrelser til en is-rygg dersom skråningen bøyer isen oppover, men motsatt hvis skråningen bøyer isen nedover. Lokalt istrykk på skrå strukturer har vært vanskelig å fastslå på grunn av mangel i tilgjenelig litteratur. Derfor har denne Masteren vurderte flere fremgangsmåter, og den mest egnede tilnærmingen for

SAMMENDRAG

skrående struktur har blitt brukt videre i oppgaven for å undersøke strukturell kapasitet i skroget.

Som en avsluttende vurdering, har en ikke-lineær statisk analyse blitt utført i ABAQUS av en lokal modell hentet fra ett Sevan Arctic Mobile Offshore Drilling Unit design som er en bøye formet flyter. ABAQUS løser elementmetoden numerisk. Derfor har en teori del blitt presentert rettet mot ABAQUS og elementetteori relevant for denne oppgaven. Videre presenteres de nødvendige stegene for å utføre en ikke-lineær statisk analyse i ABAQUS. En konvergens test rettet mot valg av element størrelse og type fastslo at lineære firkantede elementer med redusert integrasjon og global størrelse 200mm gir konservative resultater. Den lokale modellen ble sjekke mot strukturell kapasitet for jevnt fordelt istrykk. I denne Masteren, har strukturell kapasitet blitt undersøkt for stivere og plate der flytgrensen gitt av von Mises spenninger er satt som begrensning. Basert på resultatene, har det vært foreslått å ende dimensjonene slik at stiverne får høyere kapasitet og skrog platene får redusere kapasitet. Det er også blitt foreslått at strukturens dypgang i is bør være plassert slik at islasten er lastet på høyde med en horisontal bærebjelke.

TABLE OF CONTENTS

TABLE OF CONTENTS

TABLE OF CONTENTS

LIST OF SYMBOLS

Latin symbols

A	local contact design area
AR	load patch ratio
a	loaded height for local ice pressure
a_d	frame spacing
b	width of the solid ice equivalent to the keel
b_p	height of patch load
CF_C	crushing failure class factor
CF_F	flexural failure class factor
CF_D	load patch dimensions class factor
CF_{DIS}	displacement class factor
CF_L	longitudinal strength class factor
c	cohesion of ice rubble
E	elastic modulus of sea ice
E_{cl}	elastic modulus of consolidated layer
E_k	elastic modulus of keel
E_1	complete elliptical integral of first order
E_2	complete elliptical integral of second order
e	porosity of ice rubble
F	impact force
$F_{m,lower}$	managed ice force for mean trend line
$F_{m,upper}$	managed ice force for upper bound
F_H	horizontal ice force
F_V	vertical ice force
f	parameter
fa_i	shape coefficient
G	parameter
g	acceleration of gravity
g_r	parameter
H_B	horizontal ice breaking load
H_L	horizontal load required to lift ice rubble on top of advancing ice sheet prior to breaking it
H_P	horizontal load required to push ice sheet through ice rubble
H_R	horizontal load to push ice blocks up slope through the ice rubble
H_s	sail height
H_T	horizontal load to turn ice block at the top of the slope
h	level ice thickness

LIST OF SYMBOLS

h_{cl}	consolidated layer thickness
h_F	ice floe thickness
h_k	keel height
h_r	ice ride up height or rubble height
h_v	parameter
I_T	second moment of area
k_i	thermal conductivity
L	latent heat of fusion of ice
L_{cc}	parameter
L_c	characteristic length
l_c	total length of circumferential crack
L_{wl}	ship length measured at UIWL
N	normal ice force
P_{avg}	average pressure over patch
P	parameter
P_{PC}	pressure
p_L	local ice pressure
Q	line load
S_i	salinity of sea ice
T_a	top temperature of ice sheet
T_b	bottom temperature of ice sheet
T_i	absolute value of ice temperature
t	element thickness
t_t	total freezing time
$V_{1,cl}$	vertical force for consolidated layer to fail by center crack
$V_{1,k}$	vertical force for keel to fail by center crack
$V_{2,cl}$	vertical force for consolidated layer to fail by hinge crack
$V_{2,k}$	vertical force for keel to fail by hinge crack
V_B	vertical breaking force
V_R	vertical ride up force
W	parameter
W_r	width of ridge
w	width of the sloping structure
w_L	width of local ice pressure
w_p	width of patch load
w_T	top diameter of the cone
X	parameter
x	distance from forward perpendicular to station under consideration
Y	equal to 2.711 for Tresca yielding or 3.422 for Johnsen yielding
y_1	distance to top surface from the neutral axis

LIST OF SYMBOLS

Greek symbols

α	inclination angle of the sloping structure
β'	normal frame angle
Δ_{tk}	ship displacement measured from upper ice waterline (UIWL)
ζ	equals to $\left(\frac{\sin\alpha+\mu\cos\alpha}{\cos\alpha-\mu\sin\alpha}\right)$
θ	angle the broken ice sheet makes with the horizontal
θ_k	keel angle
μ	ice-structure friction coefficient
μ_i	ice-ice friction coefficient
v	Poisson's ratio
v_b	brine volume
ρ_i	ice density
ρ_w	sea water density
σ_{cl}	flexural strength of consolidated layer
σ_f	flexural strength of ice sheet
σ_k	flexural strength of keel
σ_{VM}	yield stress under uniaxial stress
σ_x	direct stress in x-pane
σ_y	direct stress in y- plane
σ_1	principle stress in x-plane
σ_2	principle stress in y-plane
τ_{xy}	shear stress in xy-plane
φ	friction angle of ice rubble

ABBREVATIONS

MODU	Mobile Offshore Drilling Unit
WMO	World Metrological Institution
OMV	Österreichische Mineralölverwaltung (oil and gas Company)
DP	Dynamic Positioning
MBL	Minimum Breaking Load
MN	Mega Newton
MPa	Mega Pascal
ISO	International Organization for Standardization
FPSO	Floating Production, Storage and Offloading
FPU	Floating Production Unit
IACS	International Association of Classification Societies
UIWL	Upper Ice Water Line
CSA	Canadian Standards Association
dof	degrees of freedom
FEM	Finite Element Method
DNV	Det Norske Veritas
RP	Recommended Practices
SALM	Single Anchor Leg Mooring
PC4	Polar Class number 4
S3	three node triangular shell element
S3R	three node triangular shell element that uses reduced integration
S4R	quadrilateral element with four nodes that uses reduced integration
S8R	quadrilateral element with eight nodes that uses reduced integration
STRI65	triangular shell element with six nodes and five degrees of freedom

1 INTRODUCTION

The Arctic is one of the last frontiers that may hold undiscovered oil and gas reserves. As much as 25 % of the world's remaining hydrocarbons are assumed to be located in the Arctic. The demand for oil and gas continuous to grow worldwide and the interest for exploration activities towards "*…the final true frontier for hydrocarbon exploration*"(Hamilton 2011, p.1) intensifies. However, the Arctic environment represents extremely difficult engineering challenges due to excessive ice loading, extremely cold temperatures, long periods of darkness and environmental impact requirements. To meet these challenges for Arctic offshore developments to have a safe, reliable, cost-efficient and possibility for a year-round operation it is recognized that a combination of traditional and innovative technology is the key. Refer to (Iyerusalimskiy, Gu et al. 2012).

There are considerable industry experiences available in near-shore, shallow water Arctic developments. On the other hand, many of the Arctic deep water regions which also hold severe ice conditions are yet to be developed. This will require a floating systems solution. Floating platform design poses significant challenges due to the harsh ice loading conditions and the demand on the hull and mooring system strength. Hull geometry must be optimized to minimize ice loads which will be transferred to the mooring system, and mooring lines must be arranged to avoid direct exposure from ice and at the same time resist overturning moments and offset due to ice actions. Floating system's hull will in reality not experience interaction of the worst ice features because mooring lines have limiting load capacity. However, analyzing hull capacity with regards to local ice actions is vital to obtain sufficient scantling and determine design limits. One key design challenge for Arctic floating systems is the requirement to resist potentially severe ice load for year-round operations. A year-round operation will be necessary to increase the potential for economic profit to become large enough. Project development in deep water Arctic will also require fields with very large discoveries to profit with today's technology. Refer to (Aggarwal and Souza 2011).

INTRODUCTION

In this thesis, the main objective is to assess aspects of ice actions on floating offshore structures located in the deep water Arctic. Sevan Marine has provided a new design of a buoy shaped offshore structure classified for Arctic environments that will be used as a reference structure throughout the thesis.

The first part of this thesis presents a study of the different aspects of sea ice, followed by a presentation of the Arctic areas relevant for oil and gas development with focus on the Barents Sea. Further, the technological challenges and solutions which the industry has experienced with regards to floating units are presented.

An exhaustive study of ice actions, both global ice actions and local ice pressure, from ice features such as level ice, ridges and managed ice has been conducted with focus on comparison of upwards breaking versus downward ice breaking hull shape. Figure 1.1 illustrates the aspects of ice actions which will be highlighted throughout this thesis. The design called Sevan Arctic Mobile Offshore Drilling Unit (MODU) provided by Sevan Marine is used as reference structure. The study also includes an investigation of the effect of increasing geometrical ice parameters such as level ice thickness, ride up height of ice, ridge consolidated layer thickness and ridge keel height.
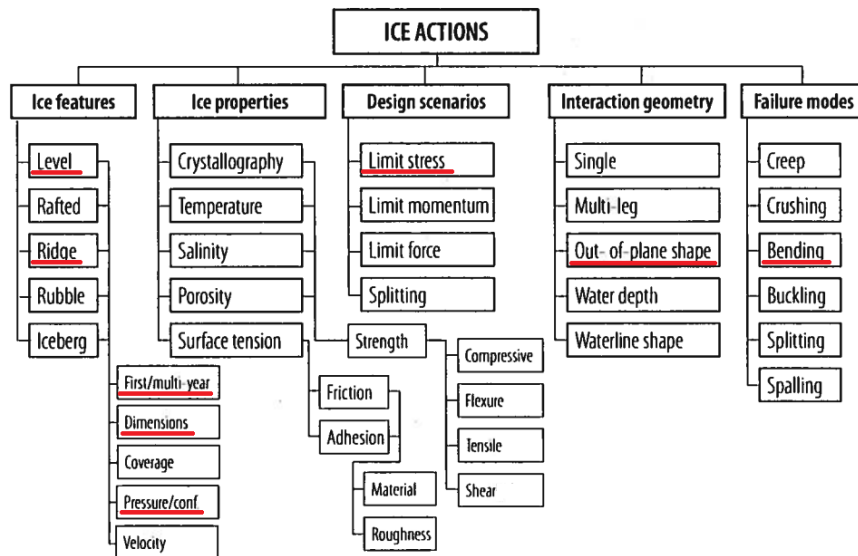
Figure 1.1: The major parameters affecting the ice action, adapted from (Løset and Gudmestad 2006)

INTRODUCTION

The final part presents nonlinear static analyses and evaluations of a local model extracted from the Sevan Arctic MODU design. The local model is subjected to local ice pressure distributed uniformly over a design area and structural capability is engaged with regards to structural yielding stresses. ABAQUS is used as the analysis tool, which is a powerful software suited for solving finite element analyses numerically. Hence, finite element method theory concerning the nonlinear static analysis is also presented, as well as the modelling footsteps necessary to perform in ABAQUS.

2 ASPECTS OF SEA ICE

Sea ice occurs in many different ways depending on many factors. Sea ice properties vary over the globe depending on salinity, oceanographic factors and others. In this thesis, only aspects of sea ice in the Arctic are of interest. The following chapter briefly presents different aspect of sea ice to easier separate sea ice types, morphology, properties and failure modes with regards to associated nomenclature.

2.1 Ice types

Sea ice types are classified by scientists based on the age of the sea ice, and are mainly developed by time and temperature. The first appearance of sea ice is a thin black-grey colored layer and as it gets thicker it changes color to a white color. The stages of development of sea ice are defined by (WMO 1989) as follow:

New ice (<1cm thickness): the starting point of sea ice development where the ice is composed of ice crystals which, as time passes, are weakly frozen together and is found as small plates or lumps. *New ice* is subdivided into frazil ice, grease ice, slush and shuga.

Nilas (1cm to 10cm thickness): a thin layer of ice that easily bends with the ocean motion. The color is greyish depending on the thickness. Hence, *nilas* is subdivided into dark and light *nilas*.

Young ice (10cm to 30cm thickness): is a transitional stage between *nilas* and *first-year ice* and subdivided into grey ice which rafts under pressure and grey-white ice which more likely ridge under pressure.

First-year ice (30cm to approx. 2m thickness): is sea ice that has only grown for one year during the winter time and may not survive the summer, see Figure 2.1. *First-year ice* is further divided into thin (30cm to 7cm thickness), medium (70cm to 120cm thickness) and thick (>120cm thickness) *first-year ice*.

Second-year ice (<2.5m thickness): is sea ice where the freezing process restarts in the autumn after *first-year ice* has survived one melting season.

Multi-year ice: all sea ice that has survived more than one melt season is denoted *multi-year ice*, also *second-year ice*, see Figure 2.2. *Multi-year ice* has a very low salinity and is considerably stronger and thicker than *first-year ice*.

The ice types of particular interest in an engineering process are the *first-year* and the *multi-year ice*. Hence, only these two ice types will be further discussed in this thesis.

Figure 2.1:Typical first-year ice condition including ice ridges, level ice and open water patches – in Gulf of Finland (Riska 2013)

Figure 2.2:Multi-year ice – ship penetrating a ridge (Riska 2013)

2.2 Ice morphology

Sea ice is also classified by form, structure and concentration. In this section, only the most relevant forms, according to the author, of sea ice are presented. It is to be noted that sea ice can also occur as iceberg and landfast ice. More ice morphology terms than is mentioned below are found in ref. (WMO 1989).

Ice floe: is a piece of floating sea ice which is relatively flat, see Figure 2.3. It arises because of movement of an ice sheet caused by thermal expansion, wind and/or currents resulting in stresses.

Brash ice: is an accumulation of *ice floes* not more than 2m across, see Figure 2.4. Often found in channels where icebreakers have made fairways for other ships (Riska 2013).

Pancake ice: is circular shaped *young ice* with 0.3 – 3m diameter and raised rims around the circumference which is formed by wave action, see Figure 2.5.

Level ice: is defined as sea ice which has not been affected by deformation. In other word, a continuous layer of sea ice with approximate same thickness, see Figure 2.6.

Rafted ice: is deformed ice defined by submersion of one ice floe beneath another ice floe, see Figure 2.7.

Figure 2.3: Ship in ice floes of concentration about 30-50% in Pechora Sea (Riska 2013)

Figure 2.4: Brash ice channel – made by an icebreaker (Riska 2013)

Figure 2.5: Pancake ice (SMHI 2012)
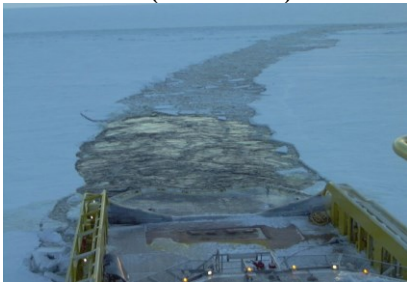
Figure 2.6: Icebreaker passing a large area of level ice (Riska 2013)

Figure 2.7: Rafted ice (SMHI 2012)

Figure 2.8: Ridge (SMHI 2012)

Ridge: a wall of deformed ice which has been forced upwards by the pressure from surrounding ice cover, see Figure 2.8. The part of the *ridge* above the waterline is termed the *sail*, and the submerged part is termed *keel* (4-5 times the *seal* height). According to (ISO19906), the cross-section of an ice *ridge* can be assumed to be symmetric for engineering design purposes. The idealized geometry of a first-year *ridge* will have a profile as illustrated in Figure 2.9.
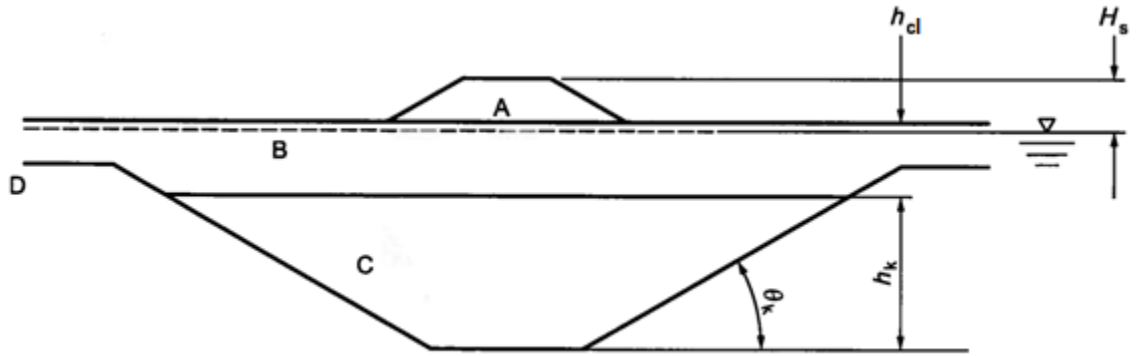
Figure 2.9: Idealized profile of a first-year ridge (ISO19906)

A – ridge sail

B – ridge consolidated layer

C – ridge keel

D – level ice

H_s – sail height

h_k – keel height

h_{cl} – consolidated layer thickness

ϑ_k – keel angle

2.3 Physical properties

In the following section, the physical factors salinity, density, temperature, ice thickness and sea ice formation and structure are given with reference to (Timco and Weeks 2010) and (Løset, Høyland et al. 1998). All these factors depend on each other.

2.3.1 Density and salinity

The density of sea ice depends roughly on the temperature and salinity, and these three factors depend strongly on each other as shown in Figure 2.10. The figure is illustrating four different salinity gas-free sea ices where density is plotted against temperature. It is observed that when the salinity is increased the temperature dependency increase. This is due to brine cells in the ice which are sensitive to temperature changes. The results in Figure 2.10 can be considered as an upper-bound for first-year sea ice density at a particular temperature and salinity. If gas is present in a sample, the density will decrease.

The density of sea ice influences the submersion of ice floes when it is forced down the structure. Small changes in density can result in a large difference in the buoyancy force.
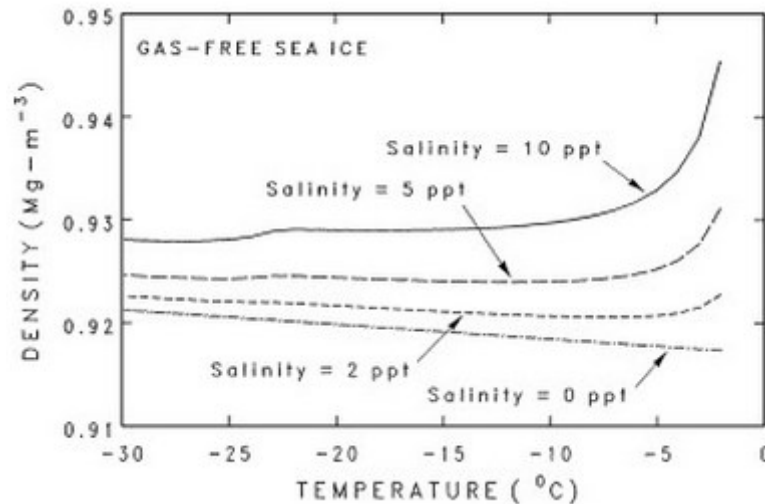
Figure 2.10: Plot of density versus temperature for four different salinities (Timco and Weeks 2010)

Salinity can be calculated if the ice thickness is known. The average salinity, S_i, of growing sea ice was examined and found that there is a consistent variation with the ice thickness. (Timco and Weeks 2010) derived the empirical equations given below:

First-year ice [‰]:
$$S_i = 4.606 + \frac{91.603}{h}$$

Equation 2.1

Multi-year ice [‰]:
$$S_i = 1.85 + \frac{80217.9}{h_F^2}$$

where

h – ice thickness [cm]

h – floe thickness [cm]

2.3.2 Sea ice formation and structure

The salt content in seawater causes ice to freeze at a temperature well below zero. The first ice crystal starts to form at -1.9 degrees, and as more and more pure ice forms brine pockets in the ice structure becomes more saline. As cooling continues, different solid salts will precipitate from the brine. In other words, sea ice contains solid ice, brine, air

and various types of solid salts. Salinity of the seawater and the growth rate of the ice affect the amount of brine trapped. Pockets of brine distributed in the sea ice reduce the strength of sea ice relative to freshwater. (Løset, Høyland et al. 1998) derived for first-year ice the relative brine volume v_b as:

$$v_b = S_i \left(\frac{45.917}{T_i} + 0.930 \right) \quad -8.2°C \leq T_i \leq -2.0°C$$

Equation 2.2

$$v_b = S_i \left(\frac{43.795}{T_i} + 1.189 \right) \quad -22.9°C \leq T_i \leq -8.2°C$$

where

v_b – brine volume per thousand

S_i – salinity of ice

T_i – absolute value of ice temperature

These equations refer to an ice density of 926kg/m3. From these equations it is observed that the ice strength will increase as the temperature decreases, ref (Løset, Høyland et al. 1998).

The growth of sea ice depends on prevailing environmental conditions and will results in different grain structures. The most common grain structure for first-year ice includes granular, columnar and discontinuous columnar. The ice microstructure will influence the mechanical and physical properties of the ice. The grain structure of multi-year ice is quite varied and can consist of a mix of granular ice, mixed granular and columnar ice, and pulverized brecciated ice. The chaotic microstructure is a result of mechanical deformation and thermal growth. Overall, first-year ice is highly anisotropic and multi-year ice is frequently isotropic. Compared to first-year ice, multi-year ice has a very low salinity. Hence, the ice is considerably stronger due to lower porosity in the ice. In many ways, the properties of multi-year ice are closer to freshwater than first-year ice.

2.3.3 Ice Thickness

Ice loads on offshore structures increase with increasing thickness. Hence, ice thickness is an important parameter when calculating the ice actions on offshore structures and

vessels. The bearing capacity, the way the ice will fail, of an ice sheet depends largely upon its thickness. If a steady state condition is assumed and the heat transfers between the water and ice is negligible, the Stefan equation can be derived as follow, Ref (Timco and Weeks 2010):

$$h = \sqrt{\frac{2k_i}{\rho_i L}(T_b - T_a)t_t}$$

Equation 2.3

where

k_i – thermal conductivity

ρ_i – ice density

L – latent heat of fusion of ice

T_a – top temperature of ice sheet

T_b – bottom temperature of ice sheet

t_t – total freezing time

Application of Equation 2.3 will always over predict the ice thickness due to the assumptions that have been made in deriving it. However, the Arctic ice has generally thicker ice than in more temperate climates largely due to the ambient air temperature and freezing time.

2.4 Mechanical properties

In this section tensile, compressive, flexural, and shear strength for sea ice is presented. The information is drawn from reference (Timco and Weeks 2010).

2.4.1 Tensile strength

Tensile strength is the maximum stress a material can withstand while being stretched or pulled, both vertical and horizontal. Tensile strength in sea ice varies in horizontal and vertical direction due to the different grain structures and growth directions. Consequently, tensile strength is found to be three times higher for vertical loading than horizontal loading. Sea ice is a brittle material. Therefore the tensile strength is a fundamental property for sea ice and a key failure mode when ice interacts with an offshore structure.

Measuring the tensile strength of sea ice is difficult and time consuming. Because of this the tensile strength for both first-year and multi-year ice have not been studied much up till now. The studies that have been performed of first-year ice up till today concludes that the horizontal value of tensile strength range from 0.2MPa to 0.8MPa and vertical value of tensile strength range up to 2MPa. Multi-year ice is concluded to vary from 0.5MPa to 1.5MPa both vertically and horizontally.

2.4.2 Compressive strength

Compressive strength is the ability of a material to resist loads that attempt to compress the material together. Sea ice failure due to compression can occur while pressure ridges are formed or by ice crushing against an offshore structure. The compressive load on an offshore structure becomes a significant design criterion for interaction with thick sea ice.

The compressive strength in sea ice has been investigated numerous times and equations based on the brine volume and the loading rate have been derived. Typical values for first-year ice range from 0.5MPa to 5MPa. Compressive strength of multi-year ice is similar to first-year strength, but can be considerably stronger compared to first-year ice if the ice is very cold.

2.4.3 Flexural strength

Flexural strength is a parameter for brittle materials and is defined as the material's capability to resist deformation under loading. For sea ice, the flexural strength is an important engineering parameter because many sea ice failures occur in this fashion, such as pressure ridge formation, ice breaking vessels failing ice and bending of ice on sloping structures.

There have been a large number of studies around flexural strength in first-year ice because the test methods are easy to perform. On the other hand, there have not been reported measurements of the flexural strength in multi-year ice. Due to the lower salinity in multi-year ice, the strength can be expected to be higher compared to first-year ice. The conclusion is that the flexural strength for first-year ice ranges from 1MPa and

decreases with brine volume and for multi-year ice the flexural strength ranges between 0.8MPa and 1.1MPa in the winter.

2.4.4 Shear strength

Shear strength for a brittle material is generally not of concern in an engineering process because it tends to fail in tension rather than shear. Shear forces produces a sliding failure in the material along a plane that is parallel to the direction of the forces. Consequently, for brittle materials the tensile strength is lower than the shear strength.

However, shear strength is an important factor to consider since ice interacting with structures is often subjected to a biaxial stress condition with tensile and compressive stresses or a shear stress.

2.5 *Failure modes*

The following theory about failure modes of ice is taken from (ISO19906), (Sanderson 1988) and (Løset and Gudmestad 2006).

The mode of ice failure against a structure has a significant effect on the magnitude of the ice action. Different types of failure take place depending on the strengths level, stress distribution, ice velocity, and shape of the structure (see Figure 2.11 and Figure 2.12). The failure modes can even replace each other during the same event. Generally ice breaks when interacting with a structure, but can deform in different ways. Structures with vertical walls in the waterline region generally experience larger ice actions than sloping ones. This is roughly due to the ice resistance to compression is significantly higher than for bending, which induce the ice failure by flexure, and will correspond to lower ice actions.
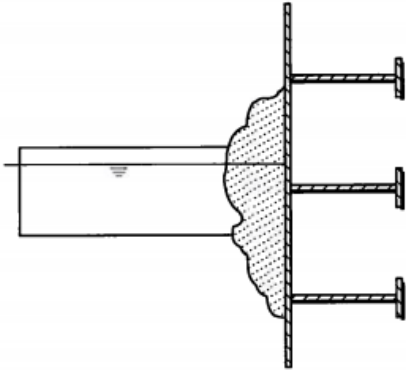
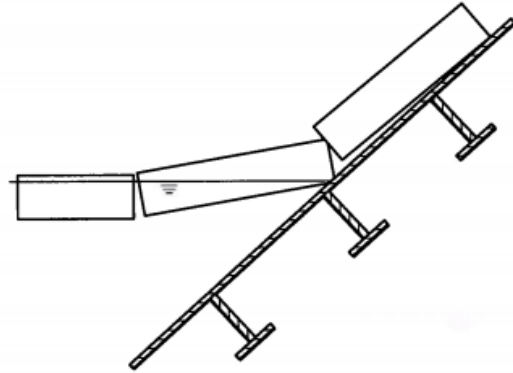**Figure 2.11: Ice crushing against a vertical structure (ISO19906)**

Figure 2.12: Ice bending upward along a sloping structure (ISO19906)

How ice behaves depends on how fast it deforms. Ice failure can be divided into continuum behavior (such as creep) and fracture behavior (such as cracking). (Sanderson 1988) classified failure types, and some common failure modes are presented below:

Creep: ice deforms in *creep* if the ice is moving very slowly like a slow-moving glacier, see Figure 2.13. It does not break up into fragments, but remains a more or less continuous solid. *Creep* loads on offshore structures in the Arctic are most critical when landfast ice undergoes thermal expansion in the spring time.

Buckling: if the ice is thin it buckles out-of-plane under edge loads applied by contact with a wide structure, see Figure 2.14. B*uckling* is likely to be the governing mode when the ice is thinner than 0.4m.

Cracking: happens both radial and circumferential. *Circumferential cracking* is a result of elastic *buckling* and *radial cracking* happens especially at high aspect ratios (typically structure corners). The *cracking* is initially stable and of limited length. See Figure 2.15.

Crushing: if the ice is thicker and loaded on a vertical structure it breaks into small fragments and causes a continuous *crushing*. The ice in the contact zone is pulverized and extruded upward and downward, see Figure 2.16. This failure mode is the case for a vertical structure and generally governs the design.
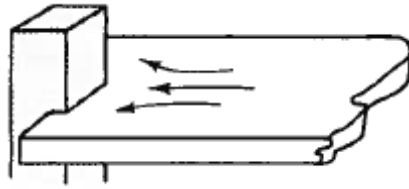
Figure 2.13: Creep (Sanderson 1988)

Figure 2.14: Buckling (Sanderson 1988)

Figure 2.16: Crushing (Sanderson 1988)

Figure 2.15: Cracking, radial and circumferential (Sanderson 1988)

Bending: last but not least, *bending* is in the majority of situations linked with ice interacting with sloping structures, see Figure 2.12. Usually *radial* and *circumferential cracking* develops due to the ice sheet *bending* while it rides up the slope. The width of the structure and ice thickness will affect the type of these cracks.

3 FOCUS AREAS IN THE ARCTIC

The most important leasing areas in the Arctic and Sub-Arctic offshore are in deep and ultra-deep water varying from 300m to 3000m water depths. The Barents Sea, the Orphan Basin, offshore Newfoundland and fields offshore Greenland are such areas of interest, see Figure 3.1. Several of these fields have exploratory drilling or in the planning stage. Due to melting of ice in the Arctic, the open water period has increased, which provides an opportunity to develop these fields with fewer concerns with regards to ice large actions. Refer to (Aggarwal and Souza 2011) .
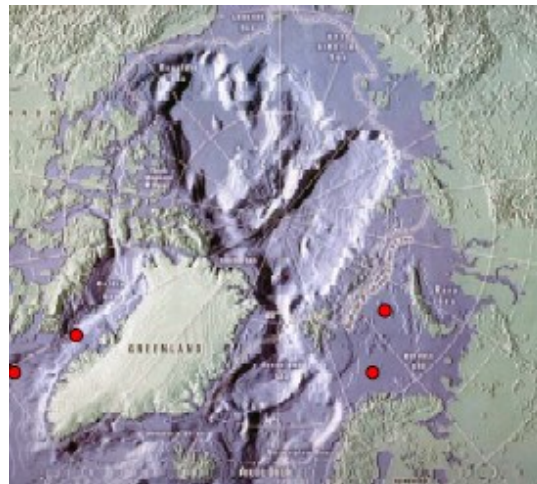
Figure 3.1: Focus areas in the Arctic with deep water (Aggarwal and Souza 2011)

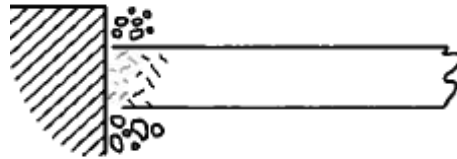The area of special interest, due to Norwegian oil companies expanding higher north, is the Barents Sea and the ice conditions here, see Figure 3.2. The most northerly oil discovery is the Wisting Central by OMV and the wildcat estimated the field to hold 165 million oil equivalents[1]. The Barents Sea holds the potential to build out an infrastructure. The Sevan Arctic MODU design provided by Sevan Marine is designed to tolerate ice condition for several areas around the world. This design is further outlined in section 5. However, ice conditions in the Barents Sea will nevertheless be of the most importance and will be investigated in this section.

---

[1] http://www.tu.no/petroleum/2013/10/03/na-pepres-barentshavet-med-bronner
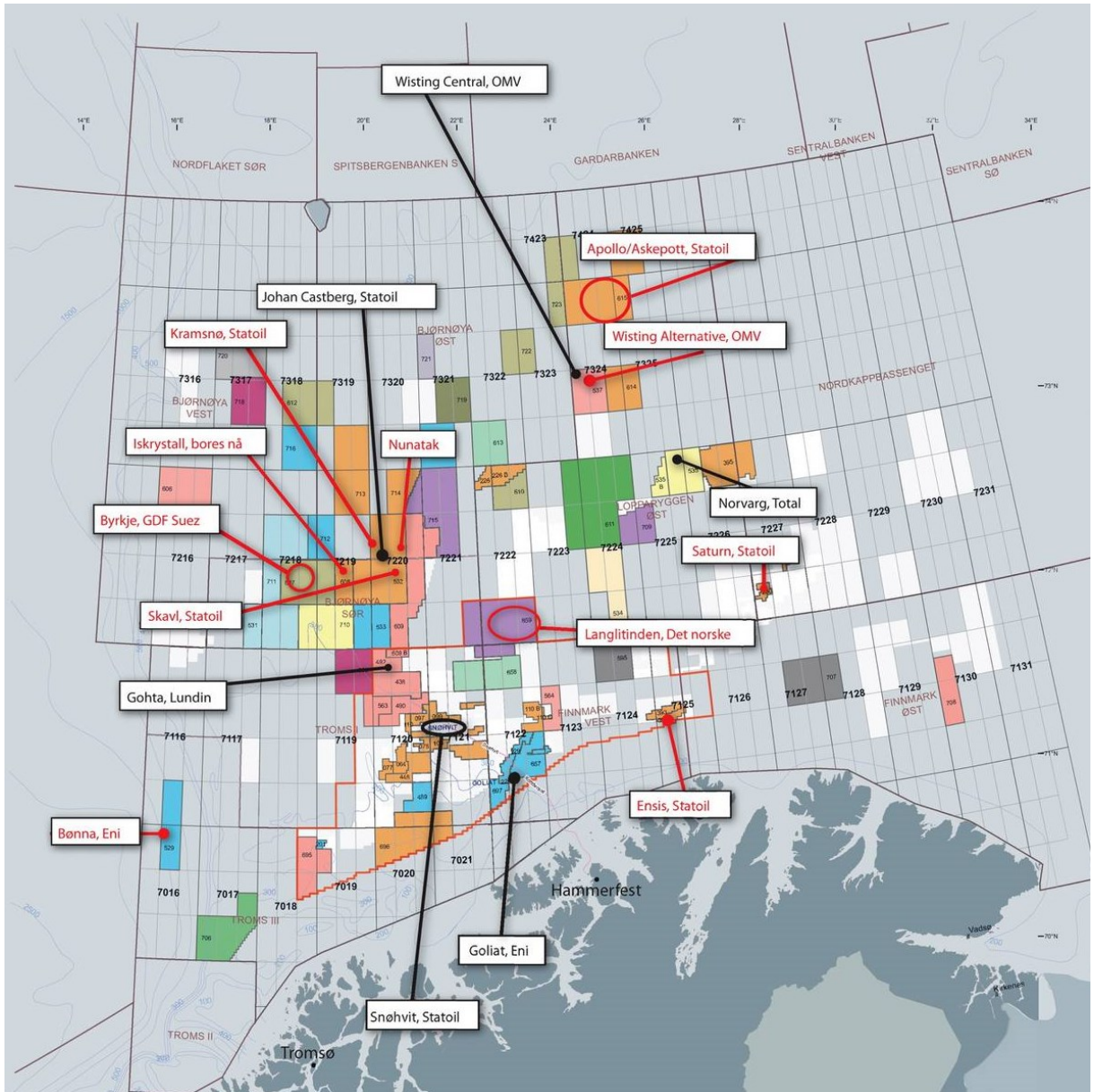
Figure 3.2: The Norwegian continental shelf of the Barents Sea (Helgesen 2013)

3.1 The Barents Sea

The information presented below about the Barents Sea is compiled from (ISO19906), (Palmer and Croasdale 2013) and (Løset and Gudmestad 2006).

The Barents Sea is a marginal sea located north of Norway and north-west of Russia. In the north the Barents Sea are bordering the Arctic Ocean. The greatest depth is up to 600m and located in the central part. This is not a very significant water depth compared to the depths elsewhere in the Arctic Ocean Basin. Due to these large depth variations,

the water exchange between the Arctic Ocean and the Barents Sea is relatively stagnating. In the Barents Sea there are four main water masses; the Atlantic water flowing from west with increased temperature and salinity, Arctic water flowing from north with very low temperature and decreased salinity, coastal water with seasonal variation in temperature and low salinity and the Barents Sea water with low temperature and high salinity. Consequently, the salinity and temperature varies within the Barents Sea throughout the season and area.

ISO 19906 divides the Barents Sea into three parts for design purposes, see Figure 3.3. The division takes into account both the physical and the geographical features like seabed relief, system of currents and ice edge position.
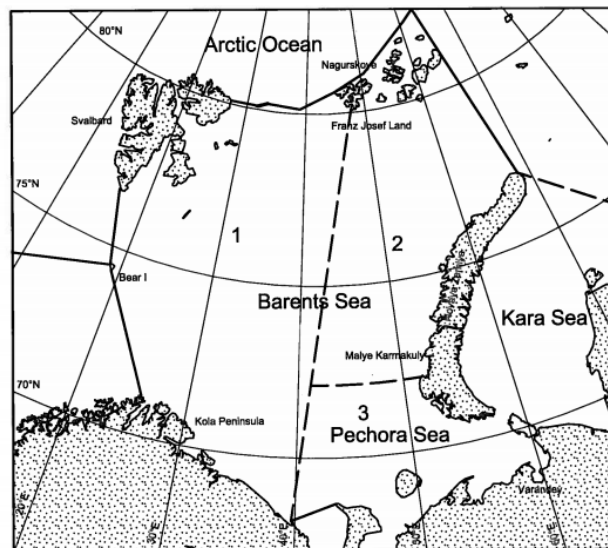
Figure 3.3: Regions of the Barents Sea (ISO19906)

1 – western region

2 – northeastern region

3 – southeastern region (Pechora Sea)

The northern part of the Barents Sea is part of the seasonal ice zone in the Arctic, which means that some years the ice melts entirely from these waters during summer while other years the ice remains. Sea ice is never completely covering the Barents Sea, approximately 55-60 % of the surface is covered during high season in March. Thus, the most common type of ice in the Barents Sea is first-year ice, which has an approximate

ice thickness of 1.5m. Multi-year ice is only found in the north of the Barents Sea between Svalbard and Franz Josef Land, and is dominating in the spring season. The seasonal variation of sea ice extension is very high with a minimum extension in September as illustrated in Figure 3.4.
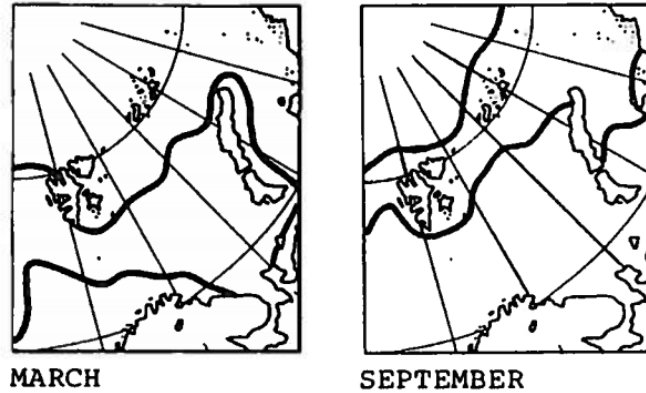
Figure 3.4: Maximum and minimum extension of sea ice in March and September (Løset and Gudmestad 2006)

Figure 3.5 shows the variation of the maximum sea ice extension. It is observed that the variation in the eastern part is considerable while variation around Bjørnøya is minor.
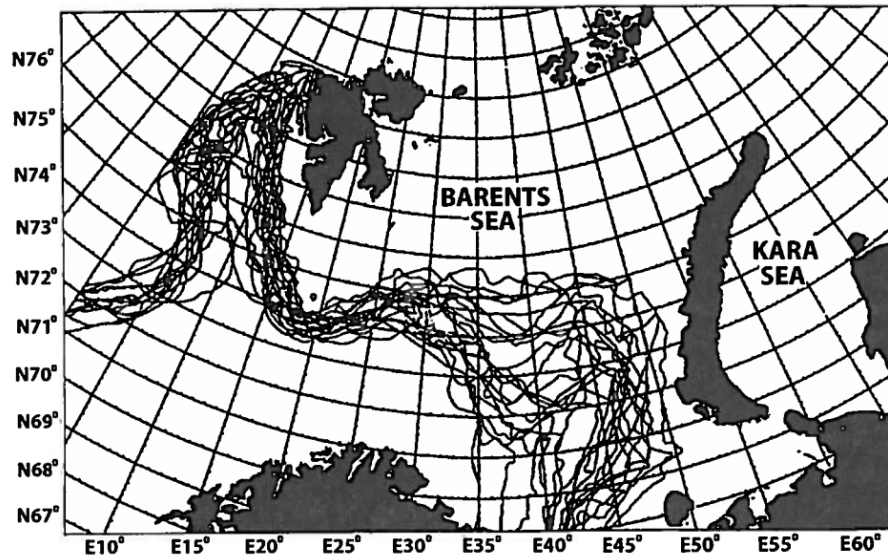
Figure 3.5: Period 1966-1989, annual maximum extension of sea ice (Løset and Gudmestad 2006)

Iceberg from glaciers on Svalbard, Franz Josef Land and Novaya Zemlya are also present in the Barents Sea. Icebergs can move large distances during their life span and drift due

18

to forces from winds and ocean currents. In the western region, there are around 10 to 40 icebergs per year and these are mainly present during the spring. Impacts from icebergs will not be looked upon in this thesis. Table 3.1 lists several parameters for the Barents Sea. Values are obtained from (ISO19906) and (Srinivasan, Singh et al. 2008).

Table 3.1: Typical environment parameters in the Barents Sea

Water salinity	‰	34.5-35.0
Water temperature	C°	5-9
Level ice thickness	m	1.3 to 1.5
Water depth	m	330
Iceberg	-	Yes
Level ice thickness (100yr)	m	2.7
Maximum ice drift (100yr)	m/s	1
Significant wave height (100yr)	m	14.3
Peak period (100yr)	s	15.3
Flexural strength of ice (max)	MPa	0.52
Maximum ridge size found	m	Width: 57 Draft:17
Wind 1 hour average for 100yr	m/s	49

4 TECHNOLOGICAL CHALLENGES AND SOLUTIONS FOR DEEP WATER ARCTIC DEVELOPMENTS

In Arctic shallow water field development the most used platform designs are fixed base or bottom founded platforms. This is because they are simpler to design and operate. However, when the field exploration expands into larger water depths there will be a demand for floating platform designs. Floating platforms have been used for centuries, but the designs need to be upgraded for their use in Arctic deep water. There will be an additional demand for technical feasibility, operability and commercial viability due to harsh weather, extreme temperatures, significant ice features and environmental impact requirements in these regions. (Aggarwal and Souza 2011) have listed the most significant challenges of deep water Arctic as follow:

- Remoteness of the fields from existing development or from shore.
- Limited access to fields due to potential impact of ice features.
- Lack of infrastructure in the fields and regions.
- Requirements of multi-year drilling program and very long project development schedule.
- Operations available with operating companies to bring the product to market.
- Lack of reliable ice and iceberg data over long period.

In the following chapter the technology challenges and solutions for offshore structures in the Artic will be looked upon.

4.1 Technological innovation

The most challenging hazard in the Arctic is the presence of large ice features of multi-year ice and icebergs. According to (Aggarwal and Souza 2011), the presence of ice will demand a technical need for the floating structure to have the opportunity to detach from the drilling and production risers and mooring lines as illustrated in Figure 4.1. This way the structure can avoid large ice loads by either being towed away until the hazard has passed or by using its own propulsion system. To perform such a disconnection-

reconnection operation is time consuming and valuable drilling time is lost. Hence, it is important to know the length and reliability of the open water season and the severity of the ice condition that can occur during the intended drilling window. There is per today a lack of reliable long term data of large ice features and icebergs in Arctic and Sub-Arctic regions. Thus, in the design of platform solutions an additional conservatism in the ice load calculations will be required. According to (Hamilton 2011), the eastern Barents Sea has a relatively long open water period of 120 days and fairly mild and predictable sea ice condition at the shoulder of the open water window. Hence, exploration wells may be drilled in a single season. However, iceberg management is required and potential temporary disconnection possibilities to avoid icebergs.
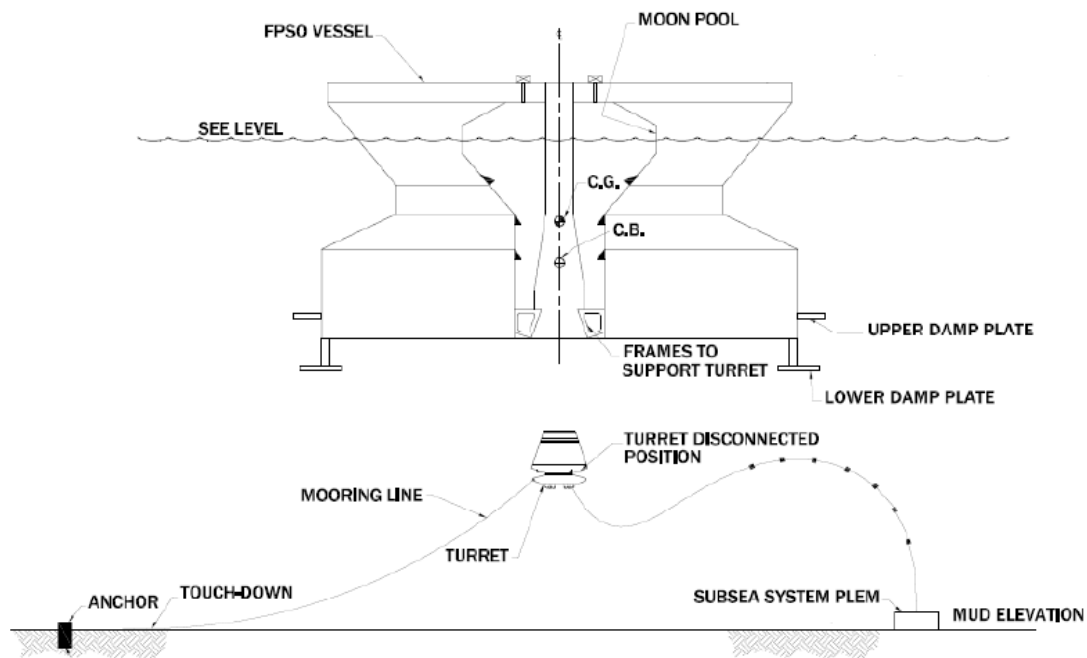
Figure 4.1: Disconnection design for FPSO located in Sakhalin-V (Srinivasan, Singh et al. 2008)

Ice management is a method that has been used since offshore structures first were located in ice infested waters and the method's function is to help withstand large ice action on the structure. The ice management icebreaking fleet's purpose is to continuously reduce the size of incoming ice sheets such that ice action on the offshore

structure stays within the capacity of its DP system or spread moorings. High reliability ice management capability will therefore be a key technology parameter for Arctic deep water development. On the other hand, because there will always be multi-year ice features that cannot be broken even by the largest icebreakers and presence of icebergs, it is essential for development of floating offshore structures to have the capability to disconnect and reconnect in dynamic ice conditions.

4.2 Ice action

A coupling of ice management, mooring line capacity and cost consideration will together determine the governing maximum ice action a floating system located in the Arctic can handle as illustrated in Figure 4.2. Global ice loads are estimated to be several times higher than the maximum storm/wave load in non-ice infested waters. Practical design of station keeping systems would be limited to loading from the first year ice or small multi-year ice features. Research work has shown that the strongest chain available has a minimum breaking load (MBL) of 31MN and with 24 mooring lines the maximum capacity would be approximate 77MN for a buoy shaped hull, and maximum offset would be 33m. Whereas the ice loads on ship shaped hulls that may be loaded up to 300MN. Refer to (Aggarwal and Souza 2011).
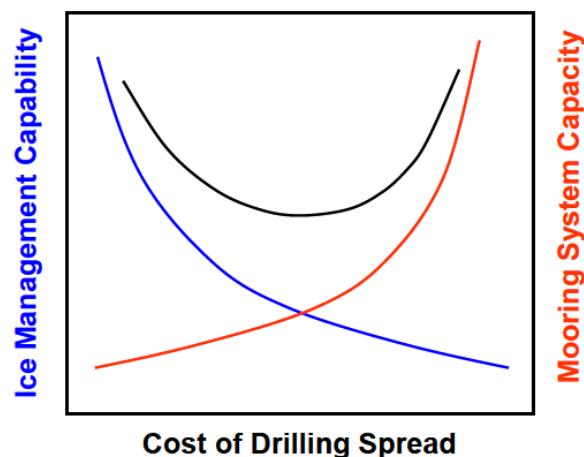
Figure 4.2: Arctic floating drilling in first-year ice trade-off between ice management and mooring system capability (Hamilton 2011)

Maximum load estimates for existing platforms in Artic areas with multi-year ice and iceberg differ from platform type and shape. The Hibernia gravity based platform was constructed to withstand large ice impacts with a maximum design load that range from 1200MN to 1500MN and the design pressure are identified to vary from 3MPa to 8MPa. These are very large design loads compared to the Terra Nova FPSO, which has a mooring system capacity of 20MN. The Terra Nova FPSO has thus a detachable design. Generally, the design ice load estimates have been reduced over the past decades due to improved understanding of the behavior of ice-structure interaction. However, there are still large uncertainties, especially towards floating platforms. Conservative estimates should therefore be used to design floating offshore structures in the Arctic.

4.3 Hull shape

Figure 4.3 illustrates some floating alternatives for deep water operations in the Arctic. Alternative (a), (b), (c) and (d) illustrate the spar, semi-submersible, ship-shaped floater and conical buoy concept, respectively. Which design that is to be preferred in the Arctic is under much debate. The debate is sometimes distorted by fashion and prejudice, but there will certainly not be a single 'right' solution.
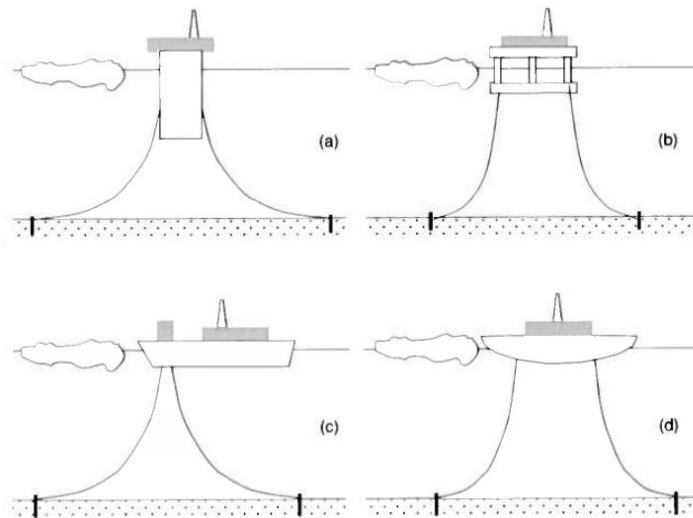
Figure 4.3: Alternative concepts for floating systems (Palmer and Croasdale 2013)

According to (Aggarwal and Souza 2011), the best hull design for Arctic ice and open water condition is a design that requires a single point detachment which will reduce time and effort to disconnect and reconnect to risers and mooring lines. A buoy shape is such a

design, see Figure 4.1. The buoy design also has the advantage compared to other platform designs to reduce ice loads because of its hull shape.

According to (ISO19906), structures with sloping hulls in the ice action areas will generally experience less ice actions compared to vertical hulls. The mode of ice failure against the structure has a significant effect on the magnitude of the ice action. Conditions that induce ice failure by bending, such as sloping structure, will result in smaller ice action than failure by ice crushing, such as vertical structure. (Aggarwal and Souza 2011) suggests that fixed platforms should bend the ice sheet upwards to reduce loads due to bending failure. On the other hand, floating platforms should bend the ice sheet downward to enable elimination of accumulation of broken ice on the platform because broken ice would clear more easily due to of the presence of water.

Buoy shaped platforms with sloping structure in the waterline region is an ideal design for deep water development in the Arctic. Additional demands and constraints for platforms in the Arctic will make the structure generally larger and heavier in size compared traditional open water platforms.

To sum up the potential operations to reduce ice loads (Aggarwal and Souza 2011) have listed the following:

- Implement variations in hull shape to reduce ice loads
- Variation in floating platform draft for ice features months from that for high wave months
- Improved understanding of ice load on different structural forms to reduce conservatism
- Risk based evaluations to enable identify appropriate ice loads
- Estimate station keeping limitations of a floating unit
- Implement ice management program for large ice features and iceberg

Major technology hurdles with regards to safety and economical procedures for the harsh environment need to be overcome to benefit from oil and gas development in the Arctic. To develop technology that can handle the Arctic and at the same time be economically

beneficial is a big challenge. In this thesis, economical influences will not be taken into consideration.

4.4 Example structures

Around the world there are just a few places where offshore development in ice infested waters has taken place. The vision for year-round operation in ice infested waters is looked upon by many oil companies. There have been drilling vessels in ice infested waters for over 40 years. The best knowledge we have on ice-structure interaction and loads is due to full-scaled experiences from structures already operating in ice infested waters. It began in the waters between Canada and Greenland, where icebergs had to be towed away from the drilling vessel. Some of the revolutionizing offshore structures, such as the Kulluk and the Molikpaq, are presented in section 4.4.1 and section 4.4.2.

4.4.1 The Kulluk vessel

Refer to (Palmer and Croasdale 2013). The Kulluk vessel was an ice-strengthened drill barge that was constructed for Arctic waters. She drilled in the Beaufort Sea from 1983-1993, and was extensively refurbished in 2005 by Shell and drilled for another 7 years around the northern coast of Alaska before she drifted and grounded in 2012 and was scraped.

Looking at the main dimensions and features, the vessel hull is 70m in diameter in the waterline and sloping inward with 30 degrees such that the ice could bend downward along the hull. The Kulluk could operate in water depths from 20m to 60m with an operating draft on about 12m. Her ultimate mooring capacity was 10MN, however during drilling operation, the maximum load tolerance was only 7.5MN. Kulluk generally only drilled in the summer season and was supported with two to four icebreakers. The icebreakers also had to tow Kulluk because she was only kept stationary by mooring lines.

**Figure 4.4: Kulluk operating in managed ice in the Canadian Beaufort Sea (Palmer and Croasdale
2013)**

Knowledge from full-scaled events on Kulluk involves both managed and unmanaged ice
conditions. Further presentation of full-scale experiences of managed ice is found in
section 6.5, where calibration results for ice load vesus ice thickness from managed ice is
highlighted.

4.4.2 The Molikpaq offshore platform

Refer to (Timco and Johnston 2003) and (Sudom and Frederking 2010). The Molikpaq
drilling and oil production platform is originally built to explore oil in the Beaufort Sea in
the 1980s. In 1998, the Molikpaq was upgraded for deeper water and towed to Russia to
be used offshore Sakhalin Island in 30m water depths. The oil is exported with tanker
during the summer months. Thus, with a FPSO moored to a SALM buoy that is
connected to Molikpaq with a pipeline, the exported could be expanded to the whole
year.

The Molikpaq structure is permanently anchored to the seabed by a concrete substructure
filled with sand. It is specially built to operate in severe ice conditions. The structure is
almost vertical in the waterline region (only 8 degrees bending upward) and 90m wide,
consequently the incoming ice will mainly fail by crushing. Generally, wide platforms in
shallow water are simpler to design and operate. However, there may be problems related
to ice rubble which will form around wide structures and not clear very easily. In May 12,

1986, Molikpaq experienced a large ice floe impact. The largest load actions ever experienced on Molikpaq platform were recorded during the impact. A closer examination of the incidence has concluded that the Molikpaq experienced a global load ranging from 195MN to 353MN.

Figure 4.5: Molikpaq operating in the Canadian Beaufort Sea (Timco and Johnston 2003)

5   THE SEVAN ARCTIC MODU

The design of the Sevan Arctic Mobile Offshore Drilling Unit (MODU) is a new, innovative design that is not yet introduced to the market. The design is still in the initial stage and continuously converging towards a better solution. Two hull shapes are investigated in this thesis, a design with downward breaking hull and a design with upward breaking hull in the waterline. Throughout the working period of this thesis Sevan continuously provided new information about the design. Thus, the design presented in this thesis may not be the final solution of the Sevan Arctic MODU, but the principles of determining ice actions will be the same.

The oil market has for a while looked upon the Arctic frontiers and its holds of hydrocarbons. Sevan Marine therefore started a process of designing an innovative oil exploration platform intended for the Arctic environment. The hull form is characterized by a cylindrical main body that is extended with a "skirt" at the lower section of the hull. The skirt below the waterline helps to maintain the structural stability. In some of the Arctic regions there is not a constant presence of ice, especially during the summer. Hence, both wave and ice actions have to be taken into consideration in the design. Sevan Marine has solved this issue by introducing a design that can operate with two drafts, one draft for wave action and one draft for ice action. At the wave action draft the hull is vertical while at the ice action draft the hull is sloping. The advantage with sloping hull in ice infested waters is as mentioned that the ice fails by bending which induce much smaller ice actions on the structure compared to a vertical hull. There are two variations of the hull that is considered in the design phase:

- Downward breaking cone, see Figure 5.1.
- Upward breaking cone, see Figure 5.2.
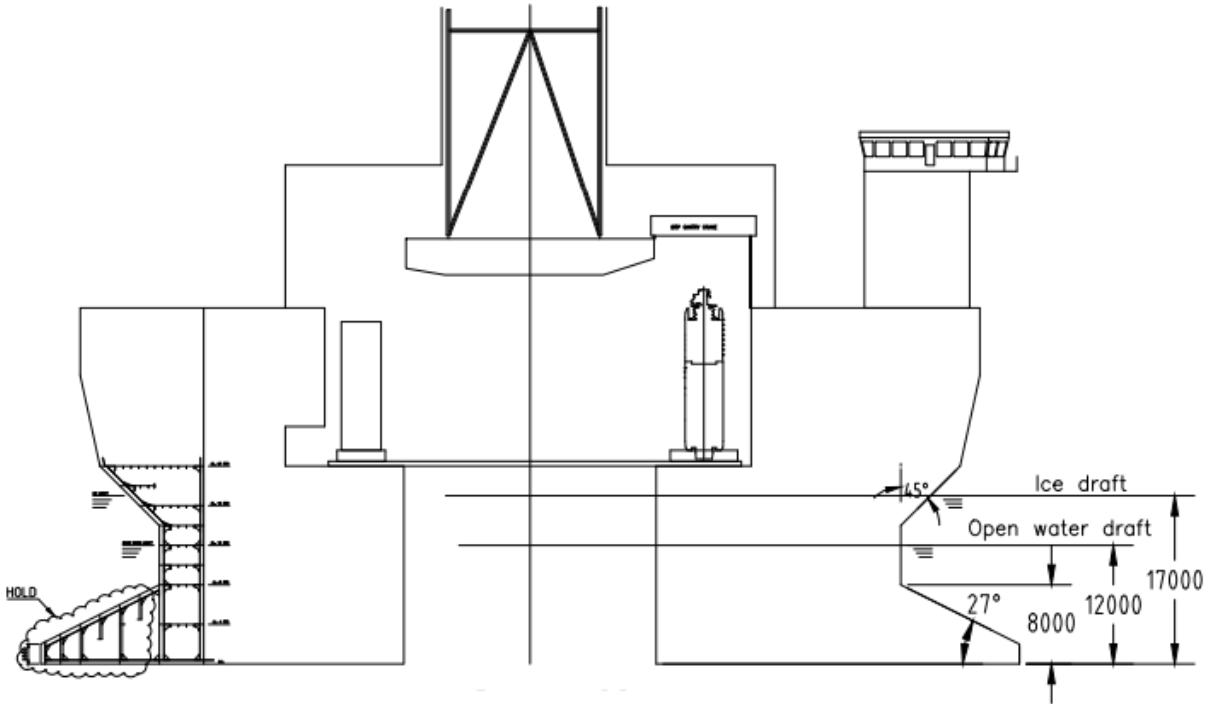
Figure 5.1: Downward sloping hull design, adapted from Appendix B1
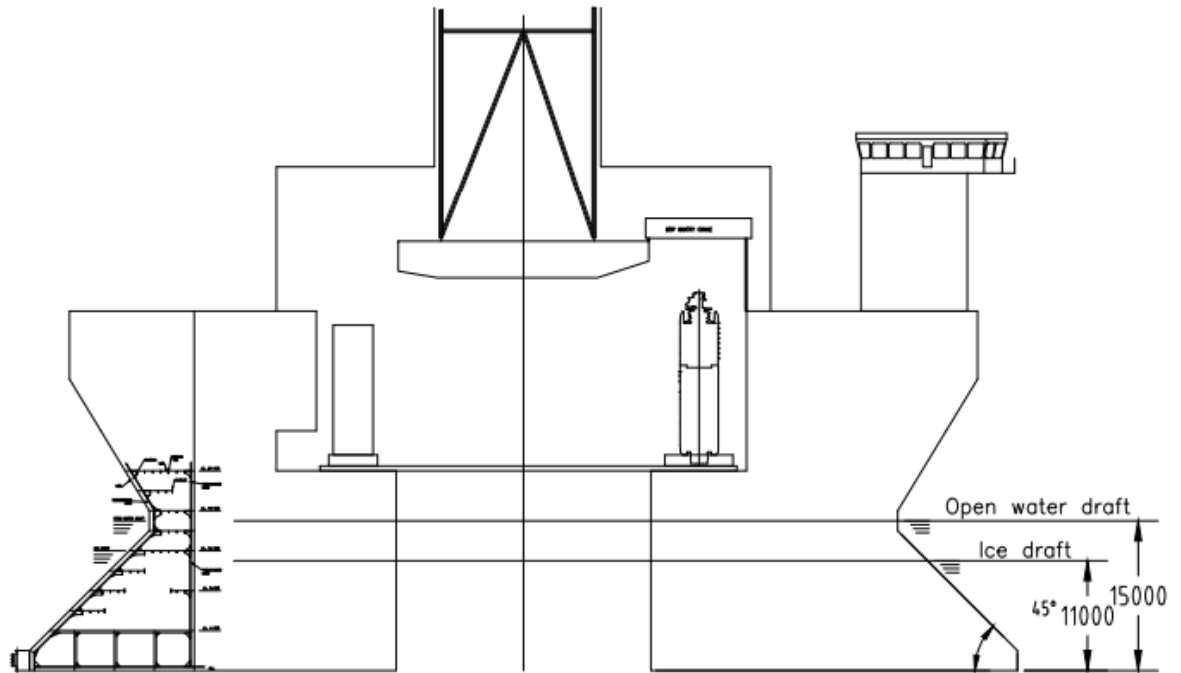
Figure 5.2: Upward sloping hull design, adapted from Appendix B2

More detailed drawings of the hulls are found in Appendix B. The structure is designed as a hexadecagon (16-sides) and can take ice loadings from any direction for the ultimate limit state, refer to Appendix A. The main advantage of this shape is that it offers the

same general shape and width to the incoming ice regardless of its direction. Another advantage with a hexadecagon compared to a circular shape is that the flat sides allow easier fabrication of the vessel. The Sevan Arctic MODU is designed in accordance to Polar Class PC4 (this is further outlined in section 6.8) and will operate in typical first-year sea ice conditions. Table 5.1 presents the main dimensions and drafts for both upward and downward breaking design, while Table 5.2 presents the ice loads scenarios provided from Sevan which is to be investigated against to the hull shapes.

Table 5.1: Main Dimensions and Drafts, adapted from Appendix A

	Downward breaking cone	Upward breaking cone
Open water Draft Diameter [m]	75	
Main Deck Diameter [m]	113	
Double Bottom Height [m]	3.5	
Double side breadth [m]	5.0	
Hull depth [m]	24	
Draft, transit [m]	10	
Draft, Ice Operation [m]	12	17

Table 5.2: Ice feature scenarios provided by Sevan, adapted from Appendix A

Ice features	Thickness [m]	Some typical ice data
Level ice	1.2	Density 890kg/m3 Bending strength 500kPa Compressive Strength 1.2MPa E-modulus 3.5GPa
Managed ice	1.2	Floe size 100mx100m Ice data as above
Ice ridge		Sail height 9.3m Keel depth 21m Consolidated layer thickness 3m Bending strength c.l. 640kPa Compressive strength c.l. 1.5MPa

6   DETERMINING ICE ACTIONS

Two types of ice actions are usually considered as most important for structural design, namely the global ice action and the local ice pressure. Global ice action is the action exerted on the whole structure at any instant time and is important to determine when stability, overturning moment or the overall strength of the structure is considered. The local pressure is the pressure exerted on a limited part of the structure, in this thesis called the local design area. This pressure is an essential factor when the local structural strength is evaluated.

(Løset and Gudmestad 2006) formulated the main problem concerning ice action of structures as "…*for a given structure form, the ice properties and environmental conditions it is necessary to find the action required to fail an ice feature*" (Løset and Gudmestad 2006, p.109). Figure 6.1 shows roughly some main factors that the global ice action may depend on. In this thesis, the highlighted factors in Figure 6.1 will be investigated and the Sevan Arctic MODU's concept will be particularly investigated with regards to these ice actions.
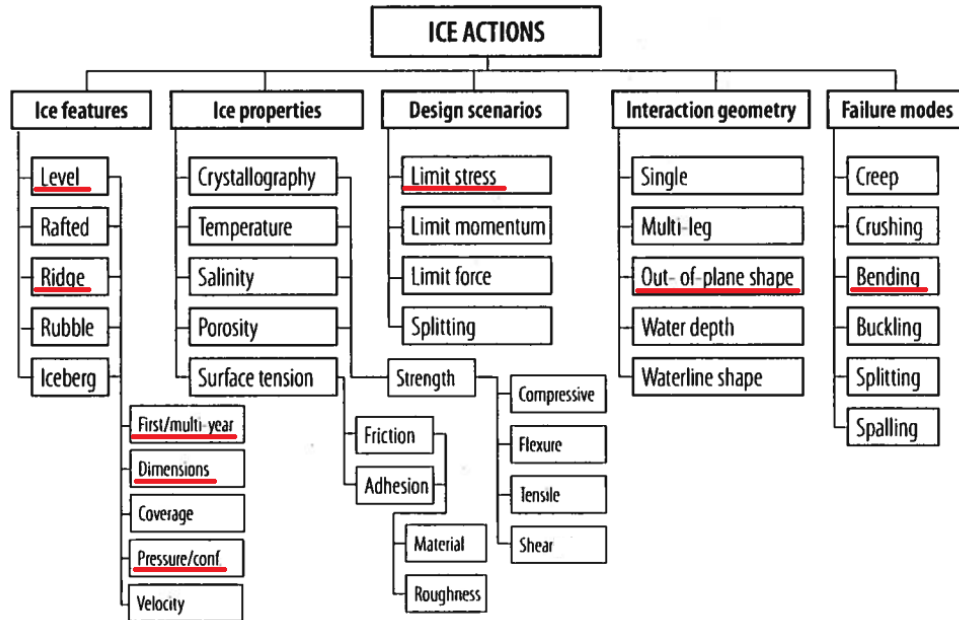

Figure 6.1: The major parameters affecting the ice action, adapted from (Løset and Gudmestad 2006)

The limit stress scenario corresponds to a situation when stress, either compressive, shear, tensile, flexural or buckling, reaches some limit. This scenario will very often control the maximum action. This is also the case in this thesis.

In addition to interaction from level ice and ridges, ice actions from managed ice will be examined. Due to ice management, sea ice reaching a floating structure is typically a slurry of broken ice pieces containing some larger floes and multi-year ice. A floater, such as the Sevan Arctic MODU, is in reality supposed to operate in managed ice. However, according to (Palmer and Croasdale 2013) it is useful to estimate loads on floaters from unmanaged ice to help define design limits.

The following sections will first present a study of previous experiences with ice acting on sloping structures, followed by a presentation of the ISO 19906 standard which is an important standard to conduct in assessment and design of offshore structures located in the Arctic. Further, a study of level ice, ridge and managed ice action on sloping structures are presented, followed by a parameter study of increasing geometrical parameters for ice. The parameter study wills also examine whether a downward sloping or an upward sloping design should be recommended for the floater. In the end, different approaches to determine local ice pressure will be presented and the most suitable approach to apply on a sloping structure in 1.2m level ice will in section 9 be used to investigate structural hull capacity of a local model extracted from the Sevan Arctic MODU design.

6.1 Sloping structure

The presence of sea ice in the Arctic and the forces it leads to proposes a design challenge of floating offshore structures. A key design driver is to optimize the hull shape to minimize the ice actions. It is long known that sloping structures may reduce ice actions significantly compared to vertical structures. The use of sloping structures reduces the load mostly because ice fails by flexural bending due to the sloping face while for vertical structures ice fails by crushing which consequently induce higher loads (see section 2.5 about ice failure modes). The sloping face can either bend the ice upward or downward. An icebreaker will for instance bend and break the ice downward with its

bow, while an upward breaking face is often used on structures in ice infested waters that are fixed to the bottom. Over the past few decades significant work has been carried out to understand the interaction between ice and sloping structures.

First of all, it is convenient to compare the effect of downward breaking face versus upward breaking face. By breaking the ice downward there is a potential to reduce the ice actions additionally compared to upward breaking. According to (Fenz, Ding et al. 2010), the peak load could be reduced with 50 % by inverting the breaking surface from upward to downward facing.

Whether the structure is sloping downward or upward has a significant effect on rubble pileup, which consequently affects the structure's behavior and resulting loads. For upward breaking structures the rubble pileup can potentially push down the structure which will add an extra stability to the structure if it is gravity-based. However, a floating structure will have to increase the required buoyancy due to the push down effect from the rubble pileup. Floating structures with a downward sloping face will, one the other hand, experience an upward lift force which may be more beneficial. Another beneficial effect with downward breaking structures is that broken ice floes will slide down along the submerged cone surface and re-emerge to the water surface due to buoyancy, see Figure 6.2. The same advantage applies to interaction with ridges, see Figure 6.3. The pileup of rubble in water rather than air will result in less pileup because the water clear away the broken ice from the structure. The additional buoyancy from the submerged ice floes needs to be balanced by the mooring system.
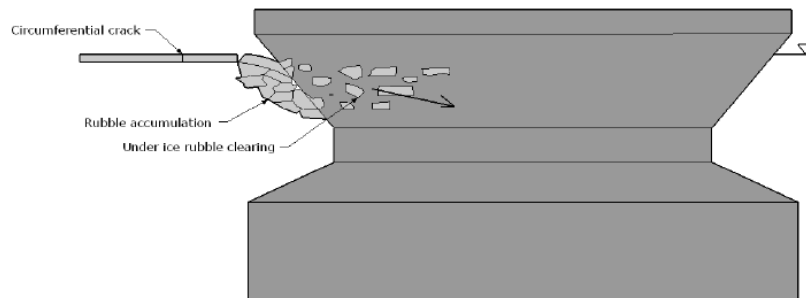
Figure 6.2: Failure of ice on a downward breaking structure (Srinivasan, Singh et al. 2008)
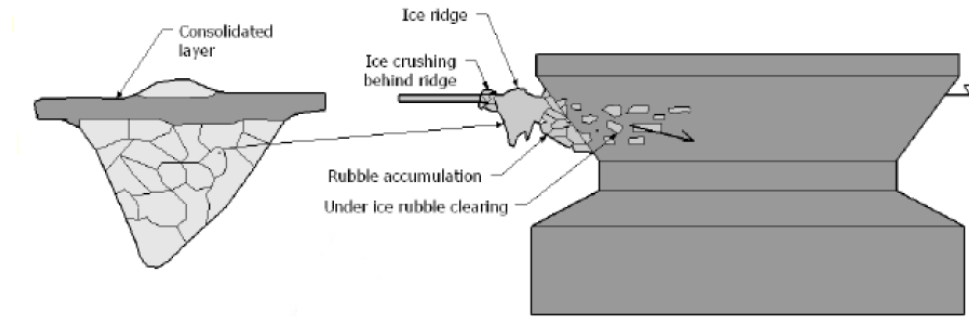
Figure 6.3: Failure of ridge on a downward breaking structure (Srinivasan, Singh et al. 2008)

(Fenz, Ding et al. 2010) did a model test on downward sloping structures with different shapes, angles, model scale, drafts and ice drift speed. Observations showed different failure modes for the same cone with different vertical clearances, see Figure 6.4. The most critical scenario occurred when there was a small vertical clearance compared to the ice thickness such that the ice sheet failed by a combination of flexural bending and crushing. Due to the crushing failure the ice loads became significantly higher compared to large vertical clearance.
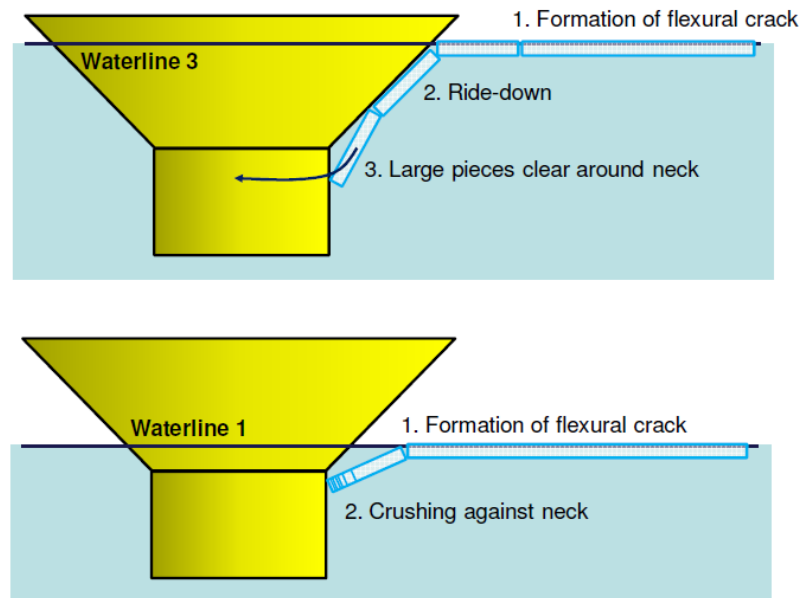
Figure 6.4: Vertical clearances effect of ice breaking failure mode (Fenz, Ding et al. 2010)

The angle of the sloping surface, ice-structure friction coefficient, ice thickness and ice drift speed also pays a significant part in resulting ice action and behaviors. Low value of all these parameters will result in dominant flexural failure of the ice sheet and with

increasing parameter values the dominant failure mode can change to shear or crushing failure and thus significantly higher ice actions. It is noted that decreasing cone angle yields smaller ice actions, however smaller anglers demand a smaller clearance distance which results in significantly higher ice crushing actions compared to larger cone angles.

6.2 ISO 19906 – Petroleum and natural gas industries- Arctic offshore structures

This section refers to (ISO19906) and will from here on be called ISO 19906. The International Organization of Standardization (ISO) is a worldwide federation of totally 164 national members. The work of preparing an International Standard is normally carried out through a technical committee where each of the 164 members has the right to participate in the committee if the member is interested in the subject. Publication of an International Standard requires approval by at least 75% of the members casting a vote. International organizations, governmental and non-governmental also take part in the work.

ISO 19906 specifies requirements and provides recommendations for design, construction, transportation, installation and removal of offshore structures related to the activities of the petroleum and natural gas industries in the Artic and cold regions. The purpose is to ensure that the structure provides an appropriate level of reliability with respect to personnel safety, environmental protection and asset value to the owner, both to the industry and to society in general. Much experience has been gained since structures, such as bridge piers, first were used in ice infested water in the 1960s. This knowledge has been incorporated into ISO 19906 and where uncertainty still exists, the standard recommends using conservative approaches and methods.

ISO 19906 provides ice action recommendations for global ice actions and local ice pressure on both vertical and sloping structures. Global loads are important for stability, overall strength and overturning moment while local ice actions are important for the design of plate and stiffeners. In this thesis, ice action for different ice scenarios such as level ice, ridges and managed ice are looked upon in ISO 19906 as well as local ice pressure. However, the ISO 19906 does not always provide the ideal method to determine

ice actions, for instance ridge loads on a sloping structure. Hence, other methods and comparisons are presented to evaluate the calculated ice actions.

6.3 Level ice

This section refers to (ISO19906). Level ice interacting with a sloping structure will fail by bending either upward or downward. The interaction process is complicated and includes failure of the ice sheet, ride up of broken ice pieces, accumulation of ice rubble on the slope and clearing of the rubble accumulation. Hence, the maximum ice action will be a function of several different parameters including geometrical parameters to the sloping structure, ice flexural strength, ice-structure and ice-ice friction coefficients, density of sea ice and sea water, and the height of rubble accumulation.

The resulting global ice action can be decomposed to a vertical and horizontal component. Level ice action components for a two-dimensional interaction with an upward breaking structure are illustrated in Figure 6.5. Mathematically the horizontal and vertical ice forces are given, respectively, by:

$$F_H = N \sin \alpha + \mu N \cos \alpha$$
$$F_V = N \cos \alpha - \mu N \sin \alpha$$

Equation 6.1

where N is the normal ice, μ is the ice-structure friction coefficient and α is the slope of the structure. In the case of a downward breaking structure, the vertical component of the ice action is directed upwards, reducing the effective shear resistance at the structure-seabed interface
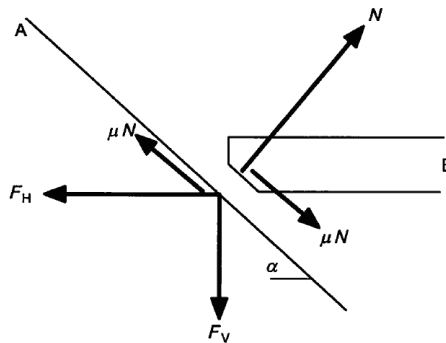
Figure 6.5: Load components on a sloping structure (ISO19906)

DETERMINING ICE ACTIONS

ISO 19906 provides two methods to determine ice actions on sloping structures. Method 1 is based on plasticity and method 2 is based in elastic beam bending. Method 1 is calculated from breaking and rid up ice action, while method 2 also take into the account of presence of ice rubble. The complexity of method 2 is greater than method 1 because several rubble ice parameters are needed. Both methods are presented below and the effect of level ice thickness and rubble ride up height are examined for upward and downward breaking structures. The values used to calculate the ice actions are based on the Sevan Arctic MODU structure geometry and values used in reference (Croasdale 2012). A list of initial values is found in Appendix C. The methods presented below are for upward breaking slopes, but are also valid for downward breaking slopes if the density of ice ρ_i is replaced by the buoyant weight of ice (ρ_w-ρ_i).

6.3.1 Method 1

This method is a plastic method which limits the solution because the method only considers the first stages of ice actions for level ice, which is flexural failure of the ice sheet and the ride up actions from the broken ice pieces. The approach is presented in this section and an examination of the effect of increasing geometrical ice parameters, both ice thickness h and ride up height h_r, on the total force will be given in section 6.3.3. The total ice action components in the horizontal and vertical direction are given by:

$$F_H = H_B + H_R$$
$$F_V = V_B + V_R$$

Equation 6.2

where subscript B and R represents breaking and ride up, respectively, and H and V represent horizontal and vertical direction, respectively. By assuming a constant ice thickness the breaking and ride up ice actions in horizontal and vertical direction for an upward breaking structure are given by:

$$H_B = \frac{\sigma_f h^2}{3} \frac{\tan \alpha}{1 - \mu g_r} \left[\frac{1 + Yx \ln x}{x - 1} \right.$$
$$\left. + G(x - 1)(x + 2) \right]$$

Equation 6.3

$$V_B = H_B h_v$$

37

$$H_R = W \frac{\tan \alpha + \mu E_2 - \mu f g_r \cos \alpha}{1 - \mu g_r}$$

$$V_R = W \cos \alpha \left(\frac{\pi}{2} \cos \alpha - \mu \alpha - f h_v\right) + H_R h_v$$

The parameters f, g_r, h_v, W and x are functions given by:

$$f = \sin \alpha + \mu E_1 \cos \alpha$$

$$g_r = \frac{\sin \alpha + \dfrac{\alpha}{\cos \alpha}}{\dfrac{\pi}{2} \sin^2 \alpha + 2\mu \alpha \cos \alpha}$$

$$h_v = \frac{f \cos \alpha - \mu E_2}{\dfrac{\pi}{4} \sin^2 \alpha + \mu \alpha \cos \alpha}$$

$$W = \rho_i g h_r \frac{w^2 - w_T^2}{4 \cos \alpha}$$

$$x = 1 + \left(3G + \frac{Y}{2}\right)^{-1/2}$$

Equation 6.4

The parameters E_1 and E_2 are complete elliptical integrals of the first and second kind which are used to account for the accumulation of rubble on the structure by using a value that exceeds the constant ice thickness for the ride up height. They are given by:

$$E_1 = \int_0^{\pi/2} (1 - \sin^2 \alpha \sin^2 \eta)^{-1/2} \, d\eta$$

$$E_2 = \int_0^{\pi/2} (1 - \sin^2 \alpha \sin^2 \eta)^{1/2} \, d\eta$$

Equation 6.5

The parameters used in the equations above are defined as:

σ_f - flexural strength of ice sheet

h – thickness of ice sheet

ρ_i – density of ice

ρ_w – density of seawater

g – acceleration of gravity

w – waterline diameter of cone or with of sloping structure

α – slope of structure, see Figure 6.5

μ – ice-structure friction coefficient

w_T – top diameter of cone

h_r – ice ride up thickness ($h_r > h$)

Y – equals to 2.711 for Tresca yielding or 3.422 for Johnsen yielding

G – equals to $(\rho_i g w^2)/(4\sigma_f h)$

It should be noted that for this method the relationship between the horizontal and vertical ice force is not given by the mathematically relationship given above in Equation 6.1. The geometrical parameters for level ice action which will be investigation for increasing value are ice thickness are h and ride up height h_r, and the results are presented in in section 6.3.3

6.3.2 Method 2

This method assesses the ice sheet as an elastic beam on elastic foundation and idealizes the fracture to occur when the bending stress reaches a critical strength. In addition, three-dimensional effects are considered, as well as the presence of ice rubble on the sloping structure. This method solves the ice action problem by dividing the force into five ice force components as given in Equation 6.6. The method is taken from ISO 19906, however (Palmer and Croasdale 2013) also recommends this approach to determine ice actions from level ice on sloping structures. The approach is presented in this section and an investigation of the ice thickness h and rubble height h_r effect on the total force will be evaluated in section 6.3.3. The elastic beam method considers the flexural failure's influence on the horizontal force in the ice sheet as the dominating force. It is given by:

$$F_H = \frac{H_B + H_P + H_R + H_L + H_T}{1 - \dfrac{H_B}{\sigma_f l_c h}}$$

Equation 6.6

$$F_V = \frac{F_H}{\zeta}$$

where

H_B – breaking load

H_P – load component required to push ice sheet through ice rubble

H_R – load to push ice blocks up slope through ice rubble

DETERMINING ICE ACTIONS

H_L – load required to lift ice rubble on top of advancing ice sheet prior to breaking it

H_T – load to turn ice block at top of slope

ζ – is equal to $\left(\frac{\sin\alpha + \mu\cos\alpha}{\cos\alpha - \mu\sin\alpha}\right)$

The different breaking and rubble loads are determined by:

$$H_B = 0.68\zeta\sigma_f\left(\frac{\rho_w g h^5}{E}\right)^{1/4}\left(w + \frac{\pi^2 L_{cc}}{4}\right)$$

$$H_P = wh_r^2\mu_i\rho_i g(1-e)\left(1 - \frac{\tan\theta}{\tan\alpha}\right)^2\frac{1}{2\tan\theta}$$

$$H_R = wP\frac{1}{\cos\alpha - \mu\sin\alpha}$$

$$H_L = 0{,}5wh_r^2\rho_i g(1-e)\zeta\left(\frac{1}{\tan\theta} - \frac{1}{\tan\alpha}\right)\left(1 - \frac{\tan\theta}{\tan\alpha}\right) \qquad \textbf{Equation 6.7}$$

$$+ 0{,}5wh_r^2\rho_i g(1-e)\zeta\tan\phi\left(1 - \frac{\tan\theta}{\tan\alpha}\right)^2$$

$$+ \zeta cwh_r\left(1 - \frac{\tan\theta}{\tan\alpha}\right)$$

$$H_T = 1{,}5wh^2\rho_i g\frac{\cos\alpha}{\sin\alpha - \mu\cos\alpha}$$

where the parameters L_{cc}, P and l_c are given by:

$$L_{cc} = \left(\frac{Eh^3}{12\rho_w g(1-v^2)}\right)^{1/4}$$

$$l_c = w + \frac{\pi^2 L_{cc}}{4}$$

$$P = 0{,}5\mu_i(\mu_i + \mu)\rho_i g(1-e)h_r^2\sin\alpha\left(\frac{1}{\tan\theta} - \frac{1}{\tan\alpha}\right)\left(1 - \frac{\tan\theta}{\tan\alpha}\right) \qquad \textbf{Equation 6.8}$$

$$+ 0{,}5(\mu_i + \mu)\rho_i g(1-e)h_r^2\frac{\cos\alpha}{\tan\alpha}\left(1 - \frac{\tan\theta}{\tan\alpha}\right)$$

$$+ h_r h\rho_i g\frac{\sin\alpha + \mu\cos\alpha}{\sin\alpha}$$

The new parameters that are included in this method that are not described in method 1 are defined as:

> E – elastic modulus of sea ice
>
> v – Poisson's ratio
>
> h_r – rubble height
>
> μ_i – ice-ice friction coefficient
>
> e – porosity of ice rubble
>
> θ – angle the ruble makes with the horizontal
>
> c – cohesion of ice rubble
>
> φ – friction angle of ice rubble

There are some values used in this method that should be commented and taken into particular consideration when selecting them. According to (Palmer and Croasdale 2013), the formulas are sensitive to the ice-structure coefficient μ and it is beneficial to apply a rugged low-friction coating as well as avoid steep cones and sudden changes in the slope when merging into a vertical wall. In this thesis is the ice-structure coefficient was selected to be 0.1 because both (Palmer and Croasdale 2013) and (Croasdale 2012) used this value in their calculations. The rubble angle θ is from experience and observations recommended to not be lower than 5 to 10 degrees of the sloping structure. In this thesis, because the sloping angle α is 45 degrees the rubble height was selected to be 40 degrees.

6.3.3 Assessment of method 1 and method 2

This section assesses and compares method 1 and 2 presented in section 6.3.1 and section 6.3.2 for resulting ice actions on upward breaking and downward breaking structures. Because structural dimensions were specified by Sevan Marine, the author decided to investigate ice geometry parameters most relevant to affect the resulting ice action, which is suggested to be the ice thickness and the rubble height/ride up height. The initial values for ice thickness h and rubble height h_r are 1.2m and 17m, respectively. Note that 17m is the Sevan Arctic MODU's draught. It is also noted that method 1 considers ride-up height, while method 2 considers rubble height which means that method 2 consider the whole rubble accumulation process while method 1 only consider presence of broken ice

DETERMINING ICE ACTIONS

in the initial stages. See Appendix D and Appendix E for more detailed calculations in excel sheet and Appendix C for initial parameter values.

First is method 1 evaluated and the results are presented in Figure 6.6, Figure 6.7, Figure 6.8 and Figure 6.9. The results for initial values found that the resulting horizontal force for downward and upward breaking structures are 12.73MN and 68.83MN, respectively. It is observed in Figure 6.6 that an increasing ice thickness h does not significantly affect the horizontal ice action. However, the selection of upward breaking structure compared to a downward structure affects the ice action considerably. A decrease in ice actions of approximately 75 % can be expected by bending the ice downward compared to upward. Figure 6.7 shows that increasing the ride up height h_r affects the horizontal ice action more significantly for upward breaking structures compared to downward breaking structures. Horizontal ice action for upward sloping structures increases more rapidly than for downward breaking structures which illustrates that upward breaking structures are more sensitive to ride up height, h_r. The theoretical formulation for method 1 results in lower ice action for downward sloping design compared to upward breaking design because the effect of calculating ice forces with (ρ_w-ρ_i) compared with ρ_i will reduce the forces considerably. However, the observations found in Figure 6.6 and Figure 6.7 could be reflected to real life experience. Due to the presence of water when the ice sheet is bent downward will clear away the broken ice pieces and consequently the forces from accumulated ice will be less.
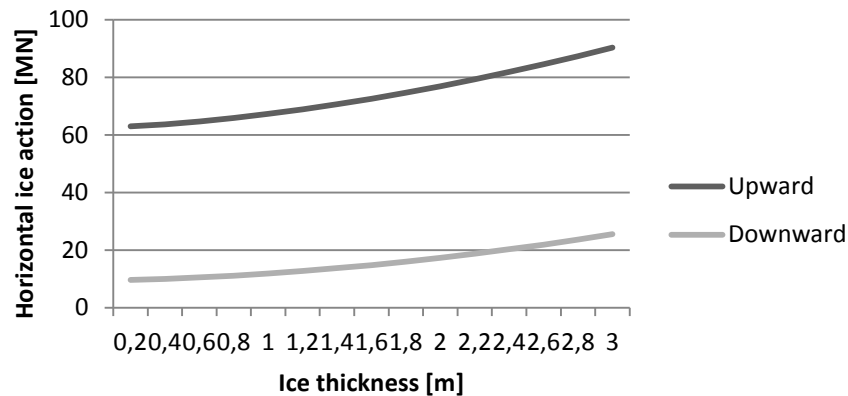
Figure 6.6: Method 1 - Upward vs. Downward: ice thickness *h*, adapted from Appendix D1
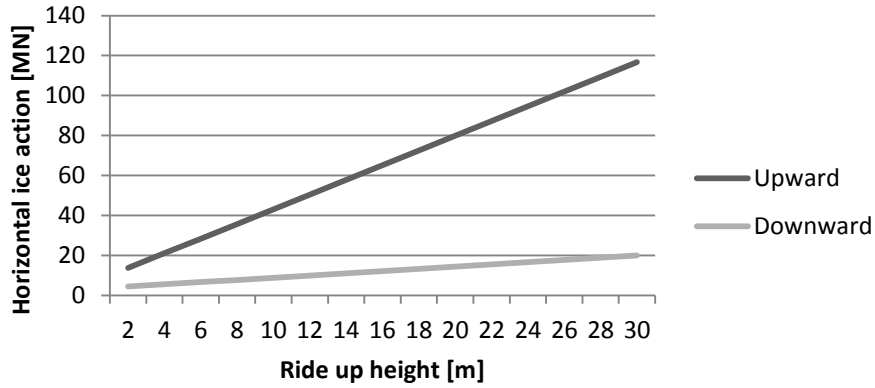
Figure 6.7: Method 1 - Upward vs. Downward: ride-up thickness h_r, adapted from Appendix D2

It is suggested that a design with downward sloping face should be implemented if ice actions are to be avoided. The horizontal and vertical ice actions, established in Equation 6.2, are compared for a downward breaking structure in Figure 6.8 and Figure 6.9. It is observed that for method 1 the vertical force and the horizontal force are not fluctuating much from each other. In reality the horizontal force is generally larger than the vertical force, and is the dominating force too. However, for this method the vertical force is only slightly larger than the horizontal force.
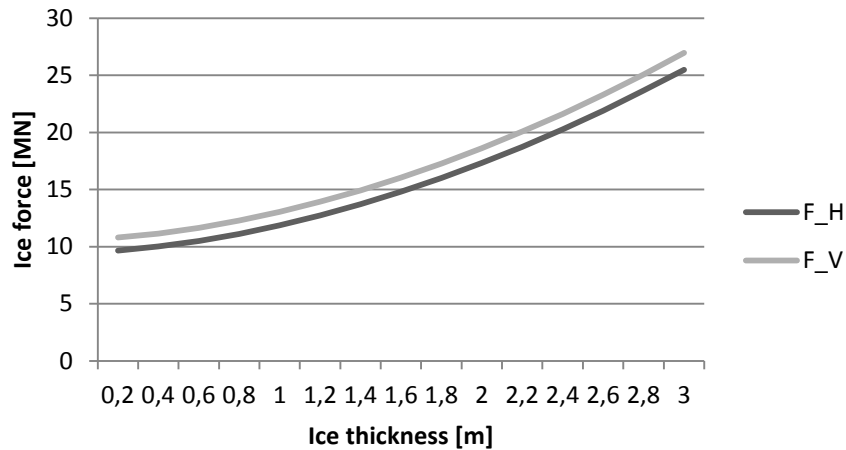
Figure 6.8: Method 1 - Ice forces versus ice thickness, adapted from Appendix D1
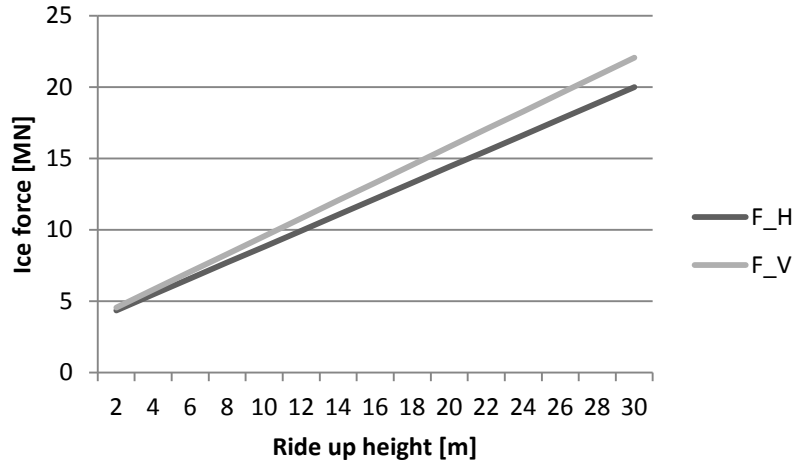
Figure 6.9: Method 1 - Ice forces versus ride up height, adapted from Appendix D2

Secondly, method 2 is evaluated and the results are presented in Figure 6.10, Figure 6.11, Figure 6.12 and Figure 6.13. The results for initial values found that the resulting normal force for downward and upward breaking structures are 15.01MN and 71.09MN, respectively. In Figure 6.10 and Figure 6.11 the normal ice forces on upward and downward sloping structures are compared with respect to ice thickness h and rubble height h_r. It is observed that for both increasing ice thickness and rubble height, the ice force increases more rapidly for upward sloping structures than for downward sloping structures. Hence, the effect of increasing level ice and rubble height is more critical for upward breaking design compared to downward breaking design. Still, it is observed that increasing rubble height is the most critical. Looking at the initial values for level ice and rubble height, the normal ice force can be reduced with 79 % by designing the structure with a downward slope rather than an upward breaking slope.
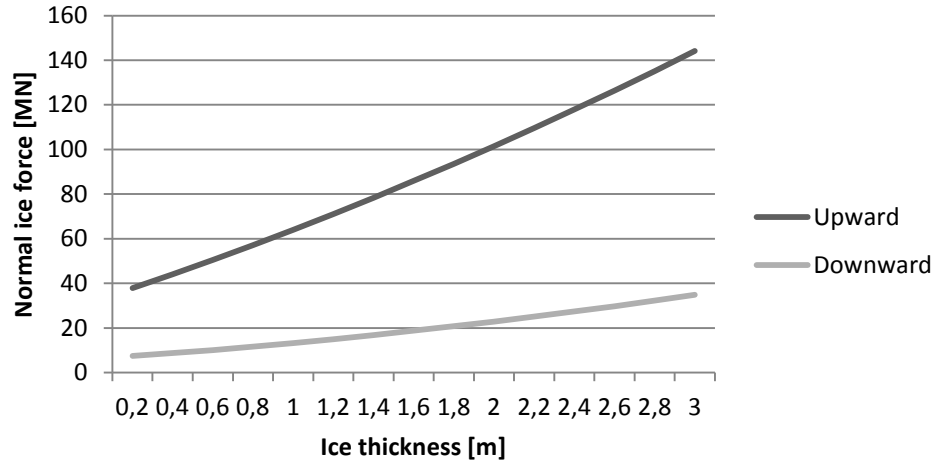
Figure 6.10: Method 2 - Upward vs. Downward: ice thickness *h*, adapted from Appendix E1
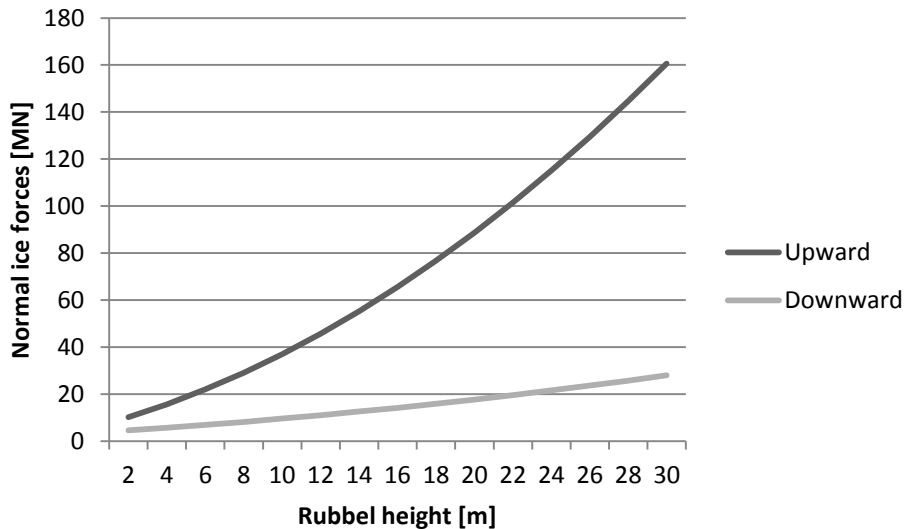
Figure 6.11: Method 2 - Upward vs. Downward: rubble height *h_r*, adapted from Appendix E2

When the ice is bent down into water the effect of friction angle of the rubble φ is negligible. Hence, $\tan(\varphi)$ equals 0 and the load required to lift the ice rubble on top of the advancing ice sheet prior to breaking it, H_L, will become lower. As for method 1, the effect of calculating with the ice buoyancy density, $(\rho_w - \rho_i)$, reduces the ice rubble forces considerably.

As for method 1, method 2 also illustrates that downward breaking structures generates less ice actions. In Figure 6.12 and Figure 6.13, the normal, horizontal and vertical ice actions are plotted for a downward breaking structure. Compared to method 1, the

expanding of vertical and horizontal force for increasing parameter is assumed to be more reliable than parallel increase (see Figure 6.8 and Figure 6.9).
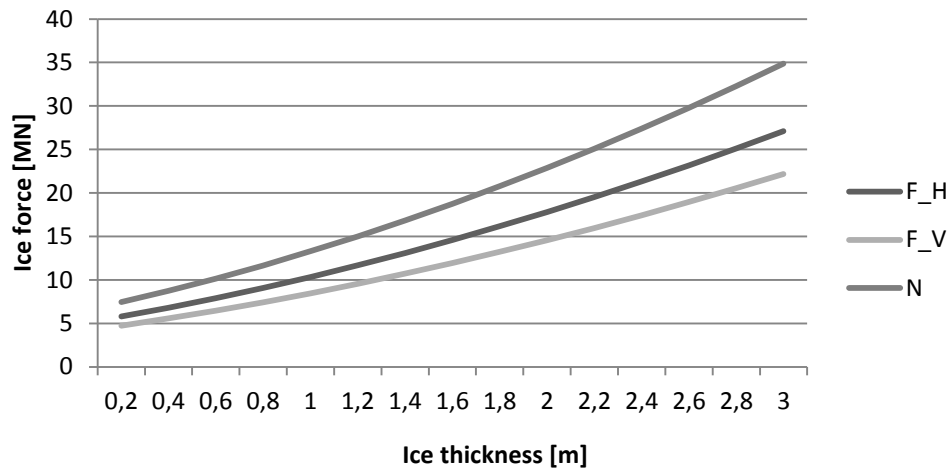
Figure 6.12: Method 2 - Ice forces versus ice thickness, adapted from Appendix E1
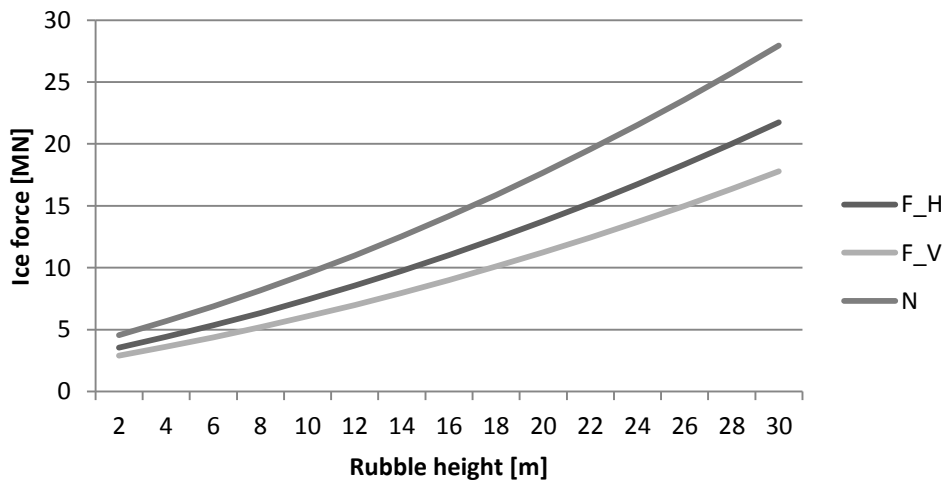
Figure 6.13: Method 2 - Ice forces versus rubble height, adapted from Appendix E2

In this thesis, the ride up height/rubble height is not investigated with regards to the width of the sloping cone. However, experiences from already existing structures show that the ride up height on cones with narrow shafts (small diameter) will not be considerably extreme because the ice may be expected to turn sideways and clear before it rides up significantly. For a wide, flat structure the ice will not clear that easily and tend to ride higher for the same ice thickness, Ref. (Palmer and Croasdale 2013).

In cases where the slope end and proceed to a vertical wall and the height of the ride up is higher than the slope, as illustrated in Figure 6.14, (Palmer and Croasdale 2013) recommend to keep the rubble height the same as expected for a structure where the slope does not end. However, an additional virtual length of ride up is added to the original ride up height. This is approximately correct for slightly lower volume of ice rubble over the real slope. In the examination above and in this thesis, the virtual length is not taken into consideration. Hence, the results may be conservative results for the Sevan Arctic MODU design which only has 2m vertical clearance.
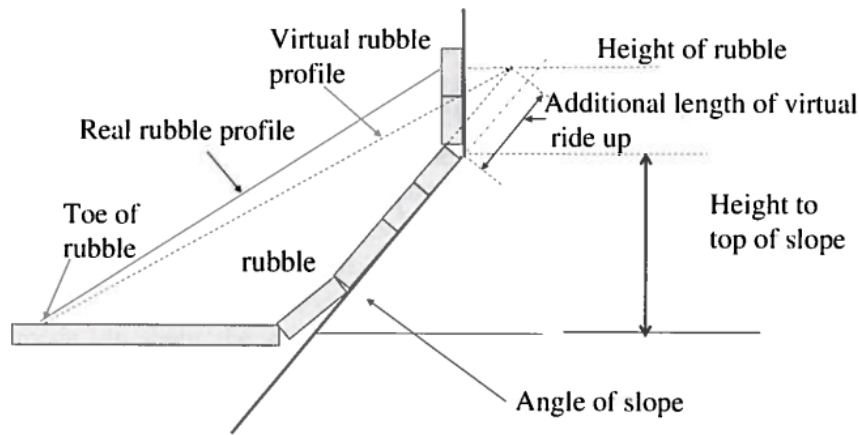
Figure 6.14: Principle of virtual ride up height due to change in geometry (Palmer and Croasdale 2013)

6.4 First-year ridges

Several approaches and theories have been proposed to calculate the global ice actions which a first-year ridge would utilize on an offshore structure. The theoretical approaches vary widely and depend upon the shape of the structure and the assumed failure mode of the ice. Reference is made to section 2.2 for idealized geometry of first-year ridges. In ISO 19906 an analytical method for first-year ridge actions is proposed, which is mainly valid for vertical structures. The ice load is estimated by adding the load from the consolidated layer to the load calculated for keel failure. The load from the consolidated layer may be calculated from Equation 6.6 for level ice actions on a sloping structure and the keel loads are calculated based on Dolgopolov, Ref. (Dolgopolov, Afanasiev et al. 1975). However, this is a very conventional approach resulting in a very large keel loads. And poses conservative results for sloping structures.

(Croasdale 2012) recently published a paper describing a simple method for calculating first-year ridge loads on sloping structures. Because full-scale experience indicates lower keel loads, (Croasdale 2012) considers an already developed theory for solid multi-year ridges that idealize the ridge to a beam and that indicates lower ice loads. The new approach assumes that the ridge is a composite beam with an upper layer based on solid ice and a lower layer based on the keel being week porous solid ice. The new method reduces the total ridge load with approximately 34 % compared to the conventional method used in ISO19906 and can be used for both downward and upward breaking structures. In this thesis, it is the new approach by (Croasdale 2012) that will be presented and evaluated for downward and upward breaking structures.

6.4.1 A simple model for first-year ridge loads on sloping structures

The following section refers to (Croasdale 2012). The first-year ridge is idealized with two materials, a top layer based on solid ice and a bottom layer based on ice rubble. Each layer is given modulus and strength properties, see Figure 6.15 and Figure 6.16. An equivalent solid ice cross-section is developed based on composite beam theory which requires that the equivalent beam is made up of one material, see Figure 6.17.
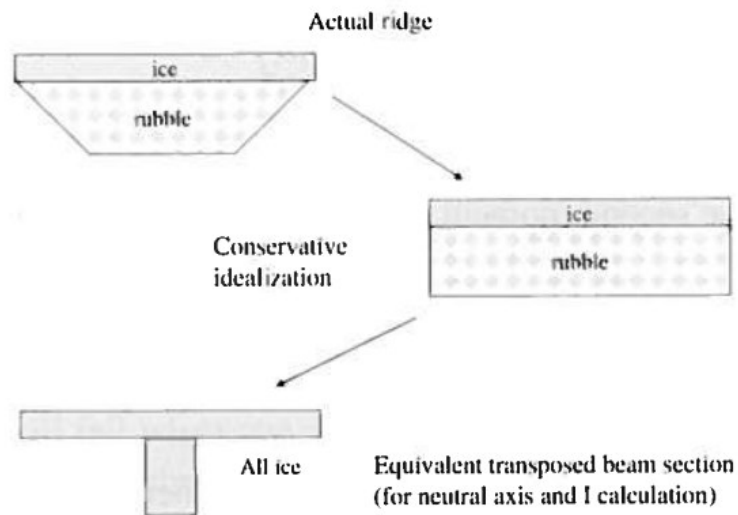
Figure 6.15: Approach to treat a first-year ridge as a composite beam (Croasdale 2012)
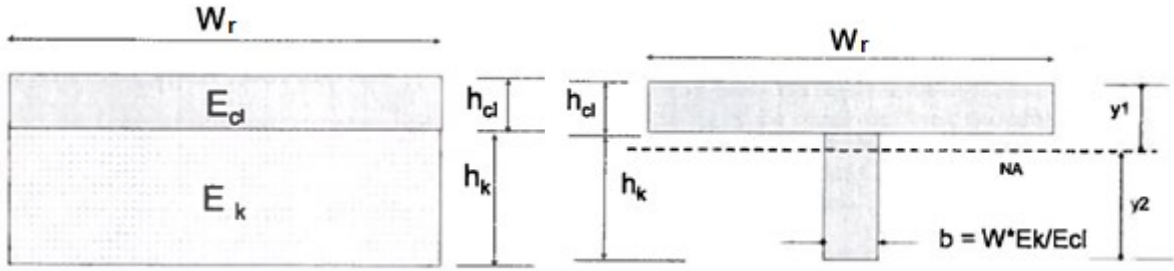
Figure 6.16: Two layer idealized ridge (Croasdale 2012)

Figure 6.17: Equivalent solid ice cross-section (Croasdale 2012)

Bending theory is used to obtain the failure stress at which the ridge will fail, for both the consolidated layer and the keel. Whichever is the lowest stress value will be the failure stress. Failure mode occurring needs to be considered when calculating the failure stress. Does the load form a hinge or a centre crack? Failure stress at where the ridge consolidate layer and keel will fail at its outer surface for center or hinge cracks are derived, respectively, to be:

$$V_{1,cl} = \frac{4\sigma_{cl}I_T}{y_1 L_c}$$

$$V_{1,k} = \frac{4\sigma_k I_T E_{cl}}{y_2 L_c E_k}$$

$$V_{2,cl} = \frac{6.17\sigma_{cl}I_T}{y_1 L_c}$$

$$V_{2,k} = \frac{6.17\sigma_k I_T E_{cl}}{y_2 L_c E_k}$$

Equation 6.9

where σ is the flexural, tensile or compressive failure strength to the ice layer, and E is the Modulus to the ice layers. The lowest value of failure strengths will be used. The parameter I_T, y_1 and L_c are the second moment of area, distance to the top surface from the neutral axis and the characteristic length, respectively, and are defined as:

$$I_T = \frac{W_r h_{cl}^3}{12} + W_r h_{cl}\left(y_1 - \frac{h_{cl}}{2}\right)^2 + \frac{bh_{cl}^3}{12}$$

$$+ bh_k\left(\frac{h_k}{2} + h_{cl} - y_1\right)^2$$

$$y_1 = \frac{0.5W_r h_{cl}^2 + bh_k(h_{cl} + 0.5h_k)}{(W_r h_{cl} + bh_k)}$$

Equation 6.10

$$L_c = \left(\frac{4E_{cl}I_T}{W_r \rho_w g}\right)^{0.25}$$

The parameters used in the equations above are defined as:

E_{cl} – elastic modulus of consolidated layer

E_k – elastic modulus of keel equal to $E_{cl}/15$

σ_{cl} – flexural strength of consolidated layer

σ_k – flexural strength of keel equal to

W_r – width of ridge

h_{cl} – consolidated layer thickness

h_k – keel height

b – width of the solid ice equivalent to the keel given by ($W_r E_k/E_{cl}$)

The same method can be used for upward sloping structures. In this case the center crack will be governed by compressive failure rather than tensile failure, and the hinge crack will be governed by tensile failure rather than compressive failure for the ice rubble at the bottom of the keel.

The results of the method given in (Croasdale 2012) are presented in Figure 6.18, Figure 6.19, Figure 6.20 and Figure 6.21. The figures illustrate increasing consolidated layer thickness h_{cl} and keel height h_k versus normal ice force for upward and downward breaking structures. The initial values for consolidated layer thickness h_{cl} and keel height h_k are 3m and 21m respectively. The width of the ridge is kept constant at 70m which is the same value used in an example in (Croasdale 2012), were approximately the same initial values for consolidated layer thickness (3.5m) and keel height (24.3m) were given. The method poses that the lowest stress value will be the failure stress. In this thesis, it is found that failure value for downward breaking structures occur due to failure of the keel

50

DETERMINING ICE ACTIONS

from hinge crack, V_{2k} equals to 29.0MN. Failure value for upward breaking structure also occurs due to failure of the keel, but from center crack, V_{1k} equals to 18.8MN..See Appendix F for an excel sheet that calculates the stress forces.

It is observed from Figure 6.18 and Figure 6.19 that the effect of increasing keel height is more significant than increasing consolidated layer thickness. The effect of choosing upward sloping structure rather than downward sloping structure results in lower ice forces, which was an unexpected result. The general assumption from an engineering perspective is that downward breaking structures will experience lower ice actions compared to upward breaking structures. This was also the result of method 1 and method 2 for level ice actions, as described in section 6.3. However, for this new method by (Croasdale 2012) this theory is not the case. This can be assumed to be due the effect of failing the keel by center crack rather than hinge crack. On the other hand, this method does not take into consideration the effect of ice breaking into sea water rather than air which will clear accumulation of rubble and reduce ice forces. It is assumed that this method may be a better approach because it gets lower results for sloping structures loaded by ridges compared to approaches for vertical structures posed by ISO 19906. However, more study on the effects by rubble accumulation from ridges should be presented into the approach, as well as geometrical parameters due to sloping dimensions and presence of sea water rather than air.
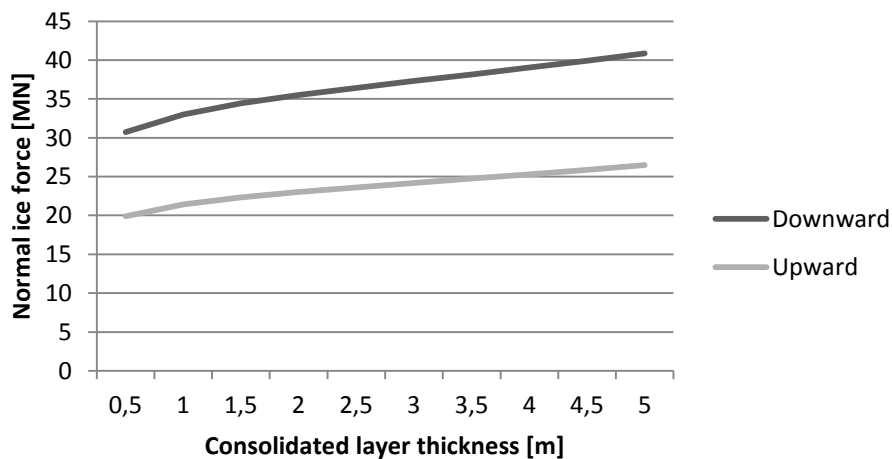
Figure 6.18: Upward vs. Downward: consolidated layer thickness h_{cl}, adapted from Appendix F1

51
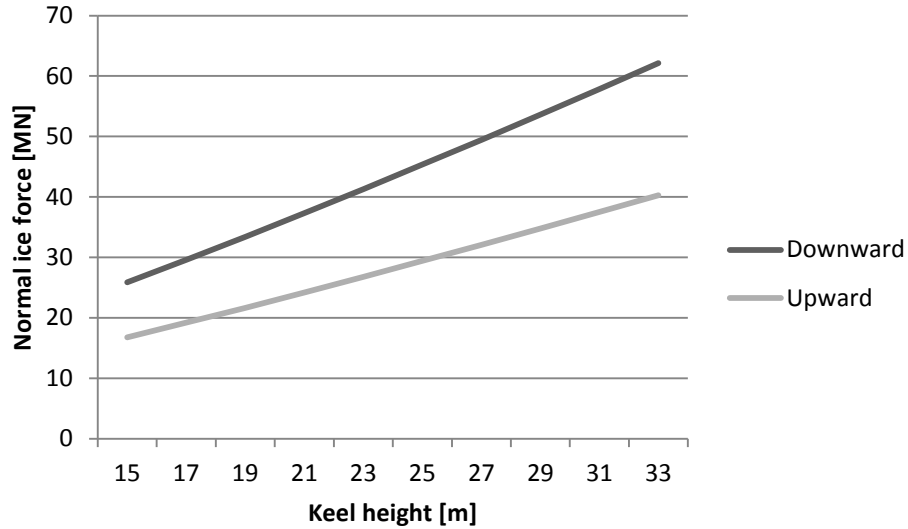
Figure 6.19: Upward vs. Downward: keel height h_k, adapted from Appendix F2

The method suggests that upward breaking structures generate less ice actions. Thus, it is recommended that the designer perform the design with an upward breaking slope to avoid large ice actions from first-year ridges. In Figure 6.20 and Figure 6.21, the normal, horizontal and vertical ice actions are compared for an upward breaking structure. Note that the horizontal and normal ice actions are determined from the ice action relationship described in Equation 6.1 in section 6.3 for level ice.
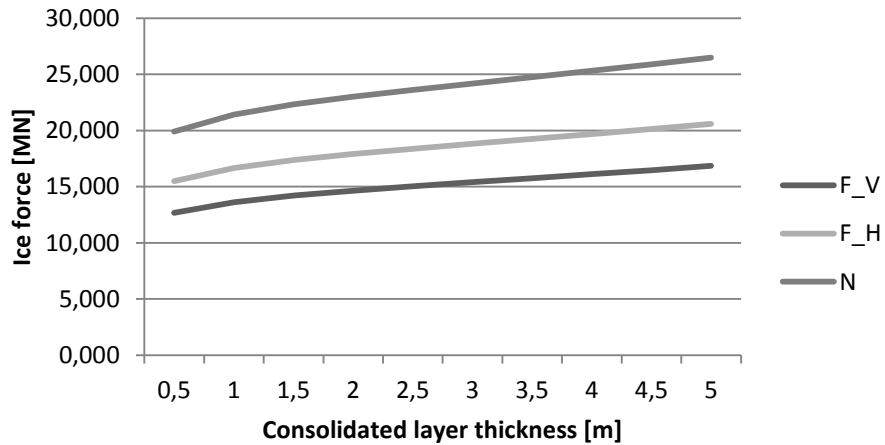
Figure 6.20: Ice forces versus consolidated layer thickness h_{cl}, adapted from Appendix F1
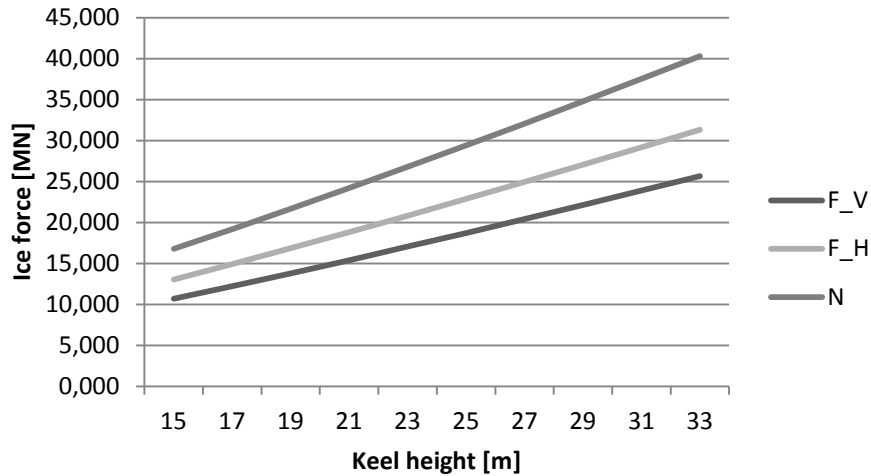
Figure 6.21: Ice forces versus keel height h_k, adapted from Appendix F2

It is observed that this method does not take geometric parameters for the interaction structure into consideration, such as width of structure or angel of slope. Because this method is a very new approach to determine ice actions from first-year ridges which is yet not used in requirements and standards it is encouraged by the author of this thesis to study the behavior of first-year ridges on a Sevan FPU-Ice design from a model test (see section 6.4.2). A model test will generally give a better solution to ice action behaviors than theoretical formulations. The model test was only performed with a downward sloping face due to purpose of the model test was for a specific design.

6.4.2 A moored Arctic floater in first-year sea ice ridges

This section refers to (Dalane, Aksnes et al. 2009). In 2009 Sevan performed a model test concerning first-year ridge loads on a Sevan FPU-Ice design. This design is of a floating circular structure similar to the traditional Sevan concept, but modified with a downward sloping cone in the ice loading waterline. The structure was loaded with several ridges that had different properties and/or boundary conditions (fully constrained, rafted ice close to the tank walls and managed level ice behind the ridge), such that the mooring force from the interactions was obtained, see Figure 6.22.
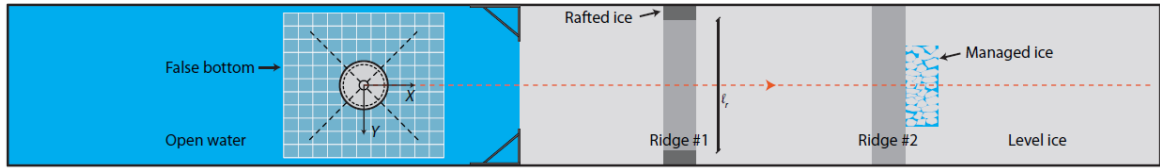
Figure 6.22: Test setup seen from above (Dalane, Aksnes et al. 2009)

Looking upon ridge behavior, in the first stage of the ridge-structure interaction the consolidated layer always failed by bending against the inclined side. However, in the last stage of the ridge-structure interaction, the consolidated layer either failed by bending by direct interaction with the floater or due to the large amount of accumulated rubble in front of the floater. The floater pushed rubble from the keel forward, such that the rubble forced the consolidated layer upward and thereby failed by upward bending due to the large presence of rubble. Due to the presence of ice rubble in front of the floater mooring peaks were observed even after the ridge had passed, see Figure 6.23. Note that the values given in Figure 6.23 and Figure 6.24 are normalized values due to confidentiality issues. However, knowledge of ridge behavior obtained from the model test is valuable.
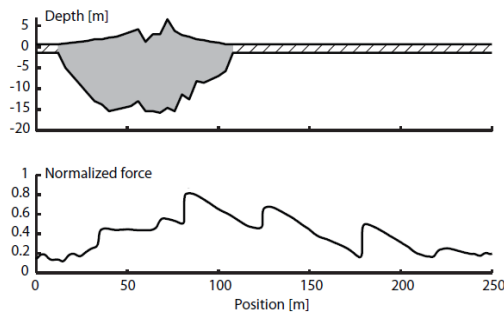
Figure 6.23: Relationship between mooring forces and position in ridge (Dalane, Aksnes et al. 2009)
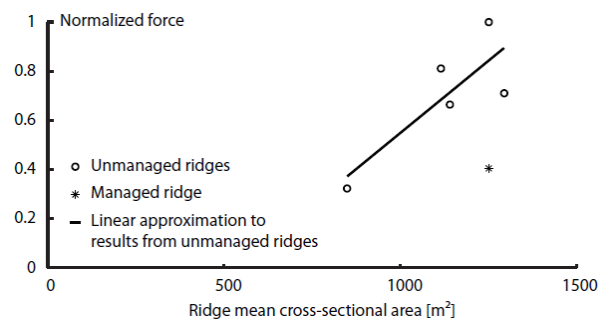
Figure 6.24: Normalized horizontal mooring forces against cross-sectional area of the corresponding ridge (Dalane, Aksnes et al. 2009)

Looking upon induced mooring forces, it was observed that forces from the unmanaged ridge increased almost linearly with increased cross-sectional area of the ridge, see Figure 6.24. This differs from ISO 19906, where keel depth is the only geometric parameter involved. If the ice after the ridge was managed, total mooring forces from ridges with was reduced by 50 % compared to similar ridges without ice management, see Figure 6.24.

6.5 Managed ice

According to ISO 19906, ice actions from managed ice on floating structures are best determined from full-scale load data from the Kulluk drilling platform. The use of approaches based on full scale experiments are in general a much more desired approach compared to theoretical formulations, and recommended to be used in most cases. Hence, the evaluation of managed ice actions on the Sevan Arctic MODU will be done based on load data from the Kulluk drilling platform (see section 4.4.1 about the Kulluk vessel). Information given in the following section is taken from (Wright 2000).

Figure 6.25 presents load data for more than 50 events in which the Kulluk experienced ice pressure. The plot represents one of the key results of (Wright 2000) study, and summarize loads on the Kulluk in a wide range of managed pack ice conditions. The dashed graph represent the mean trend line through the load data points while the upper graph represent an upper bound that is simply computed by increasing the mean trend line with 75%.
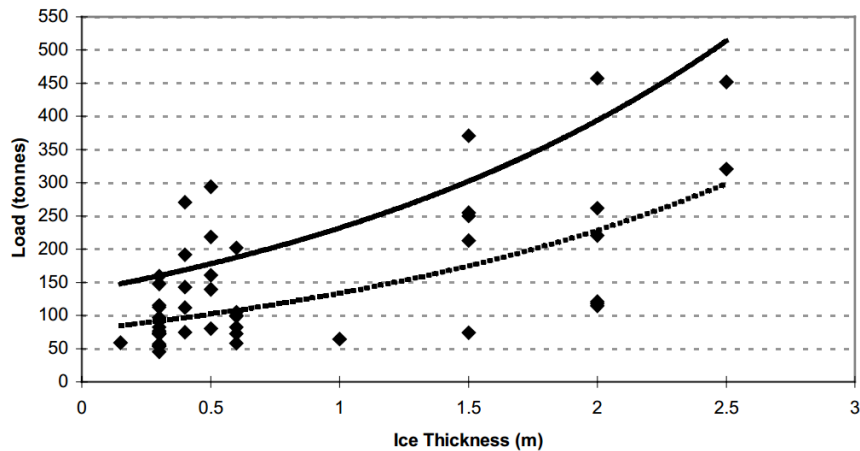
Figure 6.25: Kulluk data for all events with ice pressure (Wright 2000)

The mean trend line and the upper bound are given by:

$$F_{m,lower} = 78e^{0.53h}$$

$$F_{m,upper} = 136.5e^{0.53h}$$

Equation 6.11

where h is ice thickness in meters and F_i is the global force given in kN. This information is of high importance for ice infested areas such as the Pechora Sea and Sakhalin Island, where ice pressure events are common.

6.6 Results and comparison

Calculated ice actions for the initial values for the Sevan Arctic MODU are presented in Table 6.1. However, to understand the size of the value in a better manner the results should be compared to other experiences. Two comparison designs are presented in section 6.6.1 and section 6.6.2, and discussed in section 6.7 with regard to the values calculated in this thesis.

Table 6.1: Global ice action results from different action scenarios

Ice action scenario		Vertical force [MN]	Horizontal force [MN]	Normal force [MN]
Level ice – method 1	Upward	76.40	68.83	-
	Downward	13.92	12.73	-
Level ice – method 2	Upward	45.24	55.30	71.09
	Downward	9.55	11.67	15.01
Ridge – analytical method	Upward	15.39	18.81	24.18
	Downward	23.74	29.01	37.30
Ridge – model test	Downward	Confidential	Confidential	Confidential
Managed ice – (Wright 2000)	Downward – lower	0.147	0.147	0.147
	Downward - upper	0.258	0.258	0.258

6.6.1 Design of a non-ship shaped FPSO for Sakhalin-V deep water

Values and information for this section is obtained from (Srinivasan, Singh et al. 2008). The paper purpose a vessel design that could work in both open water and ice infested water in Arctic environment with minimal ice management requirement. The design solution suggests a non-ship-shaped FPSO design concept similar to the Sevan Arctic

MODU, see Figure 4.1 in section 4.1. The vessel is designed to resist first- and second-year sea ice and large and deep ridges.

Horizontal ice forces from level ice are computed as followed in Table 6.2. It is noted that they increase exponentially with increasing level ice thickness. Consequently, cost consideration to make the structural design withstand thick rafted ice (4m) would make the design unrealistic.

Table 6.2: Level ice forces on a non-ship-shaped FPSO with 40 degrees downward sloping face, adapted from (Srinivasan, Singh et al. 2008)

Level ice thickness [m]	Horizontal ice force [MN]
1	4.84
1.6	9.3
2.5	20.9
4 (rafted)	40.2

Compared to the resulting ice forces form level ice on downward breaking structure given in Table 6.1, the force calculated for the FPSO in Sakhalin-V is lower. This is even the case for ice force form 1.6m level ice thickness. Hence, the computed ice forces from section 6.3, both for method 1 and 2, can be considered conservative.

Calculated forces from a first-year ridge with 2.5m consolidated layer thickness and 24m keel depth are given in Table 6.3.

Table 6.3: Ridge forces on a non-ship-shaped FPSO with 40 degrees downward sloping face, adapted from (Srinivasan, Singh et al. 2008)

Forces required to break the consolidated layer [MN]	20.9
Shear forces on the ice rubble [MN]	10.9
Total ridge force on vessel [MN]	31.8

Compared to the total ridge force on downward breaking structure given in Table 6.1, the force calculated for the FPSO in Sakhalin-V is lower. Hence, the computed ice forces above can also be considered conservative.

6.6.2 Arctic Offshore Engineering

Values and information for this section is from (Palmer and Croasdale 2013). A spar shape structure with 45 degrees downward sloping face was used as an example structure to assess loads on floaters in ice. Resulting loads are presented in Table 6.4, Table 6.5 and Table 6.6 for level ice, managed ice and first-year ridge respectively.

Equations used to determine ice actions from level ice in Table 6.4 are the same as presented in section 6.3.2 (method 2). Initial values in the example presented are almost the same as used in this thesis and ride up height is set to 15m.

Table 6.4: Unmanaged ice loads from level ice on a spar vessel, adapted from (Palmer and Croasdale 2013)

Ice thickness [m]	Horizontal load [MN]	Vertical load [MN]
0.5	3.66	2.96
1.5	7.13	5.68
3	15.17	11.87

Typical managed ice loads for the same spar structure are given in Table 6.5. These loads are calculated from theoretical equations given in (Palmer and Croasdale 2013) for determining loads on floaters in managed ice. The managed ice loads are limited to about 25 % of the unmanaged ice loads.

Table 6.5: Managed ice loads as a function of ice pressure on a spar vessel, adapted from (Palmer and Croasdale 2013)

Managed ice thickness [m]	Mooring loads for various pressures [MN]			
	5kPa	10kPa	15kPa	30kPa
0.5	0.34	0.48	0.63	1.07
1.5	1.01	1.45	1.89	3.22
3	2.02	2.90	3.79	6.44

Ridge loads for four different ridge sizes are given in Table 6.6. The ridge loads are determined using the same approach as in this thesis (see section 6.4.1), namely the composite beam approach given by (Croasdale 2012).

Table 6.6: Ridge load calculated from composite beam approach for a downward breaking structure, adapted from (Palmer and Croasdale 2013)

Ridge size (width/consolidated layer thickness/ keel height) [m]	Composite beam approach (V_2)[MN]
W_r=70 h_{cl} = 3.5 h_k=24.3	28.6
W_r=60 h_{cl} = 2.5 h_k=18	16.77
W_r=50 h_{cl} = 2 h_k=15	11.07
W_r=40 h_{cl} =1.5 h_k=12	6.64

It is observed that all values calculated in Table 6.6 are lower than the values calculated for the Sevan Arctic MODU. This may be because of different input value such as the ride-up height and the width of the structure. However, it can be concluded that the Sevan Arctic MODU is on the safe side if it is designed to withstand the calculated ice actions in this thesis.

6.7 Discussion and Conclusion

Examining the results given in section 6.3.3 for resulting level ice actions on upward and downward sloping structures it is suggested to design a buoy shaped floater in ice infested water with a downward sloping hull in the ice action area. The values calculated for level ice on downward breaking face, both method 1 and 2, are higher compared to the example values given in section 6.6.1 and section 6.6.2. Hence, by applying these global ice action values to the structure concept and designing the structure mooring lines and overall stability to hold for these values it can be assumes that the structure will be ton the safe side.

Regarding ice actions from first-year ridges it is suggested to design with an upward sloping face to reduce resulting ice actions. However, the approach used to determine the ice forces are a new approach which is not taking several important parameters into the

theoretical formulation, such as structure geometry and effect of bending ice into water rather than air. Due to this, it is suggested by the author not to rely uncritically on these results before the method is improved. The example values given above are lower compared to the calculated value. Hence, the floater will be to the safe side if it is designed with the calculated values for downward braking face.

Due to the discussion above, the author suggests that the assessment of level ice action should be weighted more than ice actions from first-year ridges. Consequently a downward breaking design is proposed to be applied to a floater in ice infested waters. Results calculated for managed ice illustrates that ice actions are significantly reduced by execute ice management. Hence, it is suggested to use ice management in the highest extent it is possible.

6.8 The Polar Class rules

The following section is mainly taken from (IACS 2011). The International Association of Classification Societies (IACS) is dedicated to make safe ships and clean seas through rules and regulations for the maritime industry. More than 90 % of the world's cargo carrying tonnage is covered by IACS classification design that are made by the organization's thirteen marine classification society members[2]. In 2008, IACS approved the Polar Class rules which is a result of a large 'harmonization effort' among the classification societies, relevant governmental bodies and academic experts to develop requirements applicable for vessels operating in Polar waters.

The Polar Class rules are applicable for ships constructed of steel and intended for navigation in ice infested polar waters, except for ice breakers which may have additional icebreaking requirements. The rules consider hull structure, main propulsion, steering gear, emergency and essential auxiliary systems that are necessary to obtain the safety of the ship and crew. However, in this thesis only the hull structure will be considered and therefore only the requirements concerning hull integrity will be presented. The Polar Class classification is divided into seven levels where the severity of the ice condition intended for the ship determines the Polar Class. It is the owners' and designers'

---

[2] http://www.iacs.org.uk/

responsibility to select an appropriate Polar Class to match the ship's intended voyage or service. The Polar Class notation and description are given in Table 6.7.

Table 6.7: Polar Class description (IACS 2011)

Polar Class	Ice condition description
PC-1	Year-round operation in all Polar waters
PC-2	Year-round operation in moderate multi-year ice condition
PC-3	Year-round operation in second-year ice which may include multi-year ice inclusion
PC-4	Year-round operation in thick first-year ice which may include old ice inclusion
PC-5	Year-round operation in medium first-year ice which may include old ice inclusion
PC-6	Summer/autumn operation in medium first-year ice which may include old ice inclusion
PC-7	Summer/autumn operation in thin first-year ice which may include old ice inclusion

It should be noted that the Polar Class requirements are developed and customized for ship shaped vessels. Hence, for floating offshore installations operating in ice infested waters, the design scenarios and specific requirements given in the Polar Class rules may not necessary be considered as fully representative. According to (Nyseth 2014), if a Polar Class notation is assigned to a floating offshore structure, the requirements should be adopted as far as practical, bearing in mind that the ice class system is to be considered as a relative ranking of capabilities rather than being suitable for a defined ice conditions. Alternatively, design consideration following other recognized standards such as ISO 19906, which is presented in section 6.2, may be applicable

The Sevan Arctic MODU is classified with PC4, year-round operation in thick first-year ice which may include old ice inclusions. The hull structural requirements, such as plate

DETERMINING ICE ACTIONS

thickness and scantling, are not presented in this thesis because Sevan has determined these parameters. However, the Polar Class method to determine the Design Ice Loads to achieve the scantling requirements is presented below because the value will be used in the assessment of local ice pressure in section 6.9.

6.8.1 Design Ice Load

A glancing impact on the bow is the design scenario to consider when determining the scantling required to resist ice loads. Therefore, the Sevan Arctic MODUs' hull was considered as a bow when scantling the structure with respect to the Polar Class PC-4. In IACS, the design ice load issue is solved by applying an average pressure, P_{avg}, that is uniformly distributed over a rectangular load patch. To obtain the average pressure and load patch characteristics it is necessary to calculate a shape coefficient fa, total glancing impact force F, line load Q and pressure P_{PC} for the area and applying class factors for the selected Polar Class, see Table 6.8. The bow area load characteristics are determined as follows:

$$P_{avg} = \frac{F}{w_p \cdot b_p} \ [MPa]$$

<div align="right">Equation 6.12</div>

where w_p is the width and b_p is the height of the load patch and are determined, respectively, as follows:

$$w_p = \frac{F}{Q} \ [m]$$

$$b_p = \frac{Q}{P_{PC}} \ [m]$$

<div align="right">Equation 6.13</div>

The force, line load and pressure are determined, respectively, as follow:

$$F = fa \cdot CF_C \cdot \Delta_{tk}^{0.64} \ [MN]$$

$$Q = F^{0.61} \cdot \frac{CF_D}{AR^{0.35}} \ [\frac{MN}{m}]$$

$$P_{PC} = F^{0.22} CF_D^2 AR^{0.3} \ [MPa]$$

<div align="right">Equation 6.14</div>

where fa is the shape coefficient and AR is the load patch ratio and are given, respectively, as follow:

$$fa = minimum(fa_1; fa_2; fa_3)$$

<div align="right">Equation 6.15</div>

$$fa_1 = \left(0.097 - 0.68\left(\frac{x}{L_{wl}} - 0.15\right)^2\right) \cdot \frac{\alpha}{\beta^{,0.5}}$$

$$fa_2 = 1.2 \cdot \frac{CF_F}{\sin\beta' \cdot CF_C \Delta_{tk}^{0.64}}$$

$$fa_3 = 0.60$$

$$AR = 7.46 \cdot \sin\beta' \quad \geq 1.3$$

where the parameters and factors above are given in Table 6.8 or defined as:

Δ_{tk} – ship displacement measured from upper ice waterline (UIWL) [tk]

x – distance from the forward perpendicular to station under consideration [m]

L_{wl} – ship length measured at UIWL [m]

α – waterline angle [deg], see Figure 6.26

β' – normal frame angle [deg], see Figure 6.26
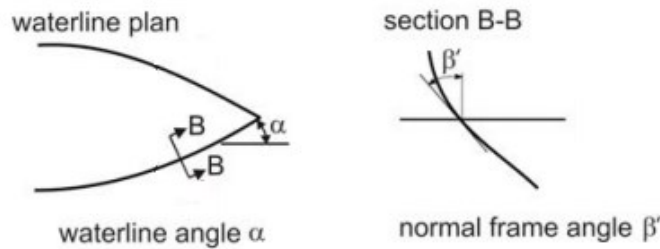
Figure 6.26: Definition of hull angles, adapted from (IACS 2011)

Table 6.8: Class Factors - Glancing impact load characteristics (IACS 2011)

Polar Class	Crushing Failure Class Factor (CF_C)	Flexural Failure Class Factor (CF_F)	Load Patch Dimensions Class Factor (CF_D)	Displacement Class Factor (CF_{DIS})	Longitudinal Strength Class Factor (CF_L)
PC-1	17.69	68.60	2.01	250	7.46
PC-2	9.89	46.80	1.75	210	5.46
PC-3	6.06	21.17	1.53	180	4.17
PC-4	4.50	13.48	1.42	130	3.15
PC-5	3.10	9.00	1.31	70	2.50
PC-6	2.40	5.49	1.17	40	2.37
PC-7	1.80	4.06	1.11	22	1.81

The hull angles and length parameters are measured at the upper ice waterline and the angles are defined in Figure 6.26. Adopting the Polar Class for ship shaped hulls to the buoy shaped Sevan Arctic MODU may introduce uncertainties to the results. To match the bow angle definitions geometrically, the waterline angle α is 90 degrees and β' is 45

degrees. The length parameters x and L_{wl} are 0m and 81m, respectively. Note that L_{wl} is equal to the Sevan Arctic MODU's diameter at the ice action waterline. See Appendix G for values and results for determining the design ice load for the Sevan's cone shaped structure.

6.8.2 Comments to the Polar Classes

Refer to (Nyseth 2014). Ice loads have a very random and complex behavior which makes it associated with high uncertainties. In the Polar Class rules the design ice load pressure and the associated patch area have been derived based on a design ship-impact scenario where ice thickness and properties are predefined parameters differentiating the ice classes. The differentiating is a stepwise increase in capacity with no clear physical boundaries which makes the ice classes very generic. The generic approach makes it apparent that the operator of the vessel is responsible to ensure safe operation. However, there is a lack of specific descriptions of the assumed capability of a vessel which makes it very difficult to evaluate the actual ice condition and the risk of operating in conditions beyond what are assumed for the Polar Classes. Hence, DNV recommends the operator of the vessel to use the Polar Class rules as a relative ranking of capabilities rather than being suitable for defined ice conditions. The values which are chosen as basis for the ice classes should be considered as differentiators between ice classes rather than actual values.

6.9 Local ice pressure

Local ice pressure calculations are used in the design of plates and stiffeners of a structure. Compared to global ice actions that are calculated from average pressure over a nominal contact area, the local ice pressure considers smaller areas that are subjected to higher local pressure. Hence, a separate consideration of local ice pressures is necessary to check the structural capability in plates and stiffeners. The pressure over such a small local area is illustrated in Figure 6.27. The local ice pressure can be considered constant over the area given by Equation 6.16, where the maximum ice action usually occurs when the height a of the loaded area equals the height of the local design area a_d, Ref (ISO19906):

$$A = a \cdot w_L$$

<div align="right">**Equation 6.16**</div>
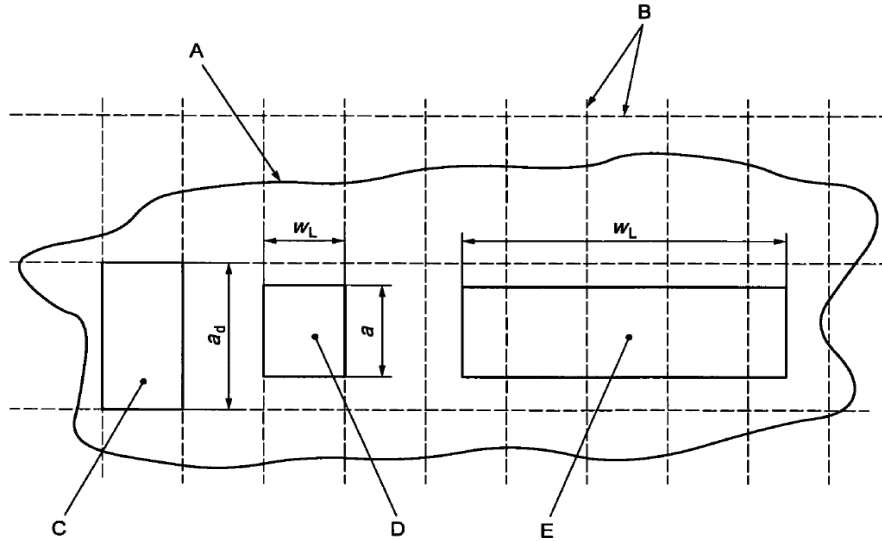
Figure 6.27: Definition of loaded area for local ice pressure (ISO19906)

A – global interaction area

B – frames and stiffeners

C – local area for plate design

D – loaded are for plate design

E – loaded are for stiffener design

a – loaded height

a_d – frame spacing

w_L – loaded width

Ever since ships started sailing in ice infested waters, designers and operators have experienced that local ice pressure can be high enough to fail steel plating, such as the sinking of the SS Titianic in 1912 after colliding with an iceberg. Designers therefore developed empirical methods for plating design such that ice pressure could be high over small areas. The consequence of this is that there are many ways to look upon the local ice pressure problem, refer to (Palmer and Croasdale 2013). However, there is actually nothing in the literature or codes that consider the local ice pressure on a sloping structure. In this section some of the methods will be presented and evaluated with regards to the Sevan Arctic MODU design. The following approaches will be presented:

- Local ice pressure for thick, massive ice features
- Local ice pressure for first-year
- Local ice pressure on sloping structure
- Polar Class – design load for scantling

6.9.1 Local ice pressure for thick, massive ice features

One of the local ice pressure curves recommended by ISO 19906 is:

$$p_L = 7.4A^{-0.7} \qquad\qquad A \leq 10m^2 \qquad\qquad \textbf{Equation 6.17}$$

The relationship should be used for ice features having a thickness larger than 1.5m and a local design area lower than 10m². Local ice pressure is constant above 10m² as 1.48MPa, see Figure 6.28. This relationship is based on the mean of data points plus three standard deviations. These data points have been derived from indentation tests in the Beaufort Sea and from measurements made on the ice pressure panels on the Molipaq structure (see section 4.4.2 about the Molipaq structure) in the same area. (Palmer and Croasdale 2013) recommend using this approach for small areas within a larger area of interaction which can occur with large icebergs, ice islands and thick multi-year floes.
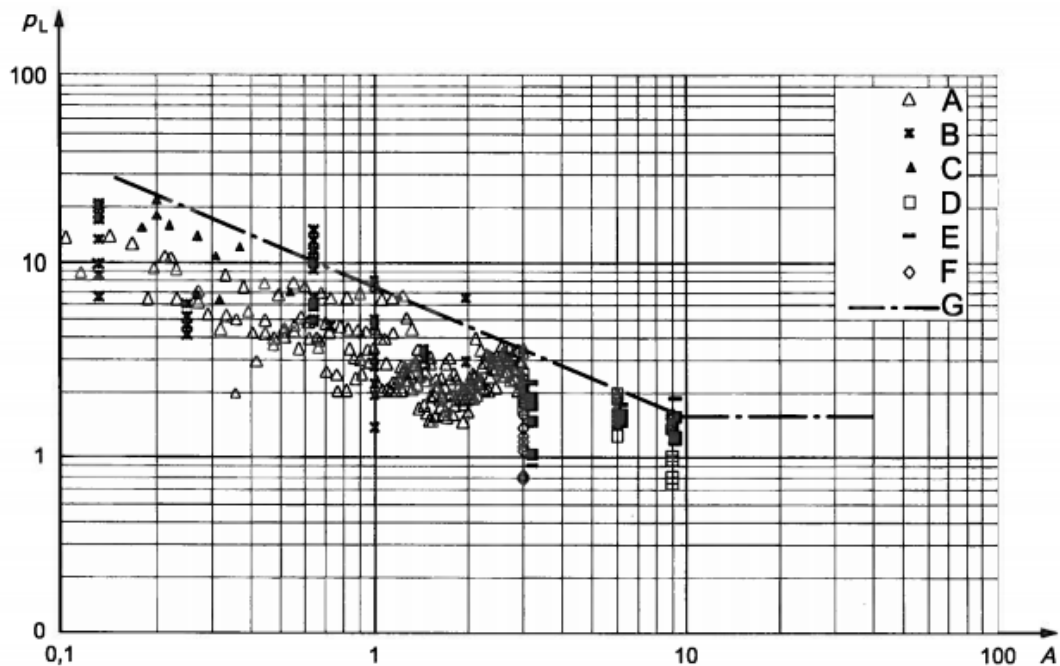
Figure 6.28: Ice pressure as a function loaded area compiled by data (ISO19906)

A – 3m^2 Pond Inlet data

B – flat jack data

C – 1989 Hobson's Choice data

D – Molikpaq Early data

E – Molikpaq N face date

F – Molikpaq E face data

G – $p_L = 7.40A^{-0.70}$

p_L – local ice pressure [MPa]

A – contact area [m^2]

However, for thinner ice and sloping structures Equation 6.17 may be very conservative.

6.9.2 Local ice pressure for first-year ice

Equation 6.17 does not take temperate variations, such as temperature and salinity, into account which has an effect on the sea ice's strength. (Palmer and Croasdale 2013) recommend a reduction of the coefficients used in Equation 6.18. A combination of the Canadian code (CSA) which takes the change of ice strength in temperate regions into account and ISO 19906's formulation for local ice pressure gives a more appropriate formulation for local ice pressure for first-year ice:

$$p_L = 4.8A^{-0.5}$$

Equation 6.18

The relationship is recommended for level ice thickness up to 2m.

6.9.3 Local ice pressure on sloping structures

Equation 6.17 and Equation 6.18 determine local ice pressure due to ice crushing on a vertical structure. However, approaches to determine local ice pressure on a sloping structure are not found in any literatures or codes. (Palmer and Croasdale 2013) looked upon the issue by using the equation for sloping structure given in ISO 19906 (see section 6.3.2). A total vertical force estimated from H_B, H_L and H_R (only using 50%) was generated to a value great enough to fail the ice sheet by bending instead of failing the ice sheet by crushing. The vertical force was resolved back into N, see Figure 6.29. Figure 6.29 also illustrated a crushing thickness that is increasing until the ice sheet fails in

bending. (Palmer and Croasdale 2013) discovered that there will be no structural design significance in specifying ice pressure greater than 1.5 MPa within the local design area.
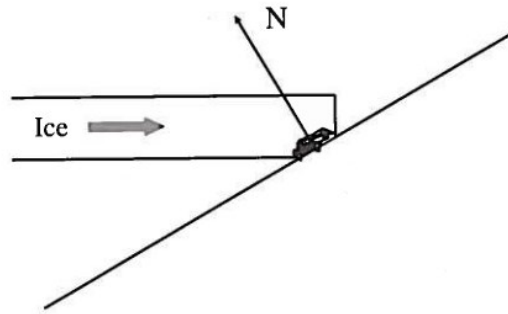
Figure 6.29: Local ice pressure on a sloping structure (Palmer and Croasdale 2013)

6.9.4 Polar Class – design load for scantling

The Sevan Arctic MODU is designed with PC4 (refer to section 5 and 6.8, respectively). In IACS, the design ice load issue is solved by applying an average pressure P_{avg} that is uniformly distributed over a rectangular load patch. The average pressure calculated for the Sevan Arctic MODU is 6.67MPa. However, the values which are chosen and calculated as basis for the polar classes should be considered as differentiators between ice classes rather than actual values.

6.9.5 Results and Discussion

Determining local ice pressure for a sloping structure becomes a matter of conservatism due to the lack of research done on the subject. The different approaches to determine local ice actions are compared in Table 6.9 and adapted from Appendix G. Local design area A for local ice pressure on plate and stiffener are determined form Equation 6.16 and are 0.48m^2 and 2.4m^2, respectively.

Table 6.9: Comparison of local ice actions

	Plate [MPa]	Stiffeners [MPa]
Local ice action for thick, massive ice features	14.0	4.55
Local ice action for first-year ice	7.6	3.4
Local ice action for sloping structure	1.5	1.5
Average pressure determined from Polar class – PC4	6.61	6.61

The results above are very spread and none of the solutions are a perfect fit for the Sevan Arctic MODU. However, the most reasonable load to apply will be a 1.5MPa ice pressure. The other approaches are either for vertical structures or deterministic values used in classification calculations. These values will be too conservative to apply on a sloping structure. The 1.5MPa ice pressure value will be applied in analysis of the Sevan Arctic MODU and investigated with regards to the structural capacity in section 9.

According to (ISO19906), local stress concentrations can occur close to discontinuities such as corners of a rectangular structure where the magnitude of the pressure can reach 2.5 to 3 times the usual pressure. The local structure considered in this thesis does not have discontinuities in the considered ice loaded area. However, it is noted that geometry will affect the local ice pressure's magnitude.

7 FEM THEORY

The Finite Element Method (FEM) is a large subject with several approaches and points to take into consideration. In this chapter a brief overview of the finite element method and its concepts is presented. The approaches relevant for the solution in this master thesis will be more closely looked upon. The following linear and nonlinear theory is mainly taken from (Moan 2003) and (Moan 2003)[3] respectively, while references about ABAQUS is taken from (ABAQUS 2013)[4].

7.1 General

The Finite Element Method is a numerical procedure for analyzing structures and is used in design of buildings, ships, airplanes etc. The method is only an approximate approach which discretizes a structural system into elements connected with nodes. The error of the result decreases by processing more equations and the results become reasonably accurate for engineering purposes. The error of the discretized structure is reduced by the number of elements that are applied; therefore more elements make the analysis converge towards the exact solution. The elements may be given physical properties such as thickness, density, Young's modulus, shear modulus and Poisson's ratio.

The FE method is based on the fundamental laws used to solve all structural problems:

- Equilibrium of stresses of all parts of the structure
- Compatibility of strains in the material
- Stress-strain relationship, expressed by Hook's law for linearly elastic material

7.2 Element theory

As the structure is discretized into elements, the choice of element type, size, geometry, number of nodes and approach for solving the fundamental laws are crucial for converging towards the exact solution. Regarding element types, beam elements are chosen for truss-type structures performing a one dimensional analysis, plate/shell

---

[3] Chapter 12 – Nonlinear analysis (Unpublished)
[4] Online documentation: http://50.16.176.52/v6.13/

elements are used for thin walled structures, while solid elements are used for complex thick structures and perform a three-dimensional analyses. For a local stiffened model as the Sevan Arctic MODU it is most appropriate to use shell elements. This is because the structural thicknesses are small compared to element dimensions and is also done in order to reduce computer time for a nonlinear analysis due to large deformation. Hence, only plate/shell elements will be presented in the next chapters.

To compute the element stress problem an approximate solution is established. A weak form of the stress problem is obtained by introducing a virtual displacement. Explanation of this theory will not be presented here, refer to (Moan 2003). However, the resulting plane element stiffness relationship is given in Equation 7.1. ABAQUS solves this virtual work problem numerically.

$$\mathbf{S} = \mathbf{kv} + \mathbf{S}^o$$

Equation 7.1

Where the element stiffness matrix k is given by:

$$\mathbf{k} = \int_V \mathbf{B}^T \mathbf{CB} dV$$

Equation 7.2

Where $\mathbf{S}$ is the force vector, $\mathbf{v}$ is the displacement vector, $\mathbf{S^o}$ is the consistent forces vector including both body forces and surface tractions, $\mathbf{B}$ is the strain-displacement matrix, V is the volume and $\mathbf{C}$ is the material stiffness.

7.2.1 Plate element

Pure plate elements where the stress distribution through the thickness is linear due to lateral loads are generally not found in today's computer programs. It is more preferable to use a more general shell element that can take both lateral and in-plane forces. Shell elements are a plate element that due to lateral loads gives a combination of membrane (in-plane) and bending stresses in the element. It is convenient to apply shell elements to stiffened panels because lateral pressure will cause bending of plates, but also cause overall bending with the stiffeners acting as beams with the plate contributing to an effective flange, see Figure 7.1.
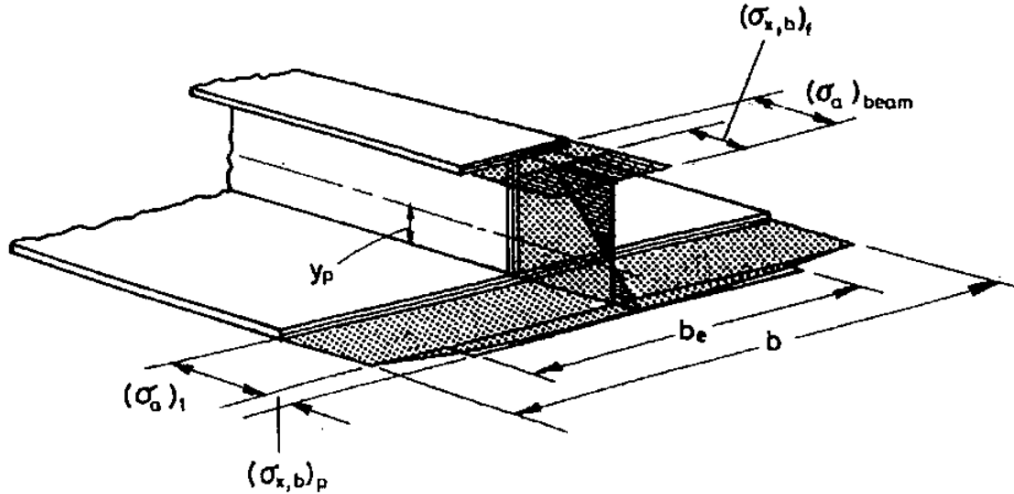
Figure 7.1 Membrane stresses in the plate and stiffeners due to in-plane and lateral loading (Moan 2003)

The interaction between membrane and bending forces occur due to curved surface of the element. Curvature of the surface will happen for large deformations and a nonlinear analysis should be performed.

The use of shell elements is thickness dependent as well as the theory to apply to the element. Kirchhoff theory (thin plate theory) and/or Mindlin-Reissner theory (thick plate theory) is used to solve the stresses within shell elements and is presented in section 7.2.2and section7.2.3. However, if distinctly thick plates are present, it is beneficial to use solid elements that capture shear strains better than shell elements. The thickness criterion is defined by the ratio of the thickness to the smaller span length and (Moan 2003) has suggested guidelines for usage of the theories:

- Kirchhoff Theory $t/L < 1/10$
- Mindlin theory $1/3 > t/L < 1/10$
- Three-dimensional theory $t/L > 1/3$

However, the distinction between thin and thick plate theory in ABAQUS is when the thickness is more than 1/15 of a characteristic length.

7.2.2 Kirchhoff theory

The thin plate theory is based on some assumptions to determine the stresses and deformations:

- A straight line normal to the mid-surface remains straight and normal to the mid-surface after deformation.
- The transverse stress is considered negligible (σ_z).
- And the transverse shear strains are considered negligible (γ_{xz} and γ_{yz}).

Hence, it is noted that bending of plates involves a plane stress-stain relationship described by the following equation:

$$\sigma = \begin{bmatrix} \sigma_x \\ \sigma_y \\ \tau_{xy} \end{bmatrix} = \frac{E}{1 - v^2} \begin{bmatrix} 1 & v & 0 \\ v & 1 & 0 \\ 0 & 0 & \frac{1}{2}(1 - v) \end{bmatrix} \begin{bmatrix} \varepsilon_x \\ \varepsilon_y \\ \gamma_{xy} \end{bmatrix} = D\varepsilon \qquad \textbf{Equation 7.3}$$

where σ and τ are the stresses, E is the material stiffness defined by Young's modulus, v is Poisson's number, and ε and γ are the strains. Displacement in vertical direction, w, may be expressed by interpolation polynomials or generalized coordinates, read more about this in (Moan 2003). However, displacements in horizontal direction are directly derived from the vertical displacement.

$$u = -zw_{,x}$$
$$v = -zw_{,y}$$

<div align="right">Equation 7.4</div>

where $w_{,x}$ and $w_{,y}$ are the slope of the mid surface in x- and y-direction, respectively.

7.2.3 Mindlin-Reissner theory

As for the Kirchhoff theory, the thick plate theory is also based on some assumptions.

- The transverse stresses is considered negligible (σ_z).
- A straight line normal to the mid-surface remains straight, but no longer normal to the mid-surface after deformation.

Thus, transverse shear deformations, γ_{xz} and γ_{yz}, are included in the solution. The stress-strain relationship will be expanded to the following equation:

$$\boldsymbol{\sigma} = \begin{bmatrix} \sigma_x \\ \sigma_y \\ \tau_{xy} \\ \tau_{xz} \\ \tau_{yz} \end{bmatrix} = \frac{E}{1-v^2} \begin{bmatrix} 1 & v & 0 & 0 & 0 \\ v & 1 & 0 & 0 & 0 \\ 0 & 0 & \frac{1}{2}(1-v) & 0 & 0 \\ 0 & 0 & 0 & \frac{1}{2k}(1-v) & 0 \\ 0 & 0 & 0 & 0 & \frac{1}{2k}(1-v) \end{bmatrix} \begin{bmatrix} \varepsilon_x \\ \varepsilon_y \\ \gamma_{xy} \\ \gamma_{xz} \\ \gamma_{yz} \end{bmatrix} \qquad \textbf{Equation 7.5}$$

$$= \boldsymbol{D\varepsilon}$$

where k is a correction factor equal to 1.2 to ensure that the shear strain energy for the plate can be correctly represented by a uniform shear stain. The transverse strains are calculated directly and the inclusion of transverse strains makes the Mindlin-Reissner theory more preferable compared to Kirchhoff theory. On the other hand, bad element performance can occur for thick plate theory due to so-called "shear-locking". By using selective integration, i.e. integrating the shear strain by a one-point integration, the performance of the element can be improved.

Compared to the Kirchhoff theory were the deformation were governed by the slopes, $w_{,x}$ and $w_{,y}$, the motion now depends on the rotation θ_x and θ_y of the lines that are straight to the mid surface.

$$u = -z\theta_x$$
$$v = -z\theta_y$$

Equation 7.6

7.2.4 Numerical integration - full and reduced

Integration in finite element method, for instance the stiffness matrix in Equation 7.2, may be difficult to solve analytically. Therefore numerical integration is frequently used. A one-dimensional integral may be computed numerically as:

$$I = \int_{-1}^{1} f(\xi)d\xi = \sum w_i f(\xi_i) \qquad \textbf{Equation 7.7}$$

where ξ is the natural coordinate, ξ_i is the integration point and w_i is the weight to the point. Sub-script i denotes number of integration points in one direction. Methods to establish ξ_i and w_i are various. The Gauss integration scheme is an optimal method and is frequently used in element analysis. In ABAQUS, for instance, the Gauss integration rule

can be used, but also the Simpson rule is selectable. However, Simpsons rule will not be presented because Gauss rule is the most preferred integration approach according to (Moan 2003). Also ABAQUS states that Gauss integration is almost always used due to its efficiency. The integral for plane stress problem, such as a rectangular area, will with numerical integration have the form:

$$I_2 = \int_{-1}^{1}\int_{-1}^{1} f(\xi,\eta)d\eta d\xi = \sum_i \sum_j w_i w_j f(\xi_i, \eta_j)$$ **Equation 7.8**

Typically, the number of integration points for FE analysis is 2x2 or 3x3 points. Hence, the natural coordinates ξ and η for 2 and 3 point one-dimensional Gauss rule correspond to location and values given in Figure 7.2. ξ and η are non-dimensional coordinates that maps the element which are used to describe numerical integration point. Number of integration points is determined by number of nodes in the element. f_i denotes the value of the integrand in the integration point (ξ_i, η_i).

a) 2 by 2 rule   b) 3 by 3 rule
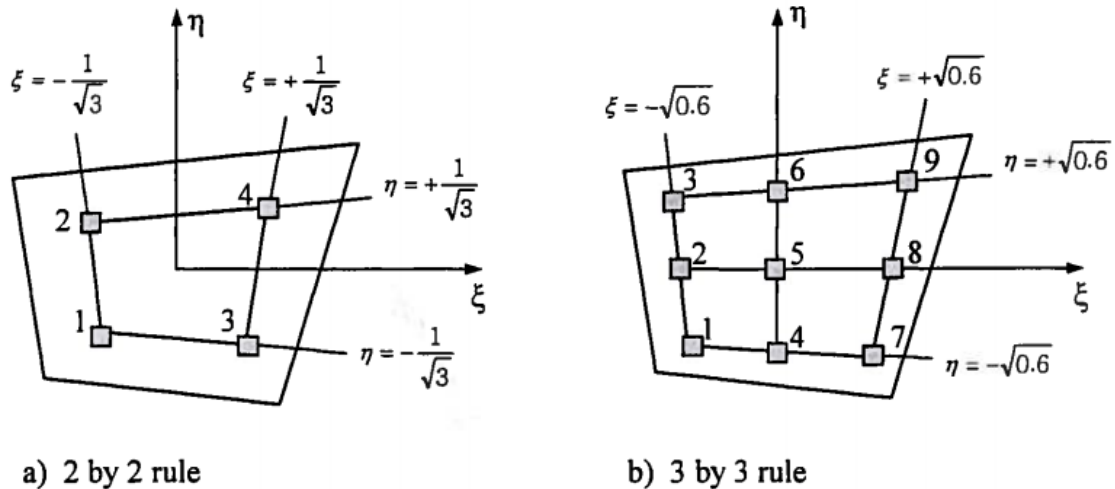
Figure 7.2: Gauss integration points in a quadrilateral element (Moan 2003)

Regarding numerical integration it is also necessary to comment on full and reduced integration. By using full integration the integral becomes exact, for instance the k_{ij} in the stiffness matrix, if element is undistorted. Undistorted means that, for instance for a rectangular element, the sides and midside nodes are straight. If the sides are curved or

midside nodes are offset from the midpoint, the integral for k_{ij} will not become exact. Thus, a desired integration rule with lower-order is preferred for two reasons. Reduced integration will first of all use lower computer time due to less integration points. Second, reduced integration tends to soften the behavior of the element. By countering the overly stiff behavior associated with an assumed displacement field, the accuracy of the FE analysis will be increased.

When reduced integration is used on a linear quadrilateral element with 4 nodes (denoted S4R in ABAQUS) the element will in bending deformation always display spurious shear strains (Mathisen 2012)[5]. This is illustrated in Figure 7.3. This parasitic shear absorbs strain energy and is called shear locking. This effect is not wanted, and because of this ABAQUS has implemented Hourglass control to minimize the problem. The hourglass principle ads an artificial stiffness to the element. Reduced integration used on quadrilateral elements with 8 nodes is generally not necessary because the element do not have the same difficulty with shear locking.
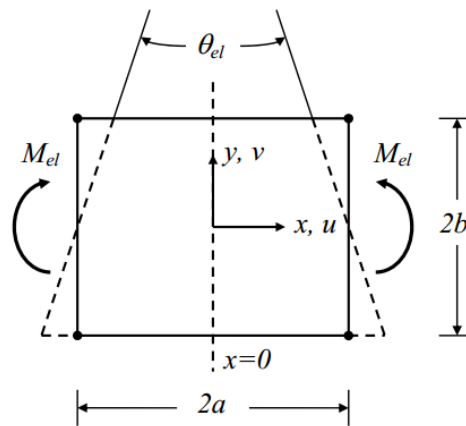
Figure 7.3: Hourglass mode, pure bending of linear quadrilateral element (Mathisen 2012)

7.2.5 Relevant elements

ABAQUS provides a large element library and the analyses procedure to be performed decides the appropriate elements for the analyses. A nonlinear static analyses is performed in this thesis, thus ABAQUS will provide stress/displacement elements for the modelling. These elements can be used for analysis involving contact, plasticity and large

---

[5] NTNU course TMR4190 – Finite element methods in structural analysis

deformations. The specific element type used in this thesis is structural shell element. Shell elements are used to model structures for which the thickness is significantly smaller than other dimensions. Presentation of relevant structural shell elements are given below.

S3/S3R is a three node triangular shell element that uses finite membrane strains. In AQABUS the element use thick shell theory as the shell thickness increases and Kirchoff thin shell theory as the shell thickness decreases. This element is a degenerated version of *S4R* and is fully compatible with *S4R*. In most loading situations the element provides accurate results. However, because of its finite bending and membrane strain approximations, a high mesh refinement may be required to capture pure bending deformations or solutions to problems involving high strain gradients.

S4R is the notation for a quadrilateral element with four nodes that uses reduced integration, hourglass control and finite membrane strains. Hourglass control is used to prevent shear locking due to usage of reduced integration. The hourglass principle ads an artificial stiffness to the element. The element allows transverse shear deformation, and as for *S3* the element use thick shell theory as the shell thickness increases and Kirchoff thin shell theory as the shell thickness decreases. ABAQUS user manual recommends using *S4R* elements when large strains or very high strain gradients are expected. Compared to S4, the S4R element uses one integration point instead of four thus reducing the computing time. First-order elements are recommended when large strains or very high strain gradients are expected.

S8R is the notation for a quadrilateral thick shell element with eight nodes that uses reduced integration. The element is used in ABAQUS for linear analysis when thick shells are needed in problems where shear flexibility is important and second-order interpolation is desired. This type of element is recommended to be used only for thick shell problems where the thickness is more than 1/15 of a characteristic length.

STRI65 is a thin conventional triangular shell element that imposes the thin shell Kirchhoff constraint numerically. The element is a six-node triangular thin shell using

five degrees of freedom per node. This element should be used in cases when transverse shear deformation is negligible. For homogeneous shells this occurs when the thickness is less than bout 1/15 of a characteristic length. Note that if this element is used to model a thick shell problem the results will become inaccurate. However, it is highly preferable for modeling bending of a thin curved shell.

7.3 Nonlinear theory

So far the structural analysis has been based upon assumptions of small displacement and linear elastic material behavior following Hook's law. Once the yield stress is reached and plastic deformations occur, linear element theory is no longer valid. Nonlinear theory is applied because of geometry, material and/or boundary condition nonlinear effects. Geometrical nonlinearity is accounted for if changes of geometry are established in the equilibrium equations. Material nonlinearities are associated with nonlinear stress-strain relationship, and solution methods will be further discussed in section 7.5. Nonlinearities due to boundary conditions are often related to contact between two surfaces. Large deformation is the most common reason for nonlinear effects such as buckling and collapse. A summary of differences between linear and nonlinear problem is shown in Table 7.1.

Table 7.1: Comparison of features for linear and nonlinear problems (Moan 2003)

Feature	Linear problems	Nonlinear problems
Load-displacement relationship	Displacements are linearly dependent on the applied loads.	The load-displacement relationship is usually nonlinear.
Stress-strain relationship	A linear relationship is assumed between stress and strain.	In problems involving material nonlinearity, the stress-strain relationship is often a nonlinear function of stress, strain and/or time.
Magnitude of displacement	Changes in geometry due to displacement are assumed to be small and hence ignored, and the original state is always used as the reference state.	Displacement may not be small; hence an updated reference state may be needed.
Material properties	Linear elastic material properties are usually easy to obtain.	Non-linear material properties may be difficult to obtain and may require additional testing.
Reversibility	The behavior of the structure is completely reversible upon removal of the external load.	Upon removal of the external loads, the final state may be different from the initial state.

Boundary conditions	Boundary conditions remain unchanged throughout the analysis	Boundary conditions may change, e.g. change in the contact area.
Loading sequence	Loading sequence is not important, and the final stat is unaffected by the load history.	The behavior of the structure may depend on the load history.
Iterations and increments	The load is applied in one load step with no iterations.	The load is often divided into small increments with iterations performed to ensure equilibrium is satisfied at every load increment.
Computation time	Relatively small compared to nonlinear analysis.	Due to many solution steps required for load incrementation and iterations, computer time is high, particularly if a high degree of accuracy is sought.
Robustness of solution	A solution can easily be obtained with no interaction from user.	In difficult nonlinear problems, the FE code may fail to converge without some interaction from user.
Use of results	Superposition and scaling allow results to be factored and combined as required.	Factoring and combining of result is not possible.
Initial state of stress/strain	The initial state of stress/strain is not important.	The initial stat of stress and/or strain is usually required for nonlinear problems.

According to (Moan 2003), nonlinear analysis may be applied for loading cases as follow:

- Design for ultimate and accidental collapse limit states.

- Assessment of existing structures whose integrity may be diminished due to aging visible damage such as cracks and corrosion etc.

- Establish the causes of a structural failure.

- Code development and research such as help to establish simple 'code-based' methods of analysis and design, help understand basic structural behavior and test the validity of proposed 'material models'.

Lately, the computes are becoming more and more efficient and powerful. Hence the solution cost decrease and less computer time is used. Because of this the analysis process is more user friendly performing nonlinear analysis rather than linear analysis becomes generally more preferably.

In the following section, nonlinear material behavior and solution techniques to solve nonlinear problems are presented.

7.4 Nonlinear material behavior

Nonlinear behavior of material happens when the stress exceeds a certain stress level, called the proportionality limit, σ_P. It is observed that metals do no longer act linear (elastic) after the proportionality limit, but by a nonlinear elasto-plastic behavior. Elasto-plastic behavior of an isotropic material in multidimensional stress state is characterized by:

- An *initial yield condition*, i.e. the state of stress for which plastic deformation first occur. In two dimension problems the yielding criterion is given by von Mises stress (this subject is further outlined in section 8.7.1).

- A *hardening rule* which describes the modification of the yielding condition due to strain hardening during plastic flow.

- A *flow rule* which allows the determination of plastic strain increments at each point in the load history. It leads to a relation between stress increment and strain increment. In one dimension the relation is simply $d\sigma = E_t d\varepsilon$, where E_t is the tangent modulus.

The expressions for elasto-plastic behavior for one-, two- and multidimensional stress states are found in (Moan 2003) and will not be presented here. However, it is noted that for analyzing thin-walled metal structures it is sufficient and more relevant to consider the stress condition as plane, i.e. in two dimensions.

Plastic deformation can weaken the structure due to permanent deflections or due to residual stresses that remain after unloading. Unloading after a stress that have exceeded the proportionality limit will create a new stress-strain curve which has a straight line parallel with the initial linear stress-strain relationship as illustrated with a dotted line in Figure 7.4.
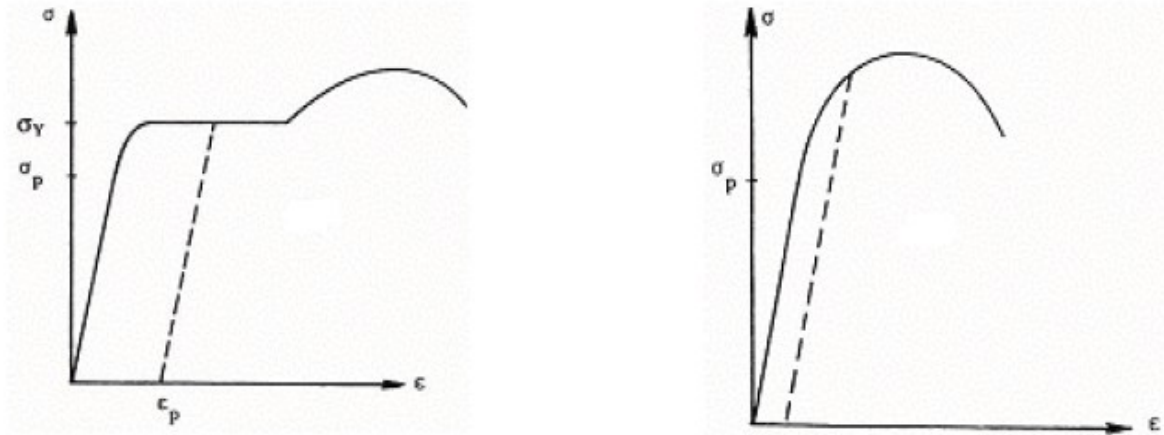
Figure 7.4: Stress-strain curve for mild steel (left) and high strength steel (right), adapted from (Moan 2003)

In Figure 7.4 σ_Y is the yield stress and ε_P is a residual plastic strain that remains when unloading the material to zero stress.

The permanent deformation, or true strain, is defined as true strain minus elastic strain, see Equation 7.9. The derivation for this equation can be found in (Moan 2003).

$$\varepsilon_{plastic} = \varepsilon_{true} - \varepsilon_{elastic} = \ln(1 + \varepsilon_0) - \frac{\sigma_0}{E}(1 + \varepsilon_0) \qquad \textbf{Equation 7.9}$$

It should be noted that the true stress-strain curve is only valid up to beginning of necking. Necking is a strain hardening phenomenon, meaning that. the material becomes harder as the strain increases, see Figure 7.5. In this area the force can no longer simply be divided by the cross-sectional area to obtain the uniaxial stress-strain curve. The formation of necking raises a complex state of stresses which is no longer uniaxial.

Figure 7.5: Nominal and true stress-strain curve illustrating necking phenomena (Moan 2003)

Typical material behavior in the plastic region is large strain increases compared to small stress increases, see Figure 7.5. The computational difficulty is that the equilibrium equations must be written using properties that depend on strain, but strains are not known in advance. Numerical methods are used in ABAQUS to solve the strain-stress curves. Some numerical solution techniques will be presented in section 7.5.
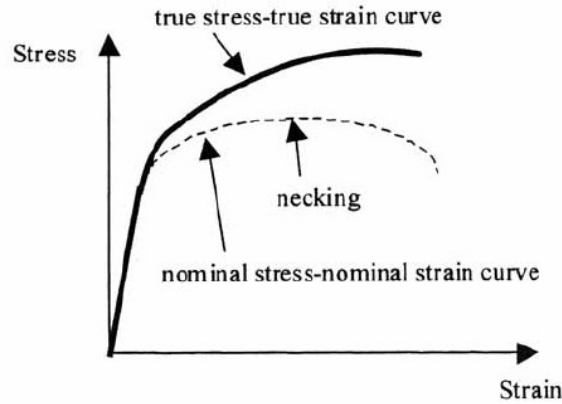
7.5 Solution techniques

In a nonlinear analyses the solution cannot be calculated by solving a single system of linear equations, as would be done in a linear problem. Various techniques for solving nonlinear problems exists where generally the equilibrium equation between external forces and internal reaction forces are solved using material stress-strain relationship.

$$\mathbf{R}_{int} = \mathbf{R}$$
$$\mathbf{K}_I(\mathbf{r})d\mathbf{r} = d\mathbf{R}$$

Equation 7.10

where $\mathbf{R}$ is the load external or internal load, $\mathbf{r}$ is the displacement and $\mathbf{K}_I$ is the stiffness. Increments and iterations are used to solve the nonlinear problem and the different techniques vary with how these increments and iterations are defined. In section 7.5.1, section 7.5.2 and section 7.5.3 the different techniques using increments (Euler-Cauchy method), iterations (Newton-Raphson method) or a combined version are described, respectively. Also a more advanced solution procedure called Arc-Length method will be

described in section 7.5.4. In section 7.5.5 a presentation of ABAQUS approach to solve nonlinearities is presented.

7.5.1 Euler-Cauchy method

The Euler-Cauchy method is a load incremental method, meaning that it provides a solution by a stepwise application of the external load. The total displacement is obtained by adding the displacement increments, $\Delta\mathbf{r}$. $\Delta\mathbf{r}$ is determined from Equation 7.11 for each step. The stiffness matrix K_I is kept constant during the increment, but recalculated for each step based on the known displacement and stress condition before a new load increment is applied.

$$\Delta\mathbf{R}_{m+1} = \mathbf{R}_{m+1} - \mathbf{R}_m$$
$$\Delta\mathbf{r}_{m+1} = \mathbf{K}(\mathbf{r}_m)^{-1}\Delta\mathbf{R}_{m+1} \qquad \textbf{Equation 7.11}$$
$$\mathbf{r}_{m+1} = \mathbf{r}_m + \Delta\mathbf{r}_{m+1}$$

With initial condition $\mathbf{r}_0=\mathbf{0}$ and step number m.

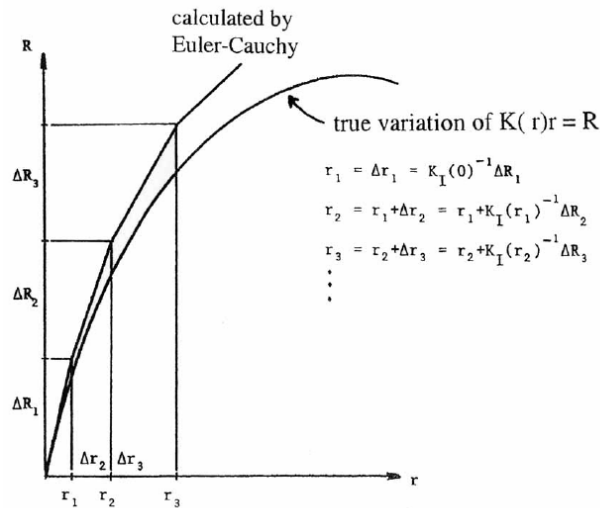**Figure 7.6: Euler-Cauchy method illustration (Moan 2003)**

It is observed in Figure 7.6 that Euler-Cauchy incrementing deviates from the equilibrium Equation 7.10. This deviation can be decreased by reducing the load increments or a simple improvement of the Euler-Cauchy method by equilibrium correction, also called modified Euler-Cauchy method. The correction can be obtained by accounting for the

residual forces when calculating the next step. The residual forces are obtained by reducing the external forces so the equilibrium is restored, see Equation 7.12. Hence, the equilibrium is restored for each step as illustrated in Figure 7.7.

$$\Delta\mathbf{R}_{m+1} = \mathbf{R}_{m+1} - \mathbf{R}_m$$

$$\mathbf{R}_r = \mathbf{R}_{int}(\mathbf{r}_m) - \mathbf{R}_m$$

$$\Delta\mathbf{r}_{m+1} = \mathbf{K}_I(\mathbf{r}_m)^{-1}\Delta\mathbf{R}_{m+1} - \mathbf{K}_I(\mathbf{r}_m)^{-1}\mathbf{R}_r$$

$$\mathbf{r}_{m+1} = \mathbf{r}_m + \Delta\mathbf{r}_{m+1}$$

Equation 7.12
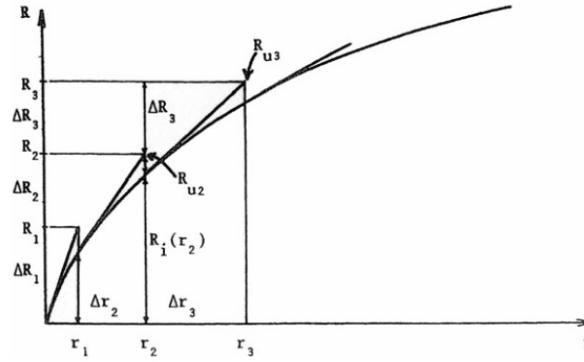
Figure 7.7: Modified Euler-Cauchy method (Moan 2003)

7.5.2 Newton-Raphson method

Compared to the Euler-Cauchy method that uses stepwise application of the external loading, the Newton-Raphson method uses stepwise application of the displacement. The Newton-Raphson method is an iterative method which is the method most frequently used to solve nonlinear problems. The relationship between strain and stress is solved by the iteration formula below and illustrated in Figure 7.8 for a single d.o.f. system.

$$\mathbf{r}_{n+1} - \mathbf{r}_n = \Delta\mathbf{r}_{n+1} = \mathbf{K}_I^{-1}(\mathbf{r}_n)(\mathbf{R} - \mathbf{R}_{int})$$

or

$$\mathbf{r}_{n+1} = \mathbf{r}_n - \mathbf{K}_I^{-1}(\mathbf{r}_n)(\mathbf{R}_{int} - \mathbf{R})$$
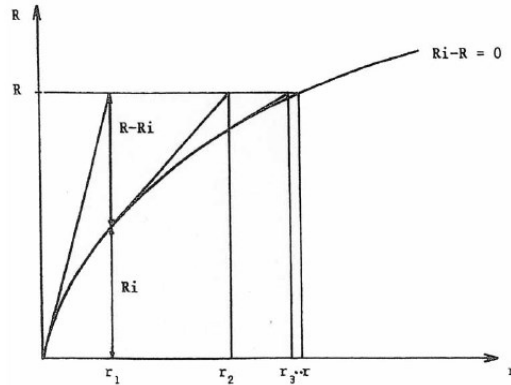
Equation 7.13

Figure 7.8: Newton-Raphson method illustration (Moan 2003)

As for Euler-Cauchy-method the stiffness of the system, $\mathbf{K}_I$, is kept constant during the step, but needs to be reestablished after each iterative step and solved for $\Delta \mathbf{r}_{n+1}$:

$$\mathbf{R} - \mathbf{R}_{int} = \mathbf{K}_I \Delta \mathbf{r}_{n+1} \qquad \text{Equation 7.14}$$

However, updating the stiffness matrix for each step is very time consuming. Therefore, a modified Newton-Raphson method can be used where the updating of $\mathbf{K}$ happens less frequently, but more iterations are needed. This is illustrated in Figure 7.9. At the same time the convergence loss will be limited. To ensure convergence, a convergence criterion is established based on the change of the displacement from one iteration to the next, and is expressed by:

$$\|\mathbf{r}_{n+1} - \mathbf{r}_n\| < \varepsilon \qquad \text{Equation 7.15}$$

where ε is of a magnitude of the order 10^{-2}-10^{-4}. The iteration procedure ends when the accuracy is acceptable.

Figure 7.9: No updating of $\mathbf{K}_I$ (left) and $\mathbf{K}_I$ updated after 1. iteration (right) (Moan 2003)

7.5.3 Combined method

This combined method is carried out by applying external loading followed by iteration to achieve equilibrium at each load level as illustrated in Figure 7.10. The iteration is

done with modified Newton-Raphson method, hence no updating of $\mathbf{K}_I$. The combined method follows the same convergence criterion as Newton-Raphson method.
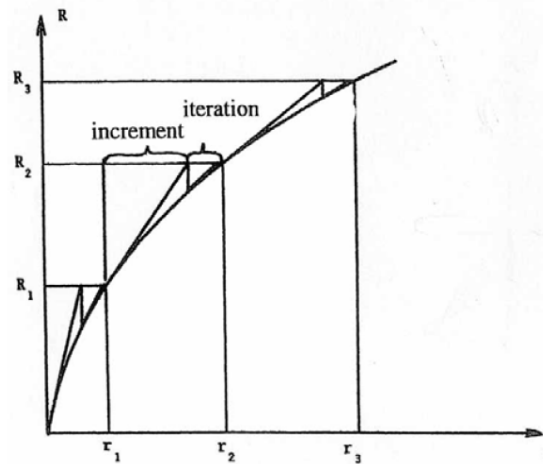
Figure 7.10: Combined method illustration (Moan 2003)

This method is only efficient as long as the load curve is monotonically increasing with displacement. If the curve includes extremal points an advanced solution procedure needs to be adopted to achieve equilibrium and convergence. One technique is the Arc Length technique which will be presented in the next section 7.5.4.

7.5.4 Advanced solution procedure

Arc-length method is a technique used to pass the limit point, also known as the ultimate strength, in the displacement-load curve. Sometimes it is necessary to describe the response after the limiting point to, for instance, know if the collapse is of ductile or brittle nature, or if a redundant structure consists of components that depend upon behavior beyond the limit point.

The arc-length method requires a combined incremental and iterative approach. To pass the limit point the increment size needs to be limited. The increment size is limited by moving a given distance along the tangent to the 'first point' and reach the 'second point' by iteration along a plane perpendicular to the 'first point's tangent that also goes through the 'second point', see Figure 7.11. Hence the equilibrium is achieved. This procedure is continued until the limit point is passed. The increment in the load-displacement space can be described by a displacement vector $\Delta\mathbf{r}$ and a load increment parameter $\Delta\lambda$, such

that $\Delta\mathbf{R}=\Delta\lambda\mathbf{R}_{ref}$, where $\mathbf{R}_{ref}$ is a fixed external load vector. Hence, and additional equation needs to be solved, but the additional equation results in a non-singular solution matrix, even at the limit points.
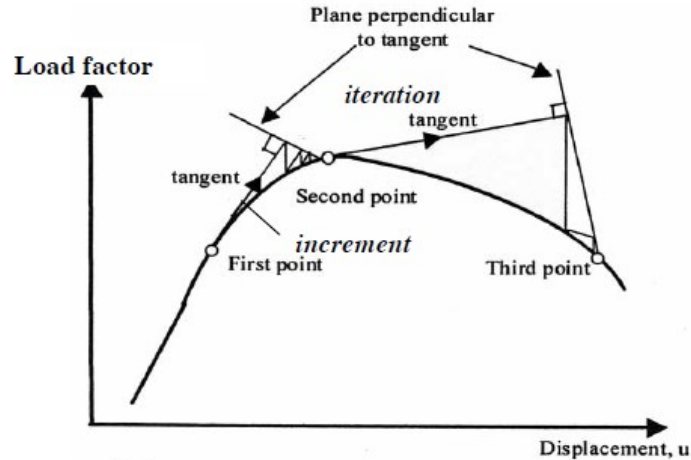
Figure 7.11: Arc length method illustration (Moan 2003)

7.5.5 Solution technique in ABAQUS

ABAQUS solves nonlinear problems with the *combined method*, as described in section 7.5.3. Newton's method is used to solve the nonlinear equations with a combination of incremental and iterative procedures. Loading is specified as a function of time and the solution is found by incrementing time to obtain the nonlinear response. ABAQUS breaks the simulation into a number of time increments and finds the approximate equilibrium configuration at the end of each time increment. The user suggests the size of the first increment, and ABAQUS will automatically choose the size of the subsequent increment. If the increment cannot find an equilibrium solution, iteration will be used until ABAQUS obtains a solution closer to equilibrium. However, if the iteration process diverges ABAQUS will terminate the iteration process and attempt to find a solution with a smaller increment size.

8   COMPUTER SETUP

As a final point in the assessment of a floater subjected to ice action, an examination of structural capability to a downward and an upward breaking design has been performed in ABAQUS 6.13. A static nonlinear analysis was performed for local models subjected to uniformly distributed ice pressure over a local design area. In this section, a presentation of the models, mesh, boundary conditions, material selection and load cases is given. In other words, all the footsteps necessary to undertake for performing a nonlinear static analysis in ABAQUS are presented. Information about ABAQUS in the following is drawn from (ABAQUS 2013)[6].

8.1   Model

The local models used in the ABAQUS analyzes were made in the Sesam GeniE software. GeinE[7] is software for designing and analyzing structures made of beams and plates. In this thesis, GeniE was only used to model the local structure because the author had much better experience with designing in the GeniE software compared to ABAQUS which provides a more difficult interface to model complicated structure geometries. The model was exported as a *.SAT – file and imported to ABAQUS were material properties and thicknesses were assigned the denoted parts as given in Appendix B.

The local structure was modelled as best as the drawings allowed, but because the design of the Sevan Arctic MODU (see section 5) is in the initial stage and still continuously iterating towards a better solution, the model may not be spot-on. However, the plate thickness, stiffener and girder sizes are more or less established and based on Polar Class PC4. Hence, the assessments should give a proper answer to whether the structure holds for local level ice pressure.

The local model is a cut-out of the global structure, see Figure 8.1. It has a width of 6.8m. This width was selected because the distance between the bulkheads is approximately 6.8m and to obtain the best boundary conditions to represent the real condition it is

---

[6] Online documentation: http://50.16.176.52/v6.13/
[7] http://www.dnv.com/services/software/products/sesam/sesam_genie/

recommended to use the presence of bulkheads as natural boundary conditions (this is further outlined in section 8.5). The Sevan Arctic MODU design is a hexadecagon (16-sided shape), thus the local model will be plane and not curved. The location of the local model coordinate system is shown in Figure 8.2.
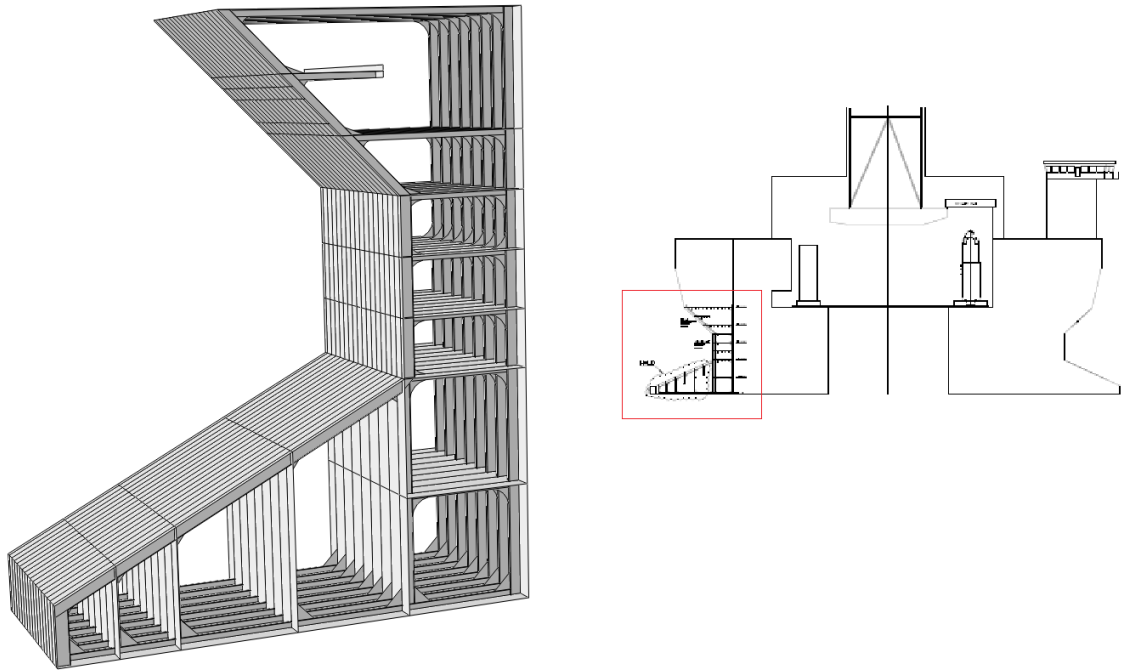

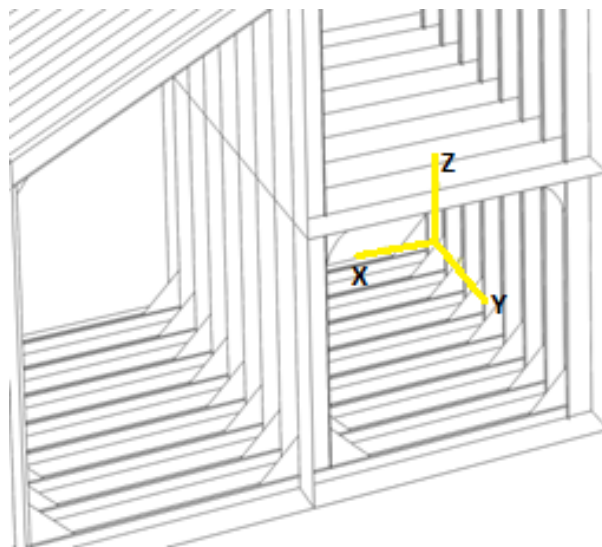**Figure 8.1: Local model extracted from global structure**

Figure 8.2: Location of coordinate system

COMPUTER SETUP

Only shell elements were used in the model, which means that also beam parts such as stiffeners were modelled with shell elements. Shell elements tend to give better results than beam elements, but are more time consuming to model. Because a local analyses is performed of the hull structure, it is recommended to use shell elements representing the same geometry as the real structure.

The model in Figure 8.1 has an upward sloping face of 27 degrees at the lower part and 45 degrees downward sloping face at the higher part which is where the ice loads are acting. The outer hull plate thickness is 34mm and internal plates range from 15mm to 20mm. Space between stiffeners that stiffen the hull is 400mm and 800mm spacing elsewhere. T450x18x100x40 stiffeners are used along the outer hull. This cross section geometry was selected by Sevan because of the small spacing between the stiffeners and to obtain the stiffening effect at the sime time as they should be possible to construct the hull at the yard efficiently. Bracket thickness is 20mm and the shape was modeled in agreement with Sevan Marine.

The effect of brackets in the ice loaded area is investigated in this thesis. Thus, an identical model as the one above was made, but without brackets. Brackets are used to connect all types of stiffeners at their ends. Their purpose is to smoothen out the transition stresses in the stiffeners and they are frequently used in marine structure design. The shape of the bracket can for instance be a simple triangular bracket or a rounded bracket, see Figure 8.3. The Sevan Arctic MODU is modeled with both simple and rounded bracket in the ice loaded area to stiffen the sloping stiffeners with the stiffeners stiffening the horizontal stringers.

Simple bracket   Rounded bracket
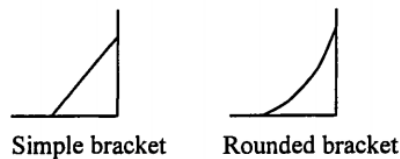
Figure 8.3: Bracket shapes (Moan 2003)

An analysis was also performed for an upward sloping design, see Figure 8.4. Roughly, the same shell thicknesses and stiffener sizes were used in this design as the downwards sloping design. This model is also assigned the same boundary conditions and material

properties as the downward sloping design. Hence, it is mainly the shape of the structure that differs.
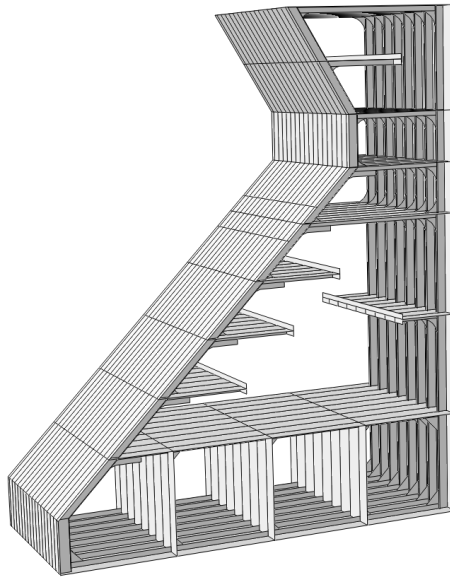
Figure 8.4: Local model of upward sloping structure

8.2 Material properties

Analysis in ABAQUS requires knowledge about the material used. ABAQUS provides a broad coverage for linear, nonlinear, isotropic and anisotropic material behaviors. The use of numerical integration of elements, including numerical integration across the cross section of shells, provides the flexibility to analyze the most complex composite structures.

Materials defined in ABAQUS can contain a number of material behaviors to specify the complete material behavior. In linear static stress analysis only, elastic material behavior may be needed, while in more complicated analysis several material behaviors may be required. In this thesis, the material is denoted both elastic and plastic properties. This is because a parameter study was performed towards structural capability for increased ice pressure. Elastic materials are relatively simple to define since only Young's modulus and Poisson's number are required. However, in the plastic regime the definition of material behaviors becomes more complicated. Data points for a stress-strain curve must be established. In this thesis the data points are obtained from (DNV 2013) for S355 steel. Presentation of the steel is given later in this section.

COMPUTER SETUP

The elastic properties used in this thesis are based on common marine construction engineering steel. The Young's modulus is 2.1GPa and Poisson's number is 0.3. A steel density of 7850kg/m^3 is also given uniformly. The material's mass density must be defined for gravity loading purposes. The steel material is selected to be isotropic, which means that it is identical in all directions.

The stress-strain data points used to determine the plastic behavior of the element are based on (DNV 2013). The idealized material curve for S355 steel is tabulated in Table 8.1 and plotted by the author in Figure 8.5. The values are given for engineering stress-strain measures which means that the values are calculated based on an initial cross section of a test specimen. S355 steel is a frequently used steel type in offshore constructions and Sevan Marine wanted the analyses to be calculated with these material properties. The properties are assumed to be within the acceptance criteria for nonlinear FEM analysis. (DNV 2013) recommends to use stress-strain curves that depend on thickness. In this thesis, it was only necessary to create two material curves because the thicknesses never exceeded 40mm plate thickness. Due to the sloping face it was necessary to denote material orientation for a local coordinate system parallel with the sloping face.

Table 8.1: Proposed non-linear properties for S355 Steel, adapted from (DNV 2013)

Strain [-]	Stress[MPa]/thickness [mm]	t<16	16<t<40	40<t<63
0	Prop.	319.5	310.5	301.5
0.004	Yield 1	355	345	335
0.02	Yield 2	358.4	348.4	338.4
0.15	Ultimate	470	470	450
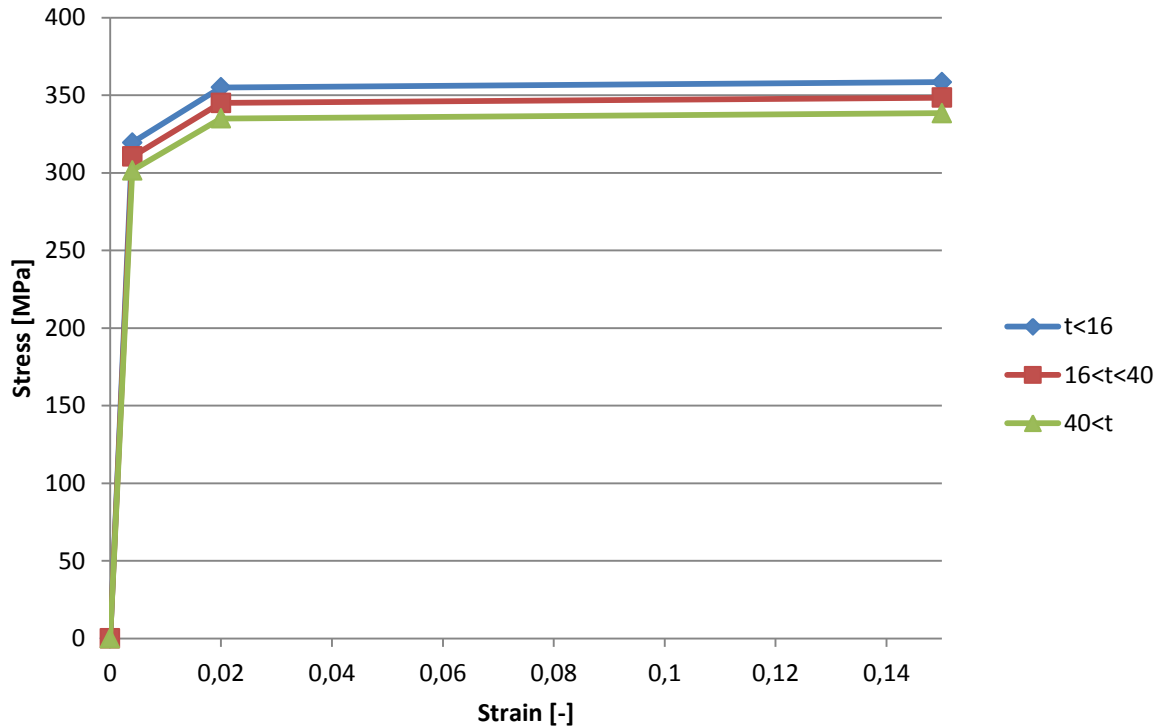
Figure 8.5: Material curve for S355 Steel

The material curve obtained from (DNV 2013) can be compared to existing material curve for the same material, see Figure 8.6. It is observed that the strain-strain curve from (DNV 2013)'s data points is significantly simplified compared to the curve in Figure 8.6. The yielding plateau and the strain hardening curvature (after yielding) are not properly achieved in Figure 8.5. However, according to (DNV 2013), the acceptance criteria for nonlinear FEM analysis should not necessarily represent the actual material curve accurately as long as the produced results are on the safe side. Because the intention of the analysis in this thesis is not to maximize the plastic potential of the structure, the shape of the graph after yielding is not of significant importance. It is the first part of the graph which will be off the most importance. In the elastic regime the strain is proportional to the stress and is linearly increasing until the stress reaches the yield limit. In this thesis the yield limit is given by the von Mises stress which is further outlined in section 8.7.1.
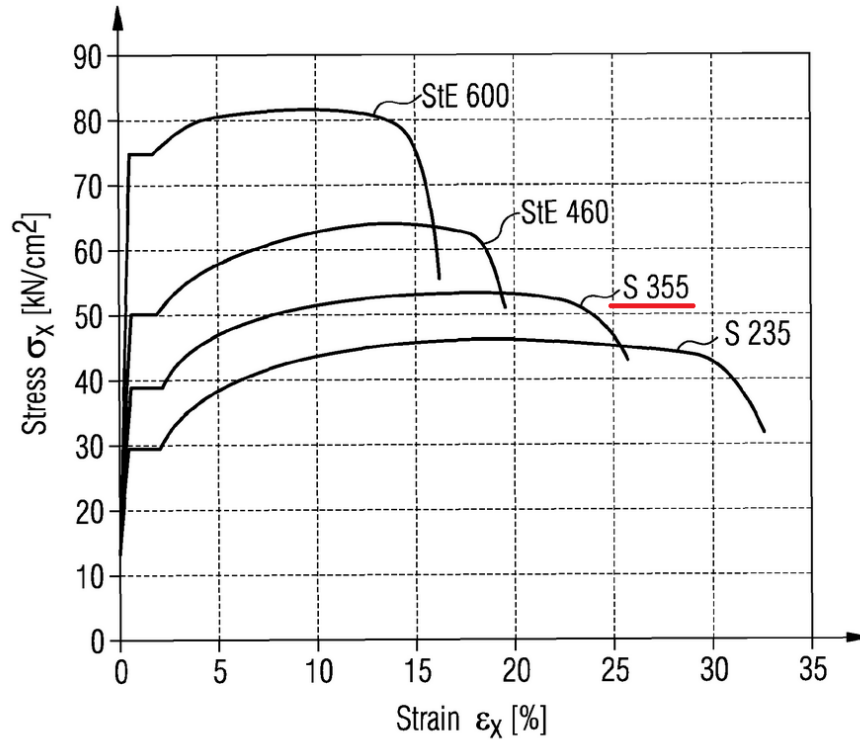
Figure 8.6: Existing stress-strain curve for steel materials, adapted from (Rasmussen 2011)

8.3 Element and mesh

The selection of element type and mesh size is based on a convergence analysis presented in section 8.4. However, a presentation of element types and sizes and the effect they have on the results is given in this section. The performance of the model is closely linked to the type-, shape- and aspect ratio of elements, as well as the topology to the mesh that is uses.

First of all, the selection of element type is strongly dependent upon the problem to be analyzed. (DNV 2013) listed several points to consider when selecting element type to be used in nonlinear FEM analysis:

- Shell elements or solid elements (see section 7.2).
- Elements based on constant, linear or higher order shape functions (see section 7.2.2 and section 7.2.4).
- Full versus reduced integration (see section 7.2.4).

94

- Number of integration through the thickness (see section 7.2.4).
- Locking effects (see section 7.2.4).
- Hourglass control (see section 7.2.4).

According to (DNV 2013), higher order elements are preferred for accurate stress estimates in general. Elements with simple shape functions will require more elements to give the same stress accuracy as higher order elements. ABAQUS provides a large element library, and the appropriate element type is decided with respect to the analyses procedure which is to be performed. A nonlinear static analyses is performed in this thesis, consequently ABAQUS will provide stress/displacement elements for the modelling. These elements can be used for analysis involving contact, plasticity and large deformations. The specific element type used in this thesis is structural shell element. Shell elements are used to model structures which have a thickness significantly smaller than the other dimensions. The relevant shell elements considered in this thesis are presented in section 7.2.5.

According to (DNV 2013), the mesh density (or element size) should be sufficiently detailed to capture the relevant failure. (DNV 1999) provides recommendations to minimum element density for performing finite element calculations of a cargo tank model:

- Between the height of girders/stringer there should be minimum three elements.
- Height of longitudinal stiffeners should include at least one element.
- Two elements between transverse girders/stiffeners.
- Large brackets it is acceptable to use the same element size as stiffeners spacing to determine stresses.

These recommendations were taken into consideration when choosing the mesh density of the local model and the number of elements in the model was never less than in the recommendations.

8.4 Convergence analysis

Finite element programs, such as ABAQUS, use numerical methods to obtain results, thus it is important to keep in mind that the results may not be correct due to boundary conditions, modeling errors and material properties. To assure that the model's mesh size and element type give converging results, a convergence test is performed in this thesis for different mesh sizes and element types. Generally, a finer mesh will provide converged results. In addition, elements with a higher order of integration points will require less elements to converge towards the exact solution and thus represent the curved surface. However, finer mesh and higher order elements will require more computer time and space. It is therefore preferred to find an element size and element type that give a converged result, but does not use much computer time and space.

Below a convergence test is performed for the local model for downward sloping design for four different element types and element sizes, thus 16 models were implemented in ABAQUS. An ice pressure of 1.5MPa was loaded uniformly over a local design area for stiffeners. The test is checked towards maximum von Mises stress and displacement in the ice loaded area. The maximum von Mises stress occurs on the flange of the middle sloping stiffener, see Figure 8.7, and maximum displacement occurs in the middle of the horizontal stringer plate, see Figure 8.8. It is assumed that it is sufficient to only check the convergence at these two points.
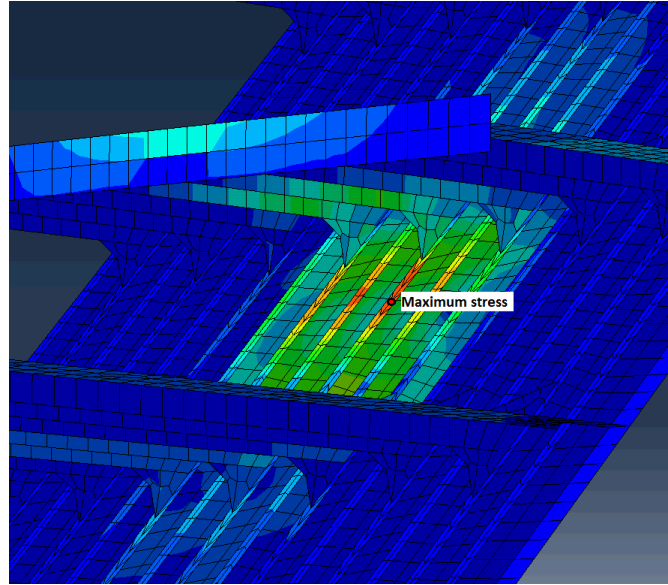
Figure 8.7: Maximum von Mises stress in ice action region for convergence analysis
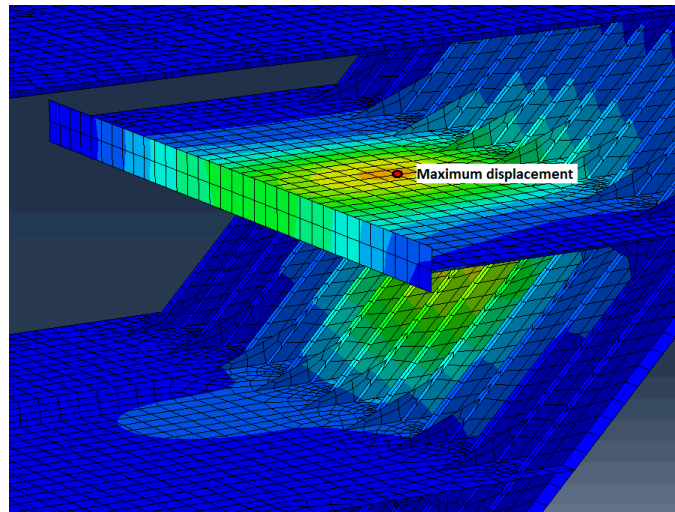
Figure 8.8: Maximum displacement in ice action region for convergence analysis

The ABAQUS library includes several of shell element types, but in this convergence study only S3, STRI65, S4R and S8R have been assessed. Description of the elements is found in section 7.2.5. These elements were chosen due to their variation in shape, integration points and shell theory. The mesh sizes vary from 200mm to 25mm and are based on monotonic convergence. It means that the accuracy requirement is configured by dividing the typical size of the previous element by two (Moan 2003). Thus, element size 200mm, 100mm, 50mm and 25mm were investigated. The convergence test for decreasing mesh size is only performed for the sloping area where the ice pressure is

applied. It is assumed that the structure actions outside this area will not affect the results considerably. The area was also selected compared to the whole structure because computer time and space increase rapidly with decreasing mesh size. Hence, to save time and computer capacity the convergence test was only considered for this area.

In Figure 8.9 and Figure 8.10, the maximum displacement and von Mises stress are plotted, respectively, for the four element types toward the four element sizes.
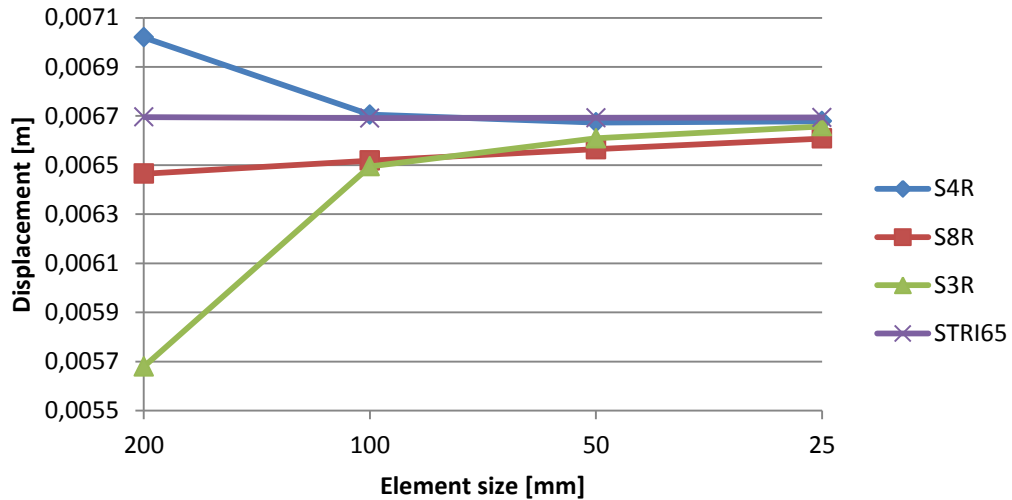
Figure 8.9: Convergence of displacement comparison, adapted from Appendix H
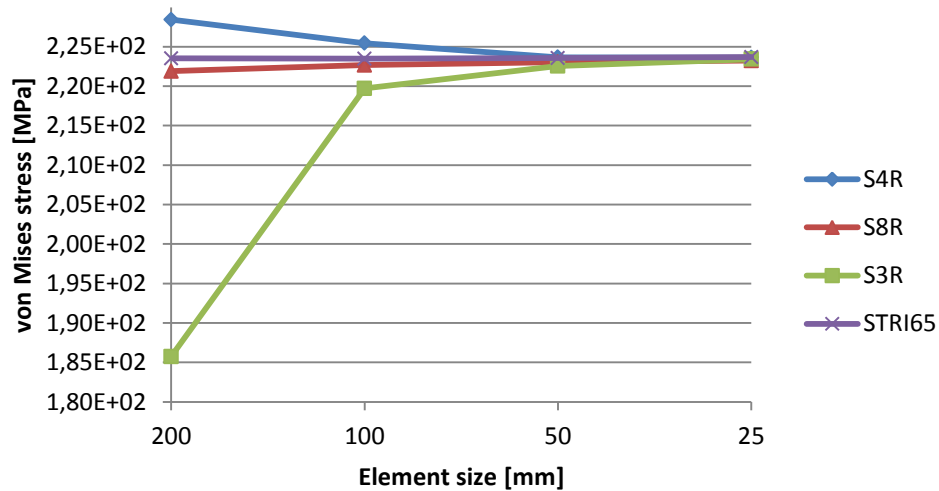
Figure 8.10: Convergence of von Mises stress comparison, adapted from Appendix H

It is observed from Figure 8.9 and Figure 8.10 that both for the displacement and stress comparisons the elements with more integration point, such as S8R and STRI65, converge faster than the elements with less integration points. Already at the element size 200mm do these elements converge. However, the analyses using the elements with more integration points used significantly longer computer time, especially for the element size 25mm.

Looking upon the element S3 and S4R (the element with less integration point) it is observed that the values are converging at 100mm-50mm, and that S4R converge faster than S3. S4R provides a more conservative result compared to S3 which is an advantage when using larger elements.

The quadrilateral elements S4R and S8R deviates less from converged value at large element size, however it is observed that S4R provides a conservative solution for increasing coarse mesh. When using first order reduced integration element such as S4R, hour-glassing (see section 7.2.4) may occur for coarse mesh. The large displacements in coarse mesh are due to this effect. Thus, a finer mesh may be required. Quadrilateral elements have a disadvantage to not adapt well to the structural geometry. A combination of quadrilateral and triangular is a recommended solution. ABAQUS provides a mesh control application which uses quadrilateral elements in the main mesh and triangular elements where quadrilateral elements are unable to adapt.

In this thesis, analysis will use quadrilateral dominant mesh with S4R and S3R elements with approximately 200mm global element size. This is because the convergence analysis illustrates that this selection provide conservative results.

8.5 Boundary conditions

The selection of boundary conditions is essential to get an accurate result. According to (DNV 2013), the selected boundary conditions need to represent the real condition in a way that will lead to results that are accurate or to the safe side. The best approach is to model the whole structure, however this is very time consuming. Because only a local analysis is to be performed in this thesis, it is assumed enough to only model a small part

of the hull because the ice load applied to the model are well within the restraints. The boundary conditions selected for the edges are illustrated in Figure 8.11.
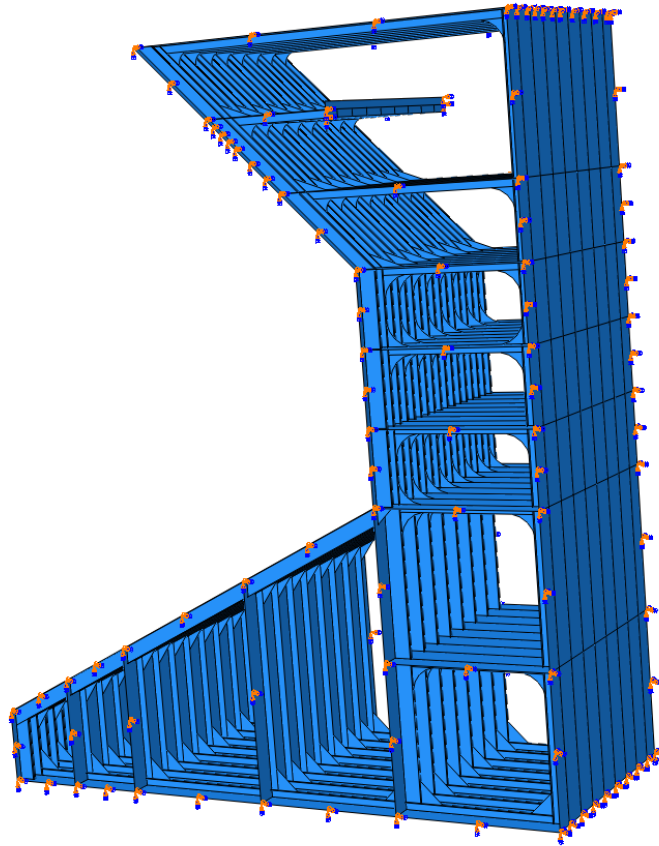
Figure 8.11: Illustration of boundary conditions

Determination of location of boundary condition is according to (Moan 2003), based on natural structural restraints or rigid supports, such as structural bulkheads. This approach is used in this thesis. In real life there is a bulkhead at the vertical plane x=0 and x=6.8m, hence the boundary location of the vertical plan is located here. One possible boundary condition is to introduce clamped edges along the vertical plane. However, when shell elements are used to model the local structure, the clamped boundary condition will introduce singularities at the corner of the boundary (Moan 2003). Singularity in a point will lead to increasing stress at the point towards infinity. To avoid the non-realistic stresses due to singularities, the boundary conditions at the vertical plane ends should be modified as illustrated in Figure 8.12. Thus at x=0 the boundary condition is fixed for all displacement and rotation except for displacement and rotation in y-direction. In

agreement with (Nyhus 2014 pers.comm. 10 May) at Sevan, the vertical plane boundary conditions at x=6.8m was only free to rotate in y-direction because this condition is assumed to represent the best real life condition.
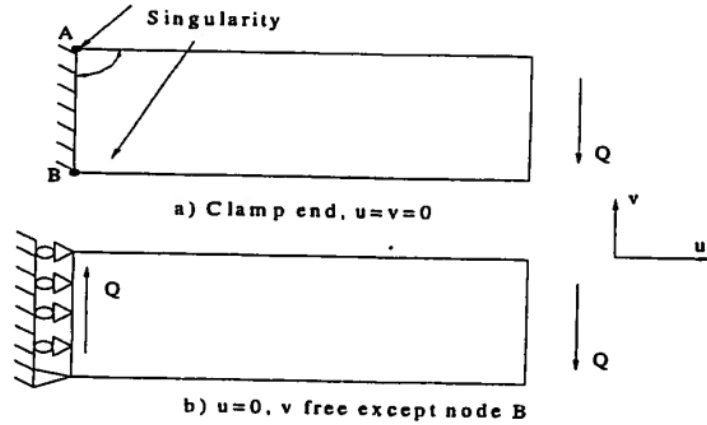
Figure 8.12: Modelling of a cantilever beam (Moan 2003)

The boundary condition along the inner wall is fixed towards all displacements and rotations. Because the main focus of the analysis are to investigate the behaviors in the local structure in the ice loaded area, the fixed boundary conditions along the inner hull are assumed to be outside the area of interest.

8.6 Analysis procedure and step

In ABAQUS the analysis problem is defined using steps. For each step an analysis procedure is chosen and the type of analysis to be performed during the step is defined. The simplest form a step can be is a static analysis where a load changes from one magnitude to another, which is the case in this thesis. Static stress analysis can be linear or nonlinear. It ignores time-dependent material effects, such as creep, but takes rate-dependent plasticity into account.

Nonlinearities arise for large displacement effects, material nonlinearity and boundary nonlinearities. A nonlinear static analysis can be performed in ABAQUS if geometrically nonlinear behavior is expected in a step which then includes large displacement

formulation. In this thesis, effects from nonlinearities from large displacements are accounted for in the performed analyses.

ABAQUS uses Newton's method to solve the nonlinear equilibrium equation. (ABAQUS 2013) recommends in most cases to use the default automatic incrementation scheme because it will select increment sizes based on computational efficiency. See section 7.5 for theory about nonlinear solution techniques. Analyses performed in this thesis used full Newton solution technique. Incrementation was performed with ABAQUS's initial values which is an increment size of 1 and minimum size $1*10^{-5}$.

There are two kinds of steps in ABAQUS, general analysis steps and linear perturbation steps. Linear perturbation steps can only be used to analyze linear problems, while general analysis steps can be used for both linear and nonlinear response. Analysis performed in this thesis was selected to use general analysis steps because nonlinearities due to large displacements are included in the analysis procedure.

8.7 Load cases

The load applied to the local model is generally the local ice pressure determined in section 6.9.5. The pressure is 1.5MPa and applied uniformly over a local design area. In the scope of work, 1.2m level ice thickness is subjected in a horizontal direction to the structure in the sloping area at draft 17m and 12m, respectively, for downward and upward sloping design. The inclining surface of 45 degrees will thus experience a local ice pressure over a local design area height with 1.7m. In ABAQUS pressure load can only be applied normal to elements. Optimally, the load should be applied parallel with the waterline, in other words 45 degrees clockwise on the sloping face. However, in analysis performed in this thesis, the ice pressure is applied normally to the sloping surface due to the restrictions in ABAQUS. The results are thus assumed to be conservative and on the safe side.

The width of the local ice pressure, according to ISO 19906 (see section 6.9), depends on whether it is the plate's or the stiffener's capacity that is looked upon. Local ice pressure for plate design has a width same as the stiffeners spacing as shown in Figure 8.13. While

local ice pressure for stiffener design are subjected such that four stiffeners are loaded as shown in Figure 8.14. An analysis was also performed to investigate the variation of shear forces if the ice pressure was moved to not be applied asymmetrically between two stringers, shown in Figure 8.15. Hydrostatic pressure was applied to the surface which is submerged, see Figure 8.17. Figure 8.16 shows the ice pressure applied to the upward sloping design.
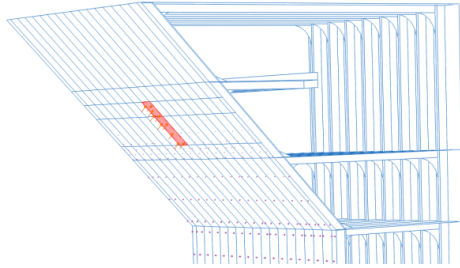
Figure 8.13: Ice pressure loaded area for plate
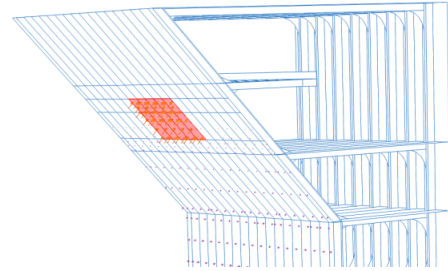
Figure 8.14: Ice pressure loaded area for stiffener
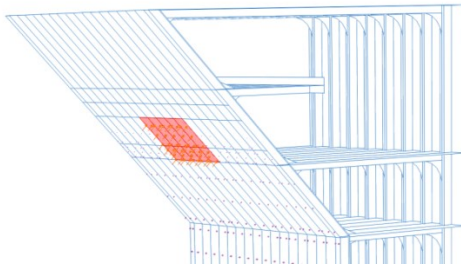
Figure 8.15: Ice pressure for shear force investigation
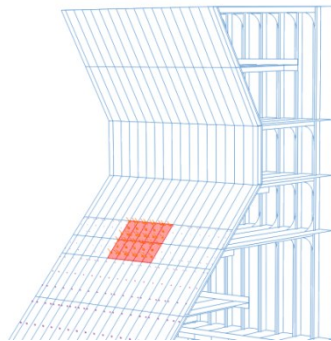
Figure 8.16: Ice pressure on upward sloping structure
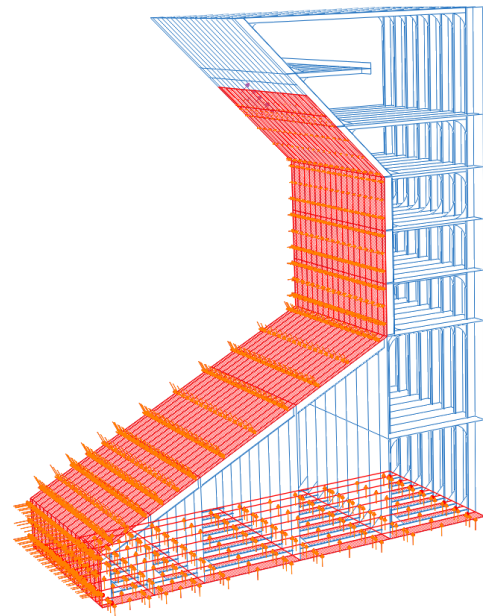
Figure 8.17: Hydrostatic pressure

In this thesis, the results of particular interest are the von Mises stresses. This is due to two-dimensional shell elements, which are used in this thesis models, are limited by

yielding criterion given by the von Mises stress. The von Mises yield criterion is presented section 8.7.1.

8.7.1 The von Mises yield criterion

The yield condition of a material defines the limit of purely elastic behavior under any combination of stress. In this thesis the results of particular interest are the von Mises yield criterion, which will be the limit for the structure from plastic behavior. According to (Moan 2003), experiments indicate that the von Mises yield condition is the best option for representing the material behavior of most metals. Hence, the von Mises yield criterion is generally used for steel material. The von Mises criterion also has the advantage that it is a simple continuous function of stress components which makes it especially attractive to numerical analysis.

The von Mises yield criterion is derived from distortion energy theory. In terms of plane stress components ($\sigma_y = 0$) the von Mises yield function is given by the following equation:

$$\sigma_{VM} = \sqrt{\sigma_x^2 + \sigma_y^2 - \sigma_x\sigma_y + 3\tau_{xy}^2} \qquad \text{Equation 8.1}$$

In which σ_x and σ_y are the direct stresses in x- and y- planes respectively, τ_{xy} is the shear stress on the plane and σ_{VM} is the yield stress under uniaxial stress. Equation 8.1 describes an ellipse, which when plotted for principle stresses in the $\sigma_1 - \sigma_2$ plane is as shown in Figure 8.18.
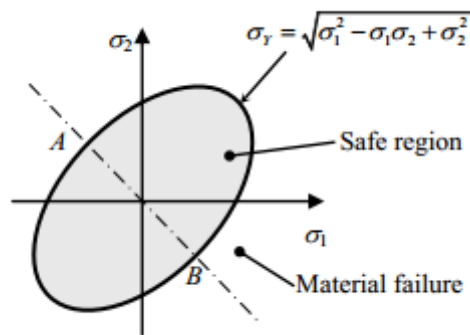
Figure 8.18: Elliptical shape of von Mises yield criterion for plan stresses (UF 2014)

COMPUTER SETUP

ABAQUS solves von Mises stress function numerically as follows, (ABAQUS 2013):

$$q = \sqrt{\frac{3}{2}\mathbf{S}:\mathbf{S}}$$

where $\mathbf{S}$ is the deviatoric stress tensor, defined as $\mathbf{S}=\boldsymbol{\sigma}+p\mathbf{I}$, where $\boldsymbol{\sigma}$ is the stress, p is the equivalent pressures stress, and $\mathbf{I}$ is a unit matrix. In index notation the Mises stress is defined as

$$q = \sqrt{\frac{3}{2}S_{ij}S_{ij}}$$

where $S_{ij} = \sigma_{ij} + p\delta_{ij}$, $p = -\frac{1}{3}\sigma_{ii}$ and δ_{ij} is the Kronecker delta.

9   NONLINEAR STATIC ANALYSIS

In this section nonlinear static analysis is performed on local models for different load cases. The following cases will be evaluated:

- Local ice pressure applied over stiffener design area.
- Local ice pressure applied over plate design area.
- Effects of brackets.
- Shear stress analysis.
- Refinement of mesh.
- Local ice pressure applied on upward breaking design.

The analysis were first of all performed to ensure that the Sevan Arctic MODU did not experience effect of severe nature due to local ice action from 1.5MPa pressure. A parameter study was preformed of increasing ice pressure to determine when the structure experienced yield stress 355MPa in both stiffener and outer hull. Effects of brackets and refinement of mesh was also examined. In the end, an upward breaking design provided from Sevan Marine loaded with 1.5MPa ice pressure was analyzed towards structural capability.

9.1 Local ice pressure applied over stiffener design area

Figure 9.1 shows the von Mises stress contour of the local model subjected to 1.5MPa pressure over the design area for stiffeners. It is observed that the maximum von Mises stress occurs in the flange of the stiffener highlighted in Figure 9.1. The element experiencing the largest von Mises stress has a value of 233MPa. Thus, at a pressure level of 1.5MPa the structural capability will not yield.

S, Mises
fraction = -0.774597
(Avg: 75%)
+2.591e+08
+2.375e+08
+2.159e+08
+1.943e+08
+1.727e+08
+1.511e+08
+1.296e+08
+1.080e+08
+8.637e+07
+6.478e+07
+4.320e+07
+2.161e+07
+1.931e+04

Maximum von Mises stress in stiffener
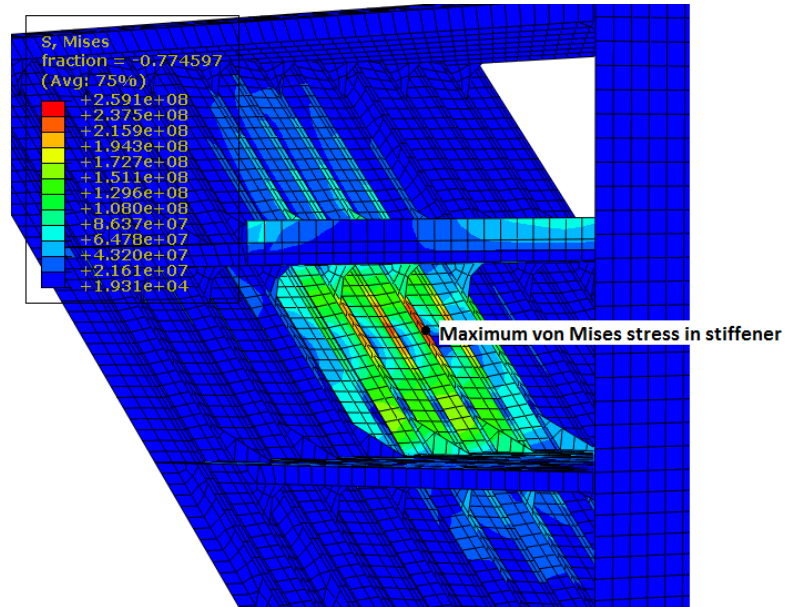
Figure 9.1: von Mises stress contour for 1.5MPa ice pressure over local design area for stiffeners

A parameter check was performed for increasing ice pressure to examine when and where the stiffener first experienced yielding. Figure 9.2 illustrates this, and it is observed that when the stiffener experience stresses near yield stress 355MPa the stiffener has a capability to resists the structural von Mises stresses to reach yield stress, illustrated in Figure 9.2 as the graph flattens. If we take a closer look at where the stiffener experiences the largest stresses it is noted that around ice pressure 4MPa the largest von Mises stress shifts from occurring in the flange to occur in the lower end of the web near the bottom stringer as illustrated in Figure 9.3. This can be assumed is due to geometrical effects to the stiffeners capability to redistributing elastic reaction forces. If we take a closer look at the deformation of the stiffener at 4MPa (see Figure 9.3) the geometrical changes of the stiffener can be better observed. It is observed that the presence of the horizontal stringer and brackets play a significant role in the stiffeners behavior. The stringers and brackets constrain the stiffeners to deform at the ends, while large deformations happen at the middle of the stiffeners.
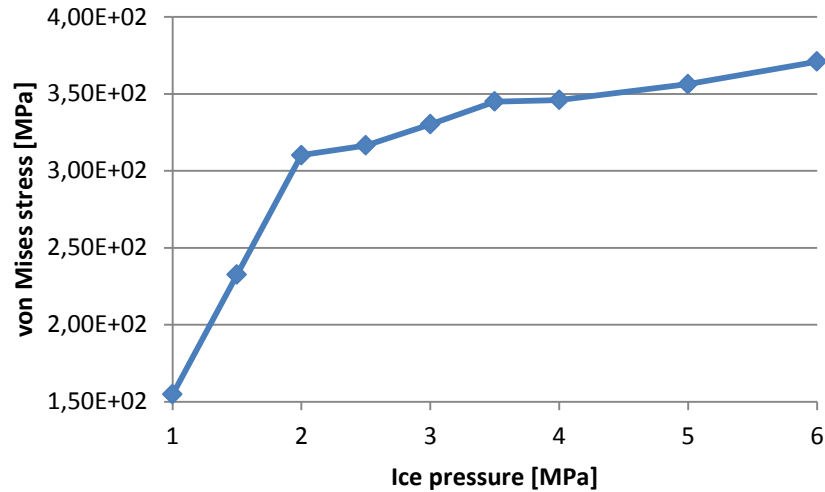
Figure 9.2: Maximum von Mises stress in stiffener versus ice pressure, adapted from Appendix I
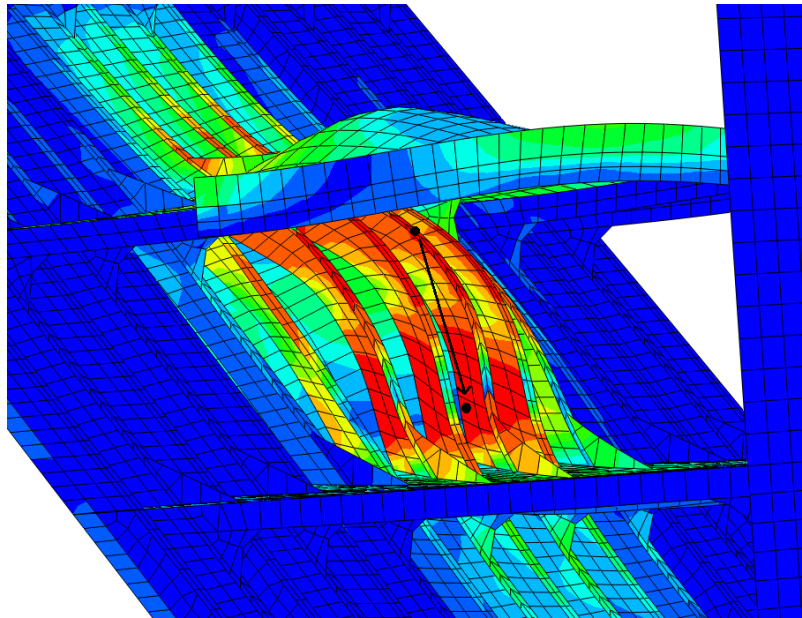
Figure 9.3: 4MPa ice pressure, shift of maximum von Mises stress in stiffeners

From the analyses it is found that yielding in the stiffener will happen around 5MPa ice pressure at the lower end of the web near the bottom stringer.

9.2 Local ice pressure applied over plate design area

The same procedure as above was performed for local ice pressure, but applied over a plate design area. Regarding the increasing ice pressure check it should be kept in mind that yielding happens in stiffeners before the plate yields. However, it is desired to investigate the plate area's behavior, thus yielding of the stiffener will be overlooked.

NONLINEAR STATIC ANALYSIS

Figure 9.4 shows the von Mises stress contour of the local model subjected to 1.5MPa pressure over the design area for plates. It is observed that the maximum von Mises stress occurs in the element highlighted in Figure 9.4. The element experiencing the larges von Mises stress has a value of is 64 MPa. At a pressure level of 1.5MPa the structural capability will not yield.
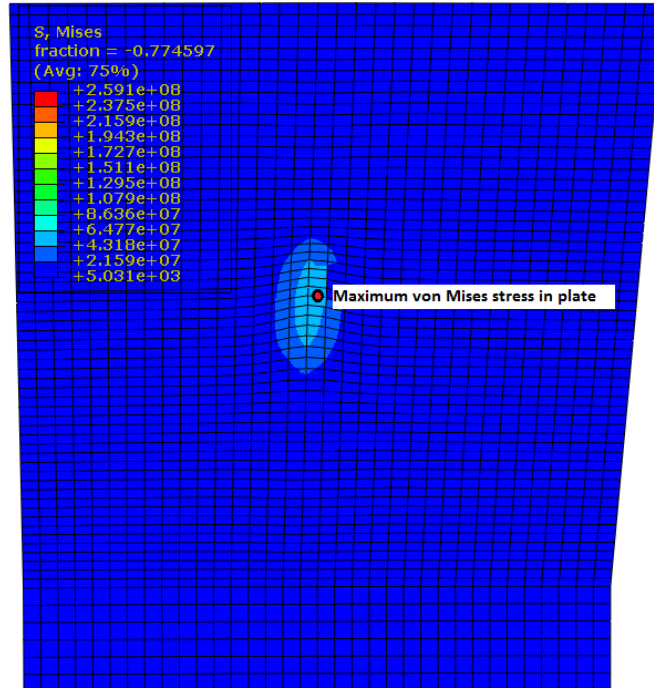
Figure 9.4: 1.5MPa ice pressure over local design area for plate design

An increasing ice pressure check was examined for the local design area for the plate. Figure 9.5 illustrates maximum von Mises stress occurring in the plate for increasing ice pressure, and it is observed that also here will the plate have a capability to resist yielding when the plate experience stresses near yield stress 355MPa. The capability of resisting yield stress is matter of structural capability rather than an isolated capability for the plate alone because the stiffeners will yield long before the plate.
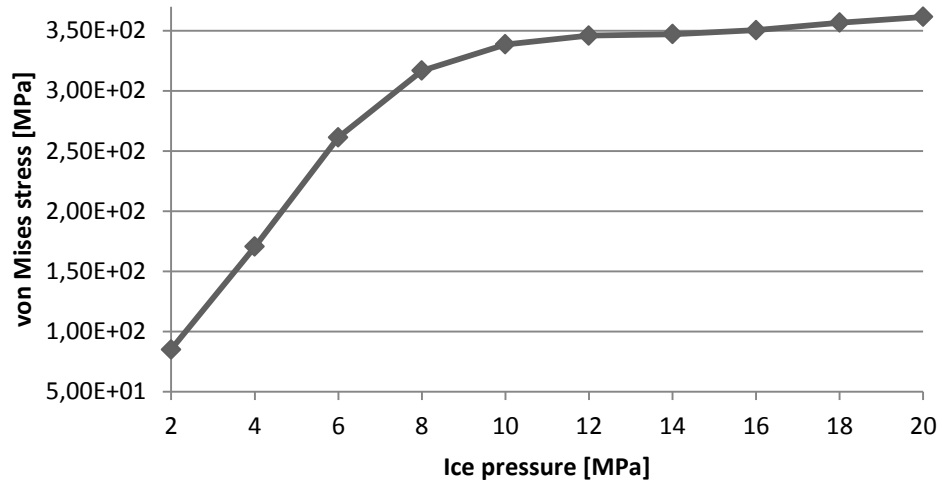
Figure 9.5: Maximum von Mises stress in plate versus ice pressure, adapted from Appendix I

The plate will start to yield around 20MPa ice pressure as shown in Figure 9.6 as the grey area. At this pressure level the stiffener has reached yielding in several locations, illustrated as gray areas in Figure 9.7.
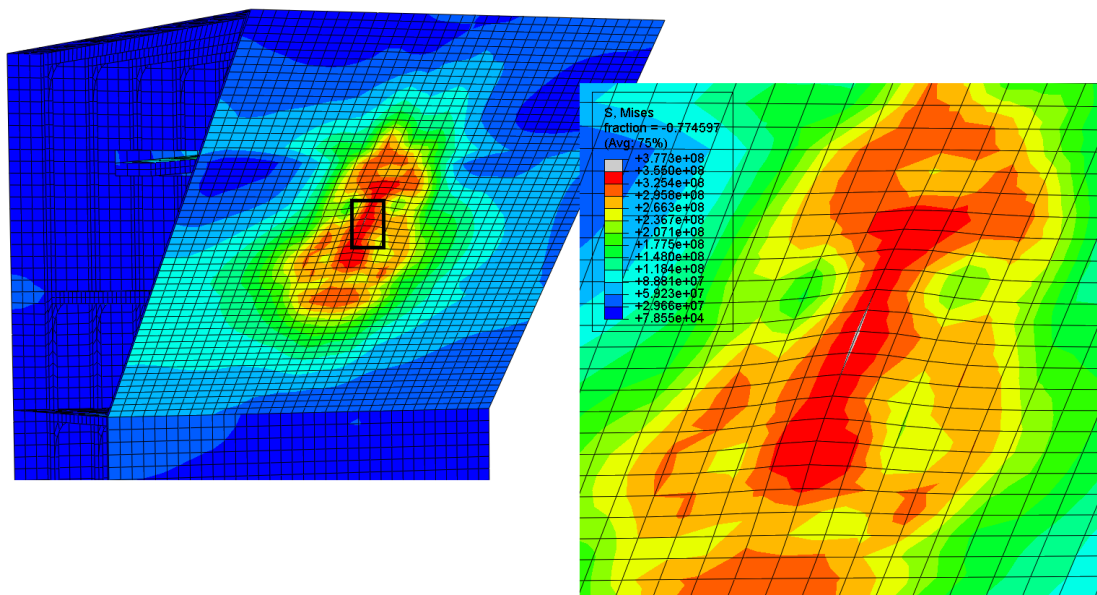
Figure 9.6: von Mises contour of 20MPa ice pressure, gray illustrates yielding in plate
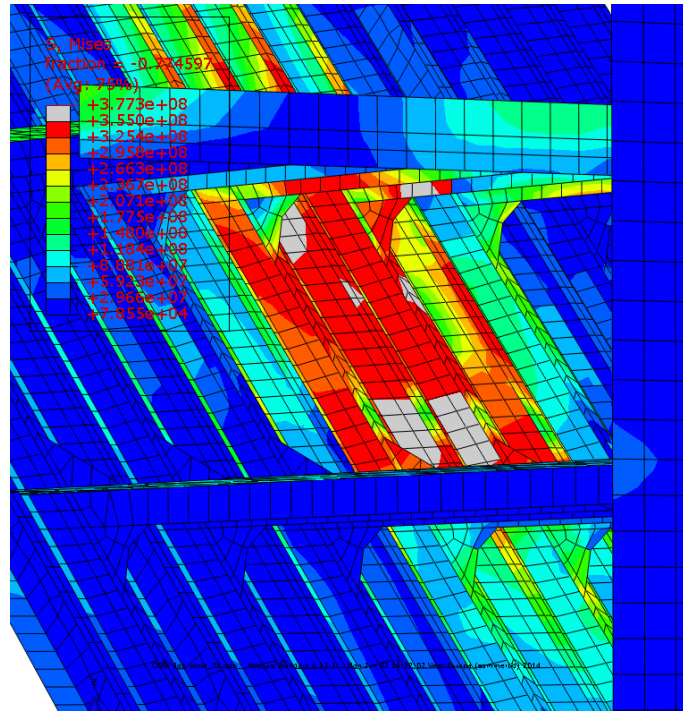
Figure 9.7: von Mises contour of 20MPa ice pressure over plate area

9.3 Effect of brackets

The variation in stress was checked along the path illustrated in Figure 9.8 for von Mises stresses. The location of the path was selected to go along the intersection of the sloping and horizontal stiffener which is the intersection experiencing the largest stresses due to ice pressure loaded over the design area for stiffeners. The same patch was selected for an identical model which used brackets.
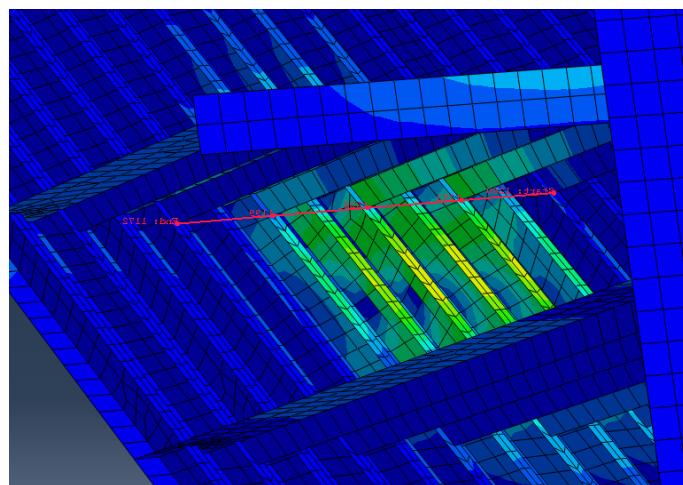
Figure 9.8: Bracket check path

111

In the model using brackets in the intersection of stiffeners, the shape of the bracket was rounded with a radius of 400 mm. Sharp corners are generally not used in design of marine structures, consequently corners are smoothened by introducing brackets.

It is observed from the results in Figure 9.9 and Figure 9.10 that stresses in the intersection corner of the stiffeners were significantly increased when the brackets was removed. The maximum stress increased with 55% by removing the brackets. The asymmetric behavior of the graphs is due to asymmetric boundary conditions and loading of the model.
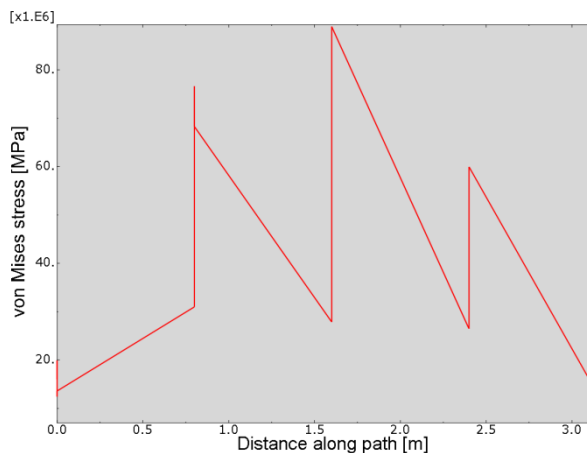
| Figure 9.9: Stress variation along path with brackets | Figure 9.10: Stress variation along path without brackets |
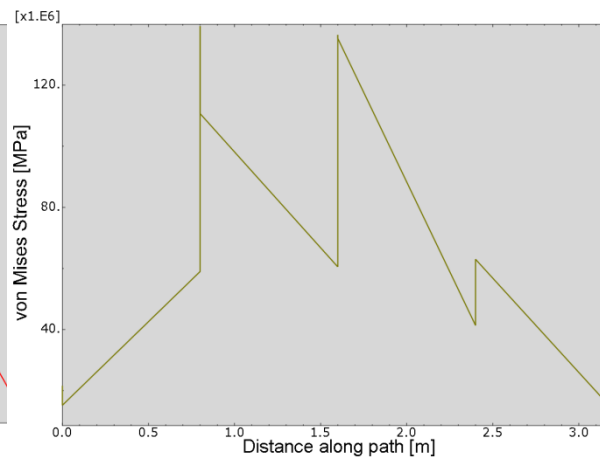
It is noted that singularities may occur in bracket toes when finite element modelling is conducted with a fine mesh (see section 8.5). Such singularity will create locally high stresses and a finer mesh would increase the stress further. In an actual structure the stresses will however not be infinitely large. Singularities will also cause problems in the interpolation of the result. In Figure 9.9 and Figure 9.10 it is observed that an infinite increase in the von Mises stress occurred at 0.8m along the path. This increase can be concluded is due to singularity which occurs in the corner. It was also observed during the convergence analysis when finer mesh was used that locally high stresses occurred in the bracket toe, see Figure 9.11. Element S4R experienced singularity for element size 25mm, 50mm and 100mm. (Moan 2003) recommends to model an even more local, adequate model to ensure that singularities do not appear en the real structure. This will not be investigated in this thesis.
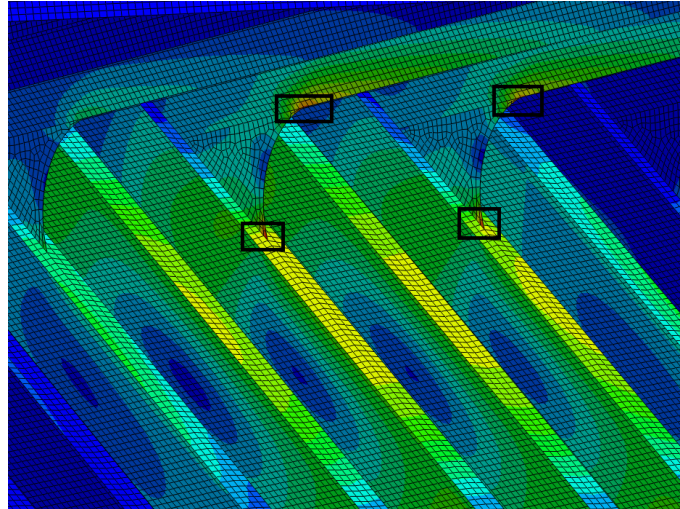
Figure 9.11: Singularity at bracket toes for mesh size 25mm

9.4 Shear stress analysis

The behavior of shear stresses along the sloping stiffeners was examined by moving the ice load to not be subjected in the middle of the two stringers, but as an asymmetric loading situation between the two stringers. A path was selected in ABAQUS for the sloping stiffener that experienced the largest shear forces. It is apparent that it is the web part of the stiffener which experiences the most significant variation in shear stress. Hence, the path was selected to go along the middle of the stiffeners web, see Figure 9.12.
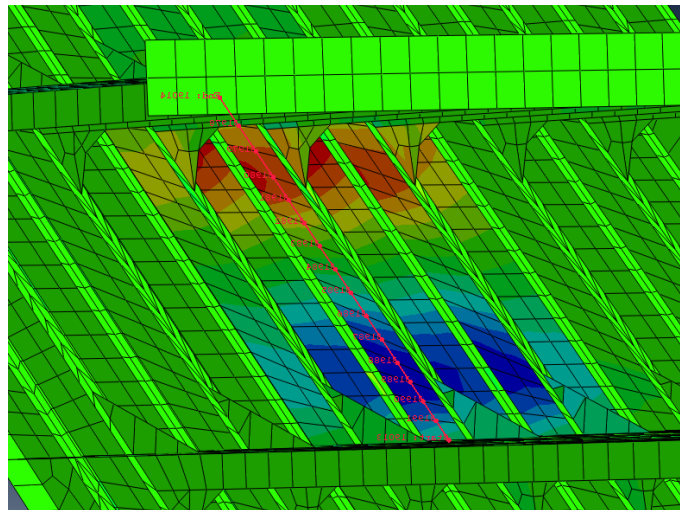
Figure 9.12: Shear check path

Figure 9.13 and Figure 9.14 shows the shear forces along the stiffener for ice pressure applied in the middle and ice pressure applied asymmetric respectively. It is observed that

moving the ice pressure from a symmetric loading to an asymmetric loading does not have a significant effect on the resulting shear forces. However, it is observed that the shape of the graphs peaks are changed from being symmetric to have a more rounded or pointed shape. The value is neither significantly increased nor decreased, but repositioned a little downward. Hence, an asymmetric loading scenario results in a smaller amount of shear forces compared to a symmetric loading scenario.
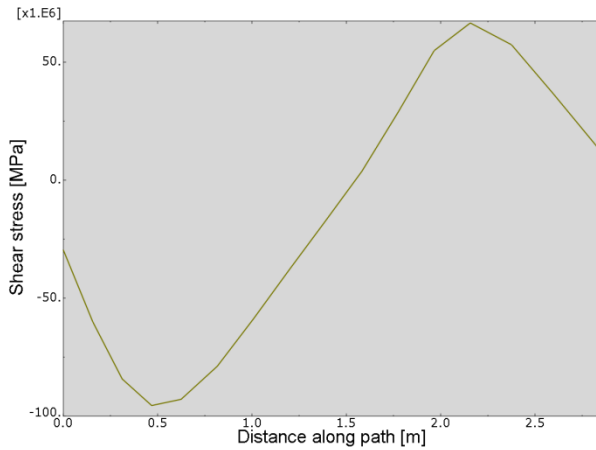
Figure 9.13: Shear forces along the path for ice pressure applied symmetric between stringer
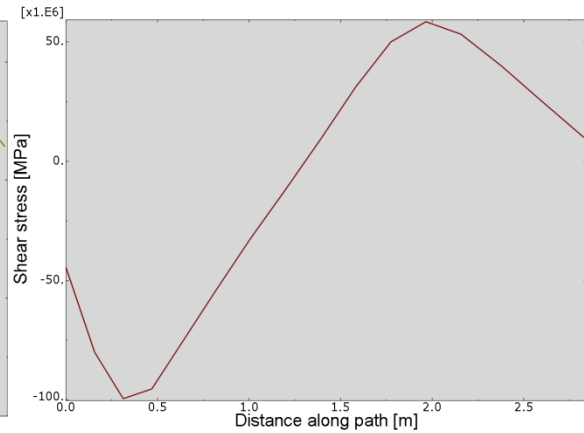
Figure 9.14: Shear forces along the path for ice pressure applied asymmetric between stringer

9.5 Refinement of mesh

ABAQUS contains a very powerful meshing tool that can mesh relatively complicated structures automatically to a relatively optimal distribution of the elements. First the author used ABAQUS's automatic meshing tool inconsequently, but throughout the analysis experienced a large number of bad element behaviors. Especially the element in the stiffeners flange behaved badly. Hence, an improved mesh was generated by the author. The element type and approximate element size were kept the same, but the shape of the elements was improved to have a more quadratic shape. Figure 9.15 and Figure 9.16 shows the mesh of the local model in the ice loaded area for mesh generated by ABAQUS and mesh refined by the author, respectively. Special attention should be directed towards the sloping stiffeners flange's elements and the brackets. The element shapes were improved significantly from a pointed parallelogram shape to a generally more square shape.
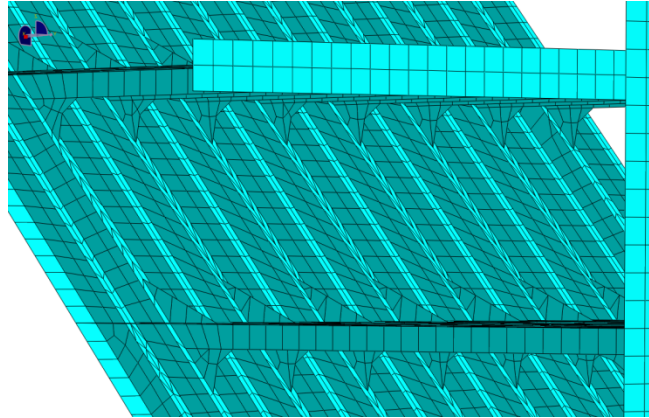
Figure 9.15: Automatic meshing by ABAQUS
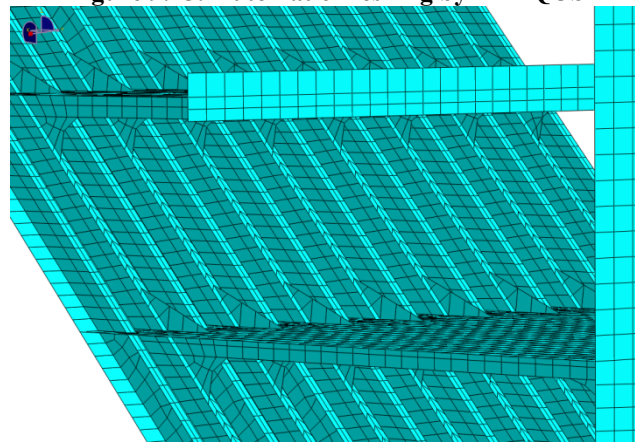
Figure 9.16: Refined mesh by the author

The effect of refining the mesh was examined against the parameter check performed on the stiffener and plate for increasing ice pressure. In Figure 9.17 and Figure 9.18 the maximum von Mises stress occurring in the plate or stiffener are compared for the two mesh alternatives due to increasing ice pressure. In is observed that the built-in meshing tool in ABAQUS and the refined mesh generally gives the same results. However, it is noted that in the cases when the same results is not achieved, the refined mesh provides a more conservative result.
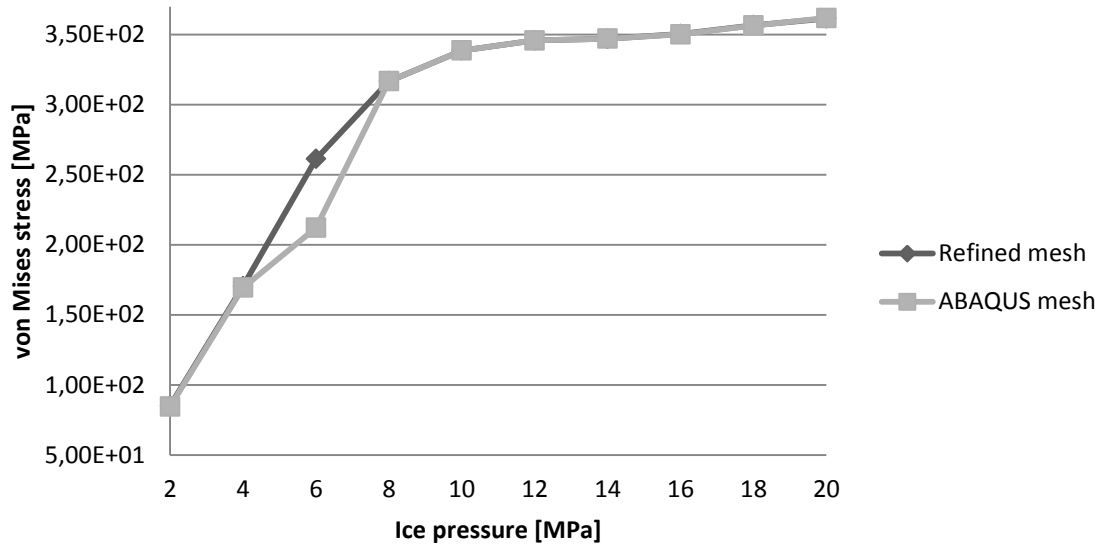
Figure 9.17: Maximum von Mises stress in plate versus ice pressure, adapted from Appendix I
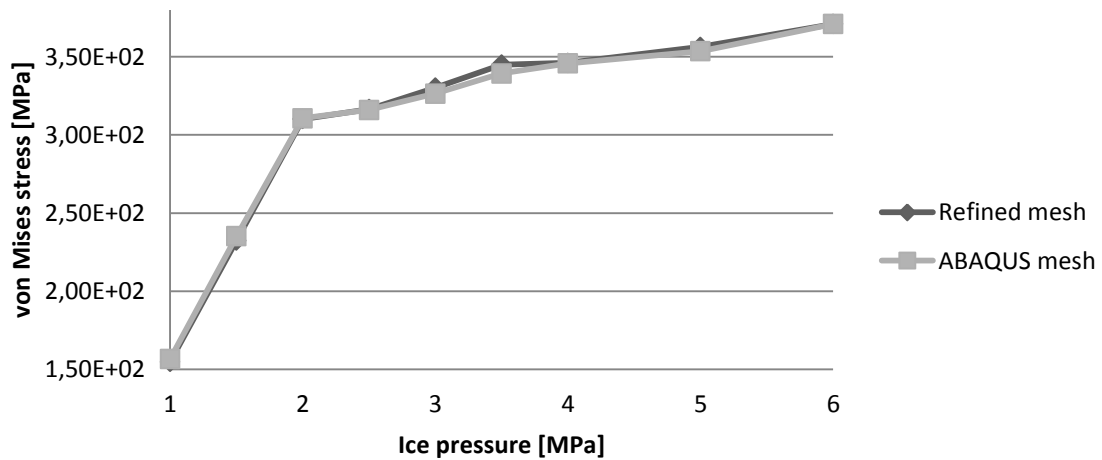
Figure 9.18: Maximum von Mises stress in stiffener versus ice pressure, adapted from Appendix I

9.6 Upward sloping structure

An examination was performed of the design given by Sevan of an upward sloping structure. Ice pressure of 1.5MPa was applied over a local design area for stiffeners design at the design ice draft (12m). Maximum von Mises stress in the outer hull was found to be 45MPa, while maximum von Mises stress in sloping stiffeners was found to be 94MPa. The maximum von Mises stress in in the stiffener occurred in the web of the stiffener just below the intersection with the stringer.
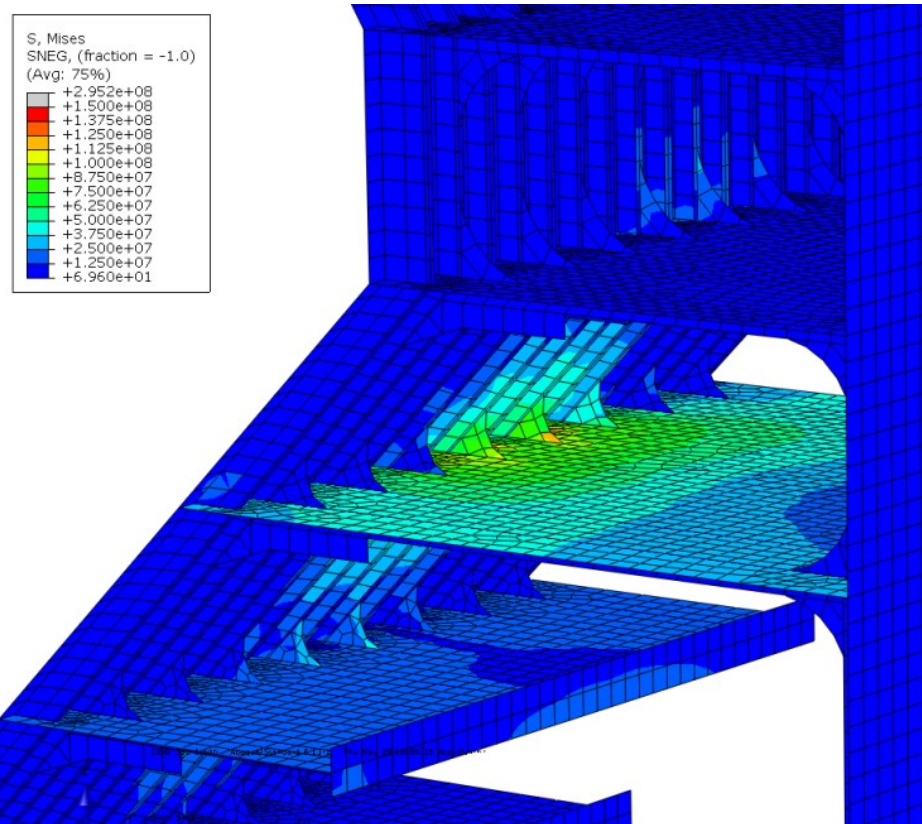
Figure 9.19: von Mises contour from 1.5MPa ice pressure on upward sloping design

Over all, it is observed that it is the horizontal stringer which experiences the largest von Mises stresses. The largest stress, 148MPa, occurs in the stringer close to the intersection between the sloping stiffener which is not stiffened with brackets. The reason why it is the stringer that experiences the largest von Mises stresses can be explained by the location of the ice loading. Compared to the downward sloping design which experiences the ice loading in the middle of two stringers, the upward sloping design experiences the ice loading at the same height as a stringer. Consequently, it is the stringer and brackets that experience the largest von Mises stresses and not the plate or sloping stiffeners. If the effect of hydrostatic pressure is overlooked, the effect of loading ice at the elevation of a stringer compared to the middle of two stringers can be reduced with 36.5 % (if the maximum von Mises stress of downward design and upward design is compared). Most likely, the von Mises stress in the upward sloping design could be reduced even more if all sloping stiffeners where supported with brackets.

It is noted that the design of the upward slope is generally a bad design because of the large empty space between the outer and inner hull. This is generally not an optimal design to obtain a decent structural capacity. If such a design is to be used, it is suggested that the inner structural design should be improved with more stringers to stiffen the structure.

10 DISCUSSION AND CONCLUSION

This thesis has discussed ice loading on a floating offshore structures located in deep water Arctic with sloping hull in the ice action water line, both global ice forces and local ice pressure. Comparison of upwards breaking and downward breaking ice forces has been performed for ice features such as level ice, ridge and managed ice. A design provided from Sevan, named Sevan Arctic Mobile Offshore Drilling Unit, has been used as a reference structure and has been numerically analyzed against local ice pressure to assess structural capability. ABAQUS has been used to perform nonlinear static analysis of a local model extracted from the global design.

Optimization of the engineering challenges presented in the Arctic due to the presence of sea ice becomes a matter of traditional and innovative solutions. A buoy shaped floater with a single point detachment is suggested. One of the reasons for this is because the hull shape has the advantage to reduce loading from ice features from all directions. Ice management will be necessary to practice around floaters in ice infested waters. However, it is useful to estimate loads on floaters from unmanaged ice to define design limits.

Structures with sloping walls in the waterline region will generally experience less ice action compared to vertical walls. Comparison of resulting ice actions on a downward sloping and upwards sloping structure obtained from theoretical formulas for level ice are examined in section 6.3. Ice actions from level ice on the reference structure are calculated to be 15.01MN for downward breaking face. For an upward breaking face the structure experiences 71.09MN. The same theoretical formulation shows that the effect of increasing ice thickness and rubble height are more significant for upwards breaking face than for downward breaking face. This is convenient because the presence of sea water when the ice is bent downward will clear away the broken ice pieces more easily.

A recently published approach by (Croasdale 2012) to determine ice actions from first-year ridges on sloping structures is examined in this thesis. The approach was applied on the reference structure and it concludes that an upwards breaking face will experience

DISCUSSION AND CONCLUSION

24.18 MN, and a downward breaking face will experience 37.30 MN. In other words, it is suggested to design a floater with upward sloping hull to reduce ice actions from first-year ridges. This approach does not take geometrical parameters such as width and angle of slope into consideration, as well as the effect of breaking ice into water rather than air. Hence, the author suggests not using the approach uncritically before it is improved to also include these parameters influences. The approach was examined for increasing ridge geometrical parameters consolidated layer thickness and keel height. It was observed that the effect of the direction of the slope is less significant for ridges than for level ice. In addition, ice forces were noted to increase slower for increasing parameters compared to level ice. Based on the theoretical formulations used in this thesis it can be concluded that increasing level ice thickness is more severe than increasing geometrical sizes of a ridge if the face is bending ice upwards, but opposite if the face is bending ice downwards.

Managed ice forces are determined from full scale experiments on the Kulluk drilling unit. The obtained ice actions on the reference structure from managed ice are considerable lower than resulting forces from level ice and ridges, and are found to have an upper limit of 0.26MN.

The effect of increasing rubble height for level ice actions has been investigated for the theoretical formulations used in this thesis. It is observed that the increasing height had a significant effect on the resulting ice action for both upward and downward face. However, the formulations do not take geometrical changes in the hull structure into consideration. Thus, the results obtained for the Sevan Arctic MODU are assumed to be conservative. The geometry of the hull and operation draft – of the present design of the Sevan Arctic MODU- are designed with a very small clearance (2m) for the sloping geometry to the vertical geometry. Rubble will easily rise and accumulate upward the vertical wall and ice pieces may fail by crushing against the vertical wall. The author suggests to improve the hull design with a draft that will give a higher vertical clearance to avoid ice crushing.

120

DISCUSSION AND CONCLUSION

Local ice pressure on sloping structures is not, as of today, discussed in any literature. Hence, several approaches to determine local ice pressure are presented and compared in section 6.9. A uniformly distributed ice pressure of 1.5MPa is concluded to be sufficient for sloping structures. The pressure was applied to a local model in ABAQUS and structural capability was investigated for plate and stiffener. Maximum von Mises stress in stiffener was 233MPa and 64MPa in plate. A parameter check of increasing ice pressure found that yielding would first happen in the sloping stiffeners web at ice pressure 4MPa, while the plate started yielding at ice pressure 20MPa. The author suggests decreasing plate thickness and increasing the stiffener capability to decrease this scattering in structural capability between stiffener and plate.

The local model has also been examined against other parameter, such as effect of brackets, asymmetric loading and refinement of mesh. Analysis of brackets' effect establishes that presence of brackets in intersections between stiffeners reduces the resulting structural stresses significantly. It is thus suggested to use brackets in marine structures, especially in areas experiencing significant load. The load reduction is due to the bracket's capacity of transporting and distributing stresses. Based on analysis performed on symmetric and asymmetric loading it can be concluded that this will not affect the resulting shear forces significantly. Examination of mesh refinement can conclude that bad shaped element results in non-conservative stresses compared to decent shaped elements. It is therefore suggested that the element mesh geometry should be refined to obtain the most conservative results.

A final examination has been performed on an upward sloping design. Interesting results from this analysis are not the effect of downward sloping face compared to upwards sloping face because the local ice pressure was applied normal to the surface either way. However, the upward sloping design is designed with an ice operational draft where the ice loads are subjected at the elevation of a stringer compared to the downward breaking design where the ice loads are subjected between two stringers. Respectively, the resulting von Mises stress 148MN was located in the stringer and had a lower value compared to the downward design which experienced 233MN in the sloping stiffeners

flange. Consequently, it is suggested to design a floater in ice-infested waters to have an ice operational draft at the same elevation as a strong stringer.

11 RECOMMENDATION FOR FURTHER WORK

In the course of working with this thesis, there have been identified issues that needs further work.

Certainly, detail can always be added to a model to be more secure about results. For instance, a global model could be model first, such that a local model could be extracted from this. The benefit of this is that correct boundary condition can be transported into the local model. Another improvement could be performed if a local model is modelled even smaller, such that only the ice action area is included (with transported boundary conditions from this thesis model). A smaller model can consequently perform analysis more easily with smaller elements, and the results will be more correct.

There are many parameters to be checked against a floater for deep water developments in the Arctic. The velocity of the drifting ice is one of them. A nonlinear analysis of the effect from transient ice loading due to ice drift should be performed, as well as impact effects over small areas. Icebergs may induce collision accidents, thus it is suggested to check the scantling against collision loads.

Due to small vertical clearance (2m) the Arctic Sevan MODU are likely to experience crushing of broken ride up ice on the vertical wall. Further investigation of the structures capability to withstand the effect of ice crushing on the vertical wall as well as the sloping face is suggested to conduct.

In this thesis, the scantling of the Sevan Arctic MODU was investigated with regards to yielding and it was recommended to decrease plate thickness and increase the stiffener capability to decrease this scattering in structural capability between stiffener and plate. A study with regards to this issue should be performed to optimize stiffener and plate scantling.

Generally model testing is wanted to confirm results. Especially if a buoy shaped interface is used.

12 REFERENCES

ABAQUS (2013). "ABAQUS 6.13 Documentation." Dassault Systèmes Simulia Corp. Retrieved 07.06.2014, from http://50.16.176.52/v6.13/.

Aggarwal, R. and R. Souza (2011). Deepwater Arctic - Technical Challenges and Solutions, Offshore Technology Conference -OTC.

Croasdale, K. R. (2012). A simple model for first-year ridge loads on sloping structures. International Conference and Exhibition on Performance of Ships and Structures in Ice 2012, ICETECH 2012.

Dalane, O., et al. (2009). A moored arctic floater in first-year sea ice ridges. Proceedings of the International Conference on Offshore Mechanics and Arctic Engineering - OMAE.

DNV (1999). Strength Analysis of Hull Structures in Tankers. Classification Note No. 31.3. Det Norske Veritas, January 1999.

DNV (2013). Determination of Structural Capacity by Non-linear FE analysis Methods. DNV-RP-C208, Det Norske Veritas AS, June 2013.

Dolgopolov, Y. V., et al. (1975). "Effect of hummocked ice on the piers of marine hydraulic structures." Proc. 3rd Int. Symp on Ice Problems: 469-477.

Fenz, D. M., et al. (2010). Multi-year ice model tests on caissons with downward breaking cones. International Conference and Exhibition on Performance of Ships and Structures in Ice 2010, ICETECH 2010.

Hamilton, J. M. (2011). The Challenges of Deep Water Arctic Development, International Society of Offshore and Polar Engineers -ISOPE.

Helgesen, O. K. (2013). "Nå pepres Barentshavet med brønner." Teknisk Ukeblad. Retrieved 07.06.2014, from http://www.tu.no/petroleum/2013/10/03/na-pepres-barentshavet-med-bronner.

IACS (2011). Requirements concerning POLAR CLASS International Association of Classificatin Societies - 2011.

ISO19906 Petroleum and natural gas industries - Arctic offshore structures Geneva, International Standards Oraganisation -2010: 465 s. : ill.

Iyerusalimskiy, A., et al. (2012). A conceptual study of deepwater arctic floater for year-round drilling and production. International Conference and Exhibition on Performance of Ships and Structures in Ice 2012, ICETECH 2012.

REFERENCES

Løset, S. and O. T. Gudmestad (2006). <u>Actions from ice on Arctic offshore and coastal structures</u>. St. Petersburg, Lan.

Løset, S., et al. (1998). <u>Ice physics and mechanics</u>. Trondheim, Norwegian University of Science and Technology.

Mathisen, K. M. (2012). Lecture notes from "TMR 4190 - Finite element methods in structural analysis". distributed by the Norwegian Uneversity of Science and Technology, autmn 2012.

Moan, T. (2003). <u>Finite element modelling and analysis of marine structures</u>. Trondheim, Marinteknisk senter.

Moan, T. (2003). <u>Finite element modelling and analysis of marine structures (chapter 12 - Nonlinear analysis UNPUBLISHED)</u>. Trondheim, Marinteknisk senter.

Nyhus, A. A. (2014 pers.comm. 10 May). Discussion about selection boundary condition.

Nyseth, H. (2014). POLAR CLASS -Brief discussion on the background and application of the rules. DNV - Maritime Advisory.

Palmer, A. and K. Croasdale (2013). <u>Arctic offshore engineering</u>. Singapore, World Scientific.

Rasmussen, A. N. (2011). Steel tower for a wind turbine, Google Patents.

Riska, K. (2013). Lecture notes from "Ship Design for Ice" distributed by the Norwegian Uneversity of Science and Technology, autumn 2013.

Sanderson, T. J. O. (1988). <u>Ice mechanics: risks to offshore structures</u>. London, Graham & Trotman.

SMHI (2012). "Sea Ice." <u>Swedish Meteorological and Hydrological Institute</u>. Retrieved 02.03.2014, from http://www.smhi.se/en/theme/sea-ice-1.11198.

Srinivasan, N., et al. (2008). <u>Design of a Non-Ship-Shped FPSO for Sakhalin-V Deepwater</u>, Society of Petroleum Engineers.

Sudom, D. and R. Frederking (2010). <u>A closer examination of the May 12, 1986 ice floe impact with the Molikpaq</u>. International Conference and Exhibition on Performance of Ships and Structures in Ice 2010, ICETECH 2010.

Timco, G. W. and M. Johnston (2003). "Ice loads on the Molikpaq in the Canadian Beaufort Sea." <u>Cold Regions Science and Technology</u> **37**(1): 51-68.

Timco, G. W. and W. F. Weeks (2010). "A review of the engineering properties of sea ice." <u>Cold Regions Science and Technology</u> **60**(2): 107-129.

REFERENCES

UF (2014). "Derivation of von Mises Criterion." University of Florida. Retrieved 01.06.2014, from http://www2.mae.ufl.edu/nkim/eas4200c/VonMisesCriterion.pdf.

WMO (1989). "Sea Ice Nomenclature." World Meteorological Organization. Retrieved 02.03.2014, from http://www.aari.nw.ru/gdsidb/docs/wmo/nomenclature/WMO_Nomenclature_draft_version1-0.pdf.

Wright, B. (2000). "Full Scale Experience with Kulluk Stationkeeping Operations in Pack Ice (With Reference to Grand Banks Developments)." Report to National Research Council of Canada.

APPENDIX

A – Memo from Sevan Marine

B – Sevan Arctic MODU drawings

      B1 – Downward sloping design

      B2 – Upward sloping design

C – Initial values

D – Excel Method 1 – Level ice

      D1 – Increasing ice thickness

      D2 – increasing ride up height

E – Excel Method 2 –Level ice

      E1 – Increasing ice thickness

      E2 – Increasing rubble thickness

F – Excel – Ridge

      F1 – Increasing consolidated layer thickness

      F2 – Increasing keel height

G – Local ice pressure

H – Convergence analysis

I – Increasing ice pressure and mesh study

APPENDIX

A – Memo from Sevan Marine

Memo		SEVAN marine	
To:	Ine Haugen	**Date:**	20.01.2014
Cc:	Otto Skjaastad, Audun Nyhus, Ragnar Thunes	**Doc. Id.:**	
From:	Hans Olav Sele	**Project No.:**	
Approved by:	Ragnar Thunes	**Project Title:**	Project work at NTNU
Subject:	Sevan Hull exposed to Ice		

Table of Contents

1 BACKGROUND

1.1 Project Work

This memo is written with intention to define a task for analysis by the student in order to understand the design of the circular hull and to define the necessary design loads to be considered in the project work.

It is suggested that the student build up a relevant model for the ice and model the relevant (exposed) parts of the structure in order to quantify the level of deformation and damage to the structure during impact.

The information in this memo may be supplemented with additional computer files etc. available for the design.

2   HULL DESIGN

2.1   Hull Form

Sevan Marine is in the process of designing an arctic intended for oil exploration in the arctic environments. The hull form is characterized by a cylindrical main body extended with a "bilge box" (skirt) at the lower section of the hull. The hull is flared in order to manage ice loads and have the possibility to break ice.There are to two variations of the hull that is considered in the design phase.

1. Downward breaking cone
2. Upward breaking cone

The difference in the hull form should be evalutated in terms of behavior in ice conditions.

Figure 2-1   Hull Form

2.1.1   Arrangement

The hull is a typical plate/beam structure featuring vertical bulkheads, horizontal stringers, decks and frames. Some of the key structural characteristics are summarized below:

- Double side structure, depth 3.5 m
- Horizontal stringers, spacing (typical) 4.0 m
- Horizontal stringers, Ice Belt 2.0 m
- Typical stiffener spacing in panels is typically in the range of 800 mm.
- Stiffener spacing in icebelt (whole side) is 400 mm

Figure 2-2 shows the structural arrangement of the hull.

Figure 2-2 Hull Section View

2.1.2   Materials

The hull will be constructed in carbon steel. The material selection for the FPSO is carbon steel with yield strength of 355 MPa (NV36 – DNV Certified steel in accordance with DNV OS-B101) will be used for plated structure including profiles.

2.1.3   Hull Size

Figure 2-3 Hull Size

Table 2-1 Main Dimensions and Draft

Item		Upward breaking Cone	Downward breaking Cone
Main Hull Diameter	(m)	75.0	
Main Deck Diameter	(m)	113.0	
Double Bottom Height	(m)	3.5	
Double Side Breadth	(m)	5.0	
Main Deck El. (Hull depth)	(m)	24.0	
Draft, Transit	(m)		10.0
Draft, Ice Operation	(m)	12.0	15.0

2.1.4 Structural Arrangement

Stiffener spacings in the side shell:

Figure 2-4 Typical Radial Cross Section

Figure 2-5 Hull Section View, Plates

Figure 2-6 Hull Section View, Profiles

APPENDIX

3 ICE LOADS

3.1 General

The hull is designed to take the ice loads from any direction for the ultimate limit state analysis.

The hull will be designed in accordance with Polar Class (DNV or equivalent), PC4. (PC4 rule formulas may be used to determine scantlings.)

The operation will be in typical 1st year ice condition.

The following data should be considered in the design:

Table 3-1 Ice Load Scenarios

Ice feature	Thickness	Comment
Level Ice	1.20 m	Some typical ice data: Density 890 kg/m3 Bending strength 500 kPa Compressive Strength 1.2 MPa Emodulus 3.5 GPa
Managed Ice	1.20 m	Floe size 100 m x 100 m Ice data as above
Ice Ridges		Sail height 9.3 m Keel depth 21 m Consolidated layer thickness 3 m Bending strength consolidated layer 640 kPa Compressive strength consolidated layer: 1.5 MPa

APPENDIX

B – Sevan Arctic MODU drawings

B1 – Downward sloping design

EL 8000

ICE DRAFT

OPEN WATER DRAFT

HOLD

2000

EL. 20 000

EL. 16 000

EL. 12 000

EL. 8 000

EL. 4 000

B.L.

VIII

B2 – Upward sloping design

LONGITUDINAL SECTION

45° 11000

15000

Ice draft

Open water draft

2000

APPENDIX

THRUSTER INSTALLATION ROOM

ROV

MOORING

BW3PS

MDO3   MDO2

MDO4

ROV   MDO1

HAZ DRAIN

NONE
HAZ
DRAIN 2

NONE
HAZ
DRAIN 1

RES5

THRUSTER INSTALLATION ROOM

THRUSTER INSTALLATION ROOM

DW2

DW1

FW3

FW2

FW1

Elevator

MOORING

MUD4   MUD3   MUD2   MUD1

DRY BULK

MOORING

BW5PS   BW6PS   BW7PS   BW5PS   BW3PS   BW2PS   BW1PS   BW2SB   BW3SB   BW4SB   BW6SB   BW7SB   BW8SB

MOORING

BW

EL 12000

X

APPENDIX

C – Initial value

Description	Parameter	Value
Sevan structure:		
Ice action line diameter	w	81 m
Waterline diameter	w_T	75 m
Draft	d	17 m
Angel of slope	α	45 degrees
Level ice:		
Thickness	h	1.2 m
Flexural (bending) strength	σ_f	$5*10^5$ Pa
Young's modulus	E	$5*10^9$ Pa
Density ice	ρ_i	890 kg/m^3
Density seawater	ρ_w	1025 kg/m^3
Poisson's ratio	v	0.3
Acceleration of gravity	g	9.81 m/s^2
Ice-structure friction	μ	0.1
Ice-ice friction	μ_i	0.05
Rubble:		
Height	h_r	17 m
Porosity	e	0.3
Cohesion	c	$5*10^3$ Pa
Friction angle (upward)	φ	40 degrees
Friction angle (downward)	φ	0 degrees
Angle of repose	θ	35 degrees
Ridge:		
Width	W	70 m
Consolidated layer thickness	h_{cl}	3 m
Consolidated layer modulus	E_{cl}	$5*10^9$ Pa
Consolidated layer flexural strength	σ_{cl}	$5*10^5$ Pa
Keel height	h_k	21 m
Keel modulus ($E_k=E_{cl}/15$)	E_k	$0.33*10^9$ Pa
Keel flexural strength (tensile failure)	$\sigma_{1,k}$	$0.25*10^5$ Pa
Keel flexural strength (compressive failure)	$\sigma_{2,k}$	$0.5*10^5$ Pa

D – Excel Method 1 – Level ice

Input	Value	Dimention	Explenation
σ_f	500000,000	Pa	flexural strength of the ice sheet
h	1,200	m	thickness of ice sheet
ρ_ice	890,000	kg/m3	density of ice (upward)
ρ_w	1025,000	kg/m4\3	density of seawater
ρ_b	135,000	kg/m3	buoyant weight of ice (downward)
g	9,814	m/s2	acceleration of gravity
w	81,000	m	waterline diameter of the cone or with the sloping structure
α	45,000	deg	slope of the structure [degrees]
α	0,785	rad	slope of the structure [-]
μ	0,100		ice-structure friction coefficient
w_T	75,000	m	top diameter of cone
h_r	17,000	m	ice ride-up thickness (h_r>h)
Y	3,422		yielding (2.711 for Tresca yielding or 3.422 for Johnsen yielding)
G_up	23,878		equal to (ρ_i*g*w^2)/(4*σ_f*h)
G_down	3,622		equal to ((ρ_w-ρ_i)*g*w^2)/(4*σ_f*h)
E_1	1,854		complete elliptical integral of first order
E_2	1,351		complete elliptical integral of second order

Parameters

f	0,838
g_r	2,028
h_v	1,021
W_up	49137814,549
W_down	7453488,724
x_up	1,117
x_down	1,282

D1 – Increasing ice thickness

UPWARD SLOPING

h	G	x	H_B	V_B	H_R	V_R	F_H	F_V
0,2	143,267	1,04814	378801,594	386749,0668	62553191,22	69994215	62,93199282	70,38096
0,4	71,633	1,067945	1110038,86	1133328,111	62553191,22	69994215	63,66323009	71,12754
0,6	47,756	1,083052	2094441,63	2138384,204	62553191,22	69994215	64,64763285	72,1326
0,8	35,817	1,095712	3296930,33	3366101,801	62553191,22	69994215	65,85012156	73,36032
1	28,653	1,1068	4697389,78	4795943,68	62553191,22	69994215	67,250581	74,79016
1,2	**23,878**	**1,116766**	**6282346,19**	**6414153,385**	**62553191,22**	**69994215**	**68,83553742**	**76,40837**
1,4	20,467	1,125877	8041975,97	8210701,197	62553191,22	69994215	70,5951672	78,20492
1,6	17,908	1,134309	9968717,57	10177866,93	62553191,22	69994215	72,5219088	80,17208
1,8	15,919	1,142182	12056525,7	12309478,46	62553191,22	69994215	74,60971693	82,30369
2	14,327	1,149586	14300429,6	14600460,76	62553191,22	69994215	76,85362085	84,59468
2,2	13,024	1,156587	16696252,6	17046549,46	62553191,22	69994215	79,24944382	87,04076
2,4	11,939	1,163239	19240424	19644098,99	62553191,22	69994215	81,79361519	89,63831
2,6	11,021	1,169583	21929848	22389948,64	62553191,22	69994215	84,4830392	92,38416
2,8	10,233	1,175652	24761809	25281325,83	62553191,22	69994215	87,31500024	95,27554
3	9,551	1,181475	27733901,3	28315774,29	62553191,22	69994215	90,28709251	98,30999

DOWNWARD SLOPING

h	G	x	H_B	V_B	H_R	V_R	F_H	F_V
0,2	21,732	1,122256	168065,96	171592,0791	9488405,411	10617100	9,65647137	10,78869
0,4	10,866	1,170726	516392,799	527227,0133	9488405,411	10617100	10,00479821	11,14433
0,6	7,244	1,206537	1007928,15	1029075,052	9488405,411	10617100	10,49633356	11,64618
0,8	5,433	1,235639	1630032,8	1664231,813	9488405,411	10617100	11,11843821	12,28133
1	4,346	1,260379	2375636,16	2425478,352	9488405,411	10617100	11,86404157	13,04258
1,2	**3,622**	**1,281978**	**3240102,29**	**3308081,474**	**9488405,411**	**10617100**	**12,7285077**	**13,92518**
1,4	3,105	1,301176	4220116,79	4308657,238	9488405,411	10617100	13,7085222	14,92576
1,6	2,716	1,31846	5313175,51	5424648,954	9488405,411	10617100	14,80158092	16,04175
1,8	2,415	1,334173	6517312,32	6654049,23	9488405,411	10617100	16,00571773	17,27115
2	2,173	1,348569	7830939,12	7995236,668	9488405,411	10617100	17,31934453	18,61234
2,2	1,976	1,36184	9252745,02	9446872,863	9488405,411	10617100	18,74115043	20,06397
2,4	1,811	1,374139	10781629,1	11007833,84	9488405,411	10617100	20,27003455	21,62493
2,6	1,672	1,385587	12416654	12677162,43	9488405,411	10617100	21,90505939	23,29426
2,8	1,552	1,396284	14157011,9	14454034,07	9488405,411	10617100	23,64541733	25,07113
3	1,449	1,406313	16002000,4	16337731,48	9488405,411	10617100	25,49040583	26,95483

Upward: Ice forces versus ice thickness
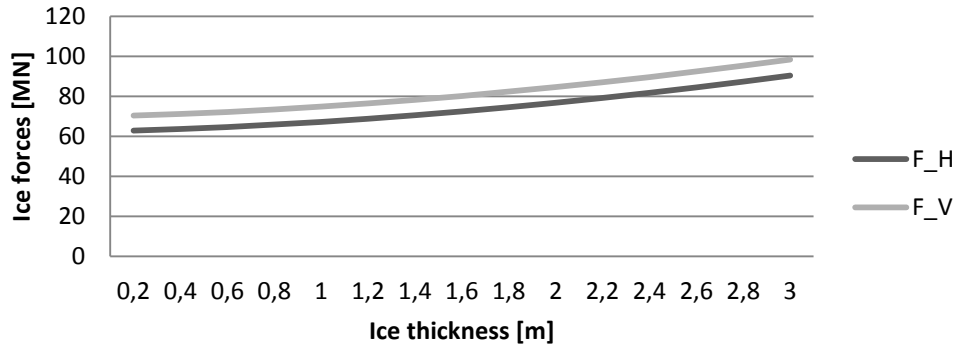
Downward: Ice forces versus ice thickness
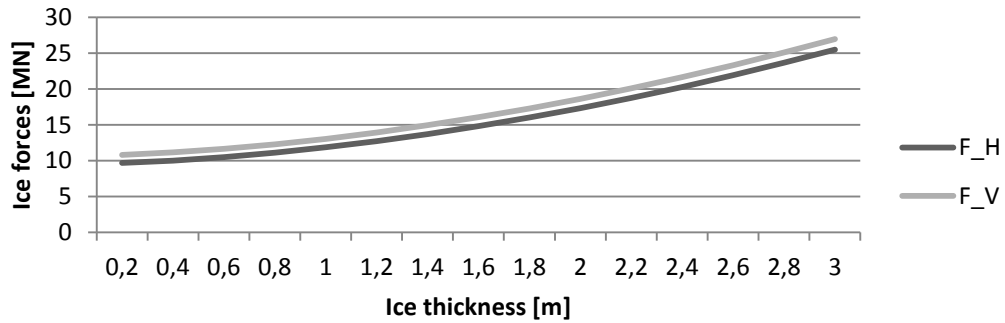
Upward vs. Downward: ice thickness *h*

D2 – Increasing ride up height

UPWARD SLOPING

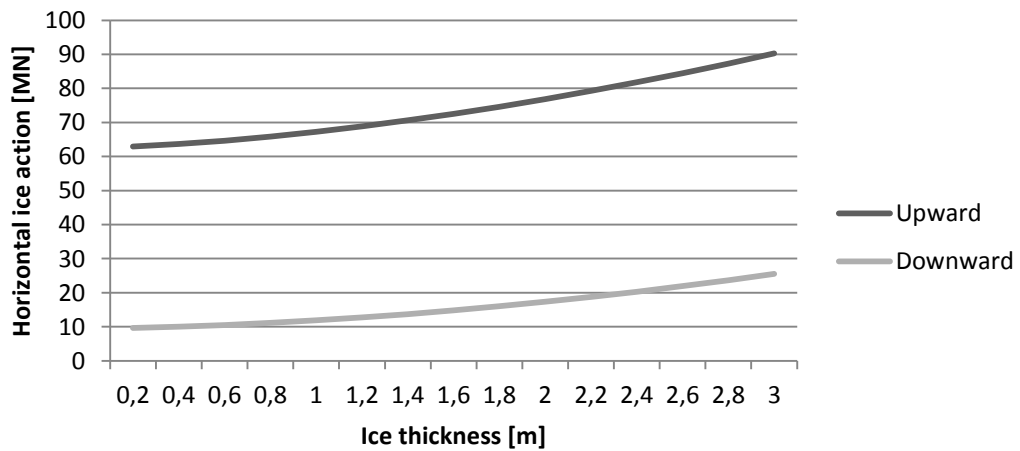| h_r	W	H_B	V_B	H_R	V_R	F_H	F_V
2	5780919,359	6282346,2	6414153,38	7359198,968	8234613,509	13,6415452	14,64876689
4	11561838,72	6282346,2	6414153,38	14718397,94	16469227,02	21,0007441	22,8833804
6	17342758,08	6282346,2	6414153,38	22077596,9	24703840,53	28,3599431	31,11799391
8	23123677,43	6282346,2	6414153,38	29436795,87	32938454,04	35,7191421	39,35260742
10	28904596,79	6282346,2	6414153,38	36795994,84	41173067,54	43,078341	47,58722093
12	34685516,15	6282346,2	6414153,38	44155193,81	49407681,05	50,43754	55,82183444
14	40466435,51	6282346,2	6414153,38	51514392,77	57642294,56	57,796739	64,05644795
16	46247354,87	6282346,2	6414153,38	58873591,74	65876908,07	65,1559379	72,29106145
18	52028274,23	6282346,2	6414153,38	66232790,71	74111521,58	72,5151369	80,52567496
20	57809193,59	6282346,2	6414153,38	73591989,68	82346135,09	79,8743359	88,76028847
22	63590112,95	6282346,2	6414153,38	80951188,64	90580748,6	87,2335348	96,99490198
24	69371032,3	6282346,2	6414153,38	88310387,61	98815362,11	94,5927338	105,2295155
26	75151951,66	6282346,2	6414153,38	95669586,58	107049975,6	101,951933	113,464129
28	80932871,02	6282346,2	6414153,38	103028785,5	115284589,1	109,311132	121,6987425
30	86713790,38	6282346,2	6414153,38	110387984,5	123519202,6	116,670331	129,933356
17	**49137814,55**	**6282346,2**	**6414153,38**	**62553191,22**	**69994214,82**	**68,8355374**	**76,40836821**

DOWNWARD SLOPING

h_r	W	H_B	V_B	H_R	V_R	F_H	F_V
2	876881,0263	3240102,3	3308081,47	1116282,989	1249070,588	4,35638528	4,557152062
4	1753762,053	3240102,3	3308081,47	2232565,979	2498141,177	5,47266827	5,806222651
6	2630643,079	3240102,3	3308081,47	3348848,968	3747211,765	6,58895126	7,055293239
8	3507524,105	3240102,3	3308081,47	4465131,958	4996282,354	7,70523425	8,304363827
10	4384405,132	3240102,3	3308081,47	5581414,947	6245352,942	8,82151724	9,553434416
12	5261286,158	3240102,3	3308081,47	6697697,937	7494423,53	9,93780022	10,802505
14	6138167,184	3240102,3	3308081,47	7813980,926	8743494,119	11,0540832	12,05157559
16	7015048,211	3240102,3	3308081,47	8930263,916	9992564,707	12,1703662	13,30064618
18	7891929,237	3240102,3	3308081,47	10046546,91	11241635,3	13,2866492	14,54971677
20	8768810,263	3240102,3	3308081,47	11162829,89	12490705,88	14,4029322	15,79878736
22	9645691,289	3240102,3	3308081,47	12279112,88	13739776,47	15,5192152	17,04785795
24	10522572,32	3240102,3	3308081,47	13395395,87	14988847,06	16,6354982	18,29692853
26	11399453,34	3240102,3	3308081,47	14511678,86	16237917,65	17,7517812	19,54599912
28	12276334,37	3240102,3	3308081,47	15627961,85	17486988,24	18,8680641	20,79506971
30	13153215,39	3240102,3	3308081,47	16744244,84	18736058,83	19,9843471	22,0441403
17	**7453488,724**	**3240102,3**	**3308081,47**	**9488405,411**	**10617100**	**12,7285077**	**13,92518148**

Upward: Ice forces versus ride up height
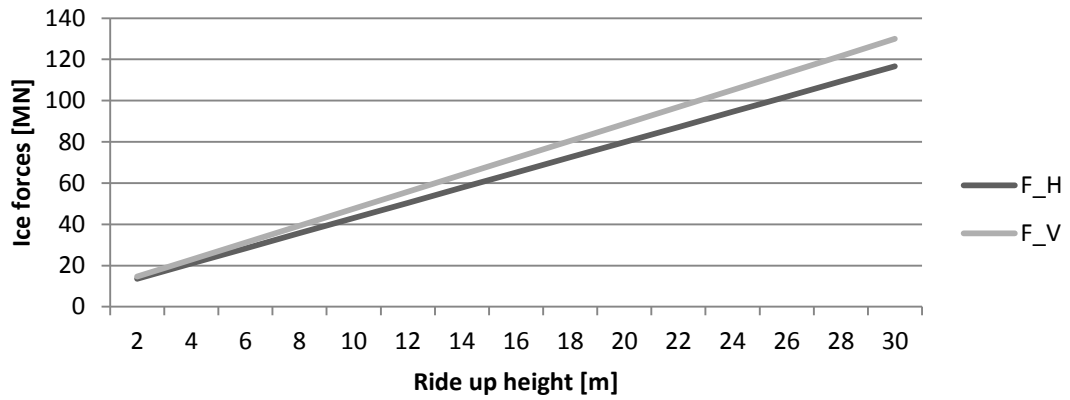
Downward: Ice forces versus ride up height
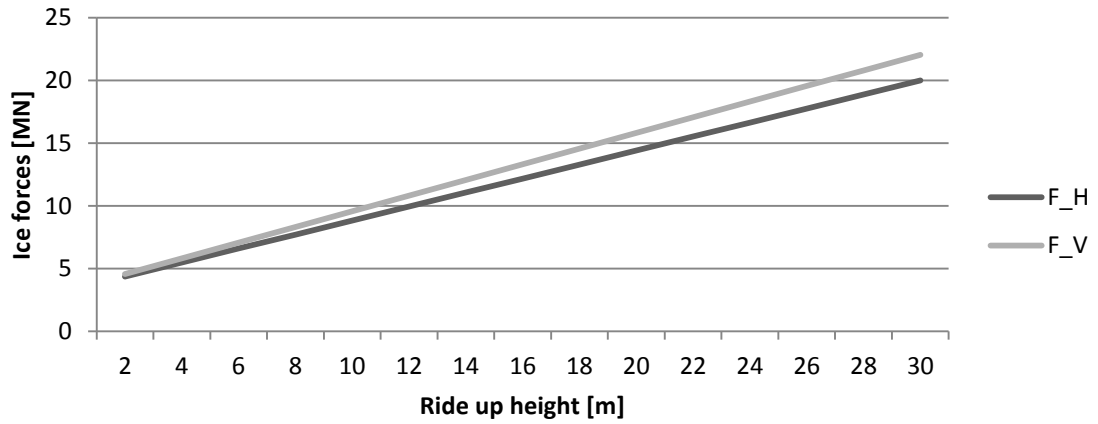
Upward vs. Downward: ride-up height
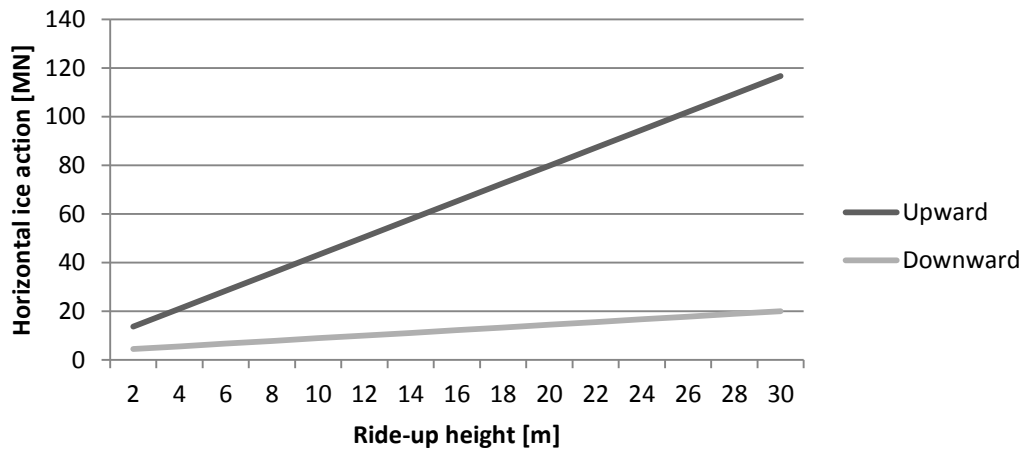
APPENDIX

E – Excel Method 2 – Level ice

Input	Value	Dimesion	Explenation
c	5000	Pa	cohesion of the ice rubble
D	81	m	Waterline diameter upward
D	81	m	Waterline diameter downward
e	0,3	[-]	porosity of the ice
E	5000000000	Pa	modulus of ice
g	9,81	m/s2	acceleration of gravity
h_r	17	m	height of ice rubble
h	1,2	m	ice sheet thickness
alfa	0,785398163	rad	slope of the structure
tetha	0,610865238	rad	angle th ruble makes
my	0,1	[-]	friction ice-structure
my_i	0,05	[-]	friction ice-ice
v	0,3	[-]	Poisson's ratio
ro_i	890	kg/m3	density ice (upward sloping)
ro_w	1025	kg/m3	density seawater
ro	135	kg/m3	density (downward sloping)
ø	0,698131701	rad	angle of internal friction of the ice rubble
	0	rad	downward
Y	500000	Pa	flexural strength of ice
zetta	1,2222222		

E1 – Increasing ice thickness

Ice thickness (h_r=17)

h	L_c	P_up	l_c	P_down
0,2	4,369	61336,3215	91,77956	9303,824
0,4	7,347	93989,8875	99,12898	14256,89
0,6	9,959	126643,453	105,5721	19209,96
0,8	12,357	159297,019	111,4892	24163,03
1	14,608	191950,585	117,0436	29116,1
1,2	**16,748**	**224604,151**	**122,3251**	**34069,17**
1,4	18,801	257257,717	127,39	39022,24
1,6	20,782	289911,283	132,2765	43975,31
1,8	22,701	322564,849	137,0122	48928,38
2	24,568	355218,415	141,6179	53881,45
2,2	26,388	387871,981	146,1097	58834,51
2,4	28,167	420525,547	150,5003	63787,58
2,6	29,910	453179,113	154,8003	68740,65
2,8	31,620	485832,679	159,0184	73693,72
3	33,299	518486,245	163,1617	78646,79

APPENDIX

Upward breaking cone

H_B	H_P	H_R	H_L	H_T	F_H [MN]	F_V [MN]	N [MN]
192096	459086,5	7806839,196	20338354,28	47146,86	29,46012769	24,10374083	37,87537466
493469,6	459086,5	11962959,63	20338354,28	188587,44	34,29609702	28,06044302	44,09273232
872414,6	459086,5	16119080,06	20338354,28	424321,74	39,29568129	32,15101196	50,52044129
1320019	459086,5	20275200,49	20338354,28	754349,76	44,46310418	36,37890342	57,16393178
1831608	459086,5	24431320,92	20338354,28	1178671,5	49,79760021	40,74349108	64,02221962
2404236	**459086,5**	**28587441,35**	**20338354,28**	**1697287**	55,29782078	**45,24367154**	**71,09357101**
3035849	459086,5	32743561,78	20338354,28	2310196,1	60,96248461	49,8783965	78,37633867
3724925	459086,5	36899682,21	20338354,28	3017399	66,7904832	54,64675898	85,86909743
4470280	459086,5	41055802,64	20338354,28	3818895,7	72,78087738	59,54799059	93,57063989
5270969	459086,5	45211923,07	20338354,28	4714686	78,93287277	64,58144135	101,4799447
6126213	459086,5	49368043,5	20338354,28	5704770,1	85,24579425	69,74655893	109,596144
7035359	459086,5	53524163,93	20338354,28	6789147,8	91,71906439	75,04287087	117,9184953
7997853	459086,5	57680284,36	20338354,28	7967819,3	98,35218591	80,46997029	126,4463593
9013214	459086,5	61836404,8	20338354,28	9240784,6	105,1447277	86,02750448	135,1791817
10081022	459086,5	65992525,23	20338354,28	10608044	112,0963138	91,71516584	144,1164793

Downward breaking cone

H_B	H_P	H_R	H_L	H_T	F_H [MN]	F_V [MN]	N [MN]
192095,97	69636,72	1184183,47	4224985	7151,49	5,799435251	4,744992478	7,456036352
493469,64	69636,72	1814606,24	4224985	28605,96	6,800571241	5,564103743	8,743145528
872414,6	69636,72	2445029	4224985	64363,41	7,89386986	6,458620795	10,14874347
1320018,6	69636,72	3075451,76	4224985	114423,84	9,073075787	7,423425644	11,66478803
1831608,1	69636,72	3705874,52	4224985	178787,25	10,33433377	8,455363992	13,2863227
2404235,9	**69636,72**	**4336297,28**	**4224985**	**257453,64**	11,67505312	**9,552316187**	**15,01001678**
3035849,3	69636,72	4966720,05	4224985	350423,01	13,0933707	10,71275785	16,83347493
3724924,5	69636,72	5597142,81	4224985	457695,36	14,58787989	11,93553809	18,75488871
4470280,1	69636,72	6227565,57	4224985	579270,69	16,15747985	13,21975624	20,77284286
5270968,8	69636,72	6857988,33	4224985	715149	17,80128508	14,56468779	22,8861989
6126212,7	69636,72	7488411,09	4224985	865330,29	19,51856765	15,96973717	25,094021
7035359,4	69636,72	8118833,86	4224985	1029814,56	21,30871864	17,43440616	27,39552627
7997853	69636,72	8749256,62	4224985	1208601,81	23,17122123	18,95827192	29,7900503
9013213,5	69636,72	9379679,38	4224985	1401692,04	25,10563153	20,54097125	32,27702236
10081022	69636,72	10010102,1	4224985	1609085,25	27,11156428	22,18218895	34,85594718

Upward: Ice forces versus ice thickness
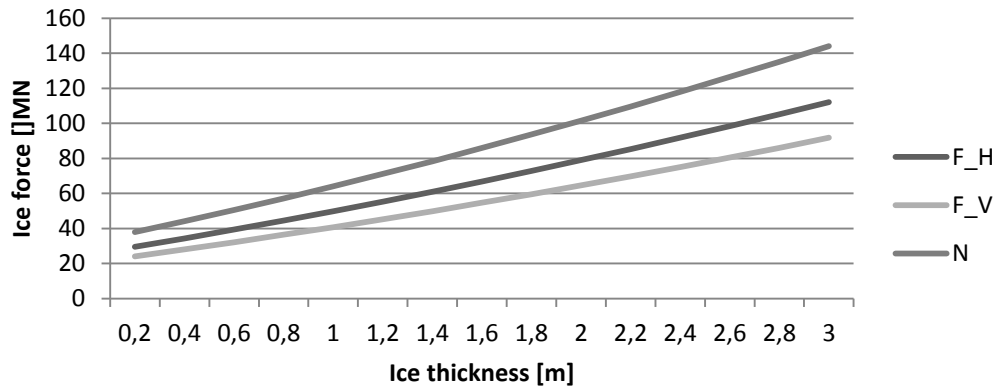
Downward : Ice forces versus ice thickness
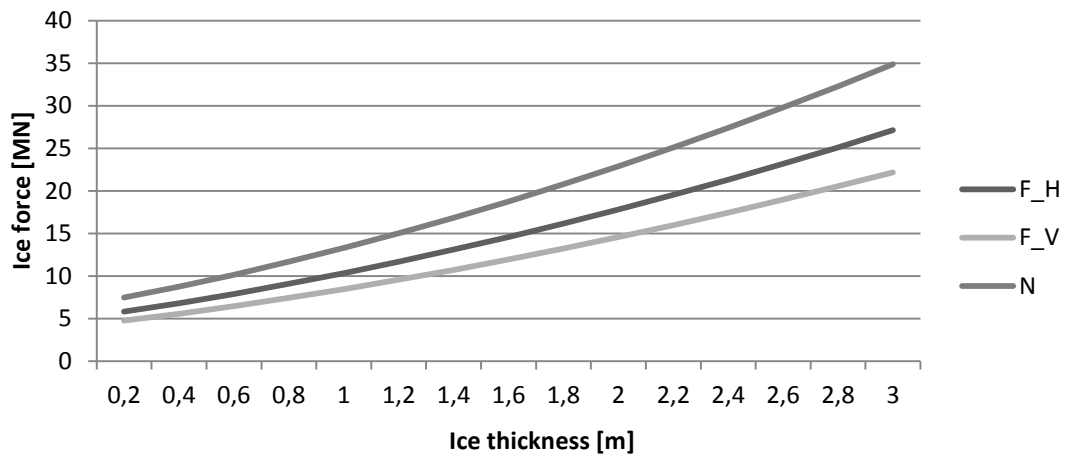
Downward versus Upward

E2 – Increasing rubble thickness

Rid-up height (h=1,2)

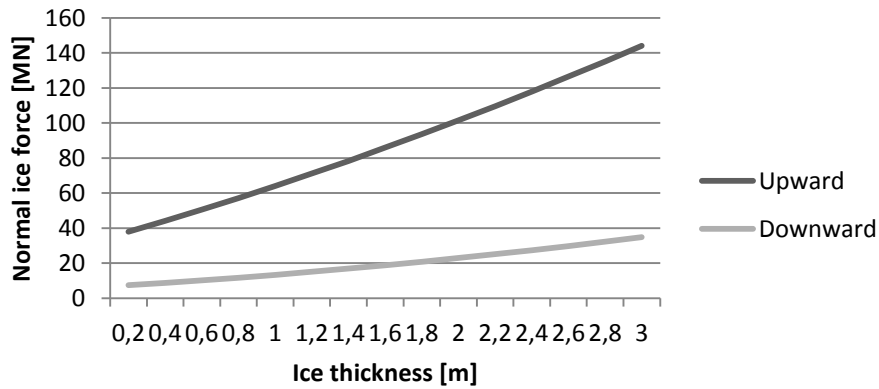| h_r	L_c	P_up	l_c	P_down
2	16,748	23446,5692	122,3251	3556,502
4	16,748	47687,1246	122,3251	7233,44
6	16,748	72721,6664	122,3251	11030,81
8	16,748	98550,1945	122,3251	14948,63
10	16,748	125172,709	122,3251	18986,87
12	16,748	152589,21	122,3251	23145,55
14	16,748	180799,697	122,3251	27424,67
16	16,748	209804,17	122,3251	31824,23
18	16,748	239602,63	122,3251	36344,22
20	16,748	270195,076	122,3251	40984,65
22	16,748	301581,508	122,3251	45745,51
24	16,748	333761,926	122,3251	50626,81
26	16,748	366736,331	122,3251	55628,54
28	16,748	400504,723	122,3251	60750,72
30	16,748	435067,1	122,3251	65993,32

			Upward breaking cone				
H_B	H_P	H_R	H_L	H_T	F_H [MN]	F_V [MN]	N [MN]
2404236	6354,139	2984261,048	543377,246	1697287	7,894106119	6,458814097	10,14904721
2404236	25416,56	6069580,055	1579919,91	1697287	12,17527024	9,961584739	15,65312027
2404236	57187,25	9255957,021	3109627,991	1697287	17,08392087	13,97775344	21,96392054
2404236	101666,2	12543391,95	5132501,49	1697287	22,62005801	18,50732019	29,08144802
2404236	158853,5	15931884,83	7648540,407	1697287	28,78368167	23,550285	37,00570272
2404236	228749	19421435,67	10657744,74	1697287	35,57479184	29,10664787	45,73668464
2404236	311352,8	23012044,47	14160114,49	1697287	42,99338853	35,1764088	55,27439378
2404236	406664,9	26703711,23	18155649,66	1697287	51,03947173	41,75956778	65,61883013
2404236	514685,3	30496435,95	22644350,25	1697287	59,71304145	48,85612482	76,7699937
2404236	635413,9	34390218,63	27626216,26	1697287	69,01409768	56,46607992	88,72788448
2404236	768850,8	38385059,27	33101247,68	1697287	78,94264042	64,58943307	101,4925025
2404236	914996	42480957,87	39069444,52	1697287	89,49866968	73,22618428	115,0638477
2404236	1073849	46677914,42	45530806,78	1697287	100,6821854	82,37633355	129,4419201
2404236	1245411	50975928,93	52485334,46	1697287	112,4931877	92,03988087	144,6267198
2404236	1429681	55375001,41	59933027,55	1697287	124,9316765	102,2168263	160,6182467

Downward breaking cone

H_B	H_P	H_R	H_L	H_T	F_H [MN]	F_V [MN]	N [MN]
2404235,9	963,8301	452668,811	320354,8	257453,64	3,552032567	2,906208464	4,566666028
2404235,9	3855,32	920666,638	687830,2	257453,64	4,41879006	3,615373686	5,681011666
2404235,9	8674,471	1403993,48	1102426	257453,64	5,352105065	4,378995053	6,880926882
2404235,9	15421,28	1902649,34	1564143	257453,64	6,351977582	5,197072567	8,166411676
2404235,9	24095,75	2416634,22	2072980	257453,64	7,41840761	6,069606227	9,537466049
2404235,9	34697,88	2945948,11	2628938	257453,64	8,551395151	6,996596033	10,99409
2404235,9	47227,67	3490591,02	3232016	257453,64	9,750940204	7,978041985	12,53628353
2404235,9	61685,12	4050562,94	3882215	257453,64	11,01704277	9,013944083	14,16404664
2404235,9	78070,24	4625863,88	4579534	257453,64	12,34970284	10,10430233	15,87737932
2404235,9	96383,01	5216493,84	5323974	257453,64	13,74892043	11,24911672	17,67628158
2404235,9	116623,4	5822452,81	6115535	257453,64	15,21469553	12,44838725	19,56075343
2404235,9	138791,5	6443740,8	6954216	257453,64	16,74702814	13,70211394	21,53079485
2404235,9	162887,3	7080357,81	7840018	257453,64	18,34591827	15,01029676	23,58640584
2404235,9	188910,7	7732303,83	8772940	257453,64	20,0113659	16,37293574	25,72758642
2404235,9	216861,8	8399578,87	9752983	257453,64	21,74337105	17,79003086	27,95433658

Upward: Ice forces versus rubble thickness
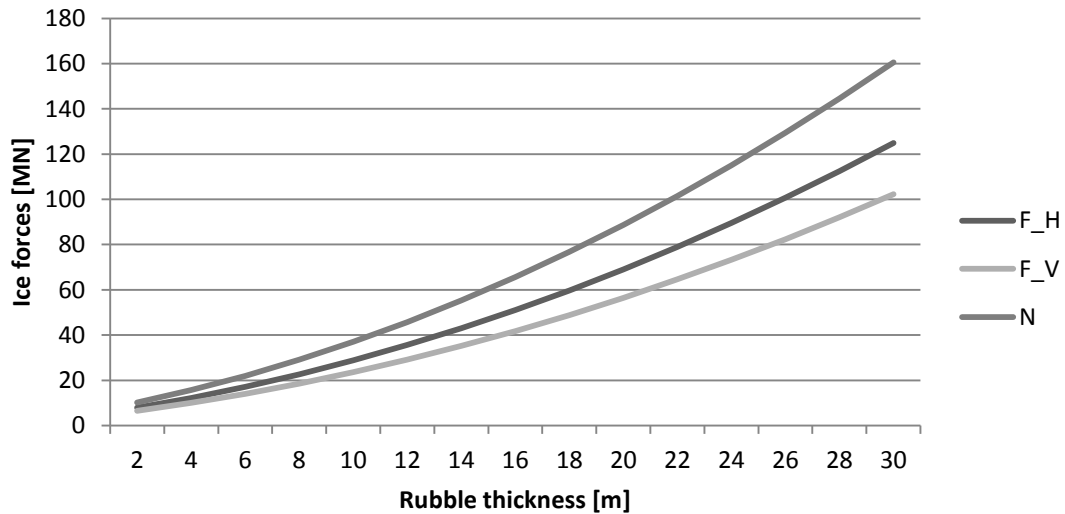
Downward: Ice forces versus rubble thickness
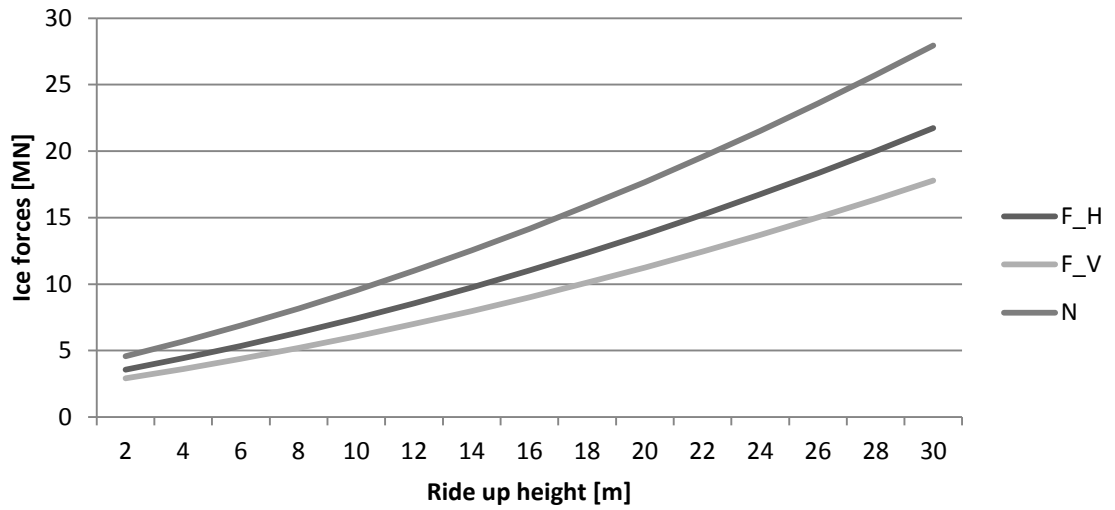
Upward versus downward
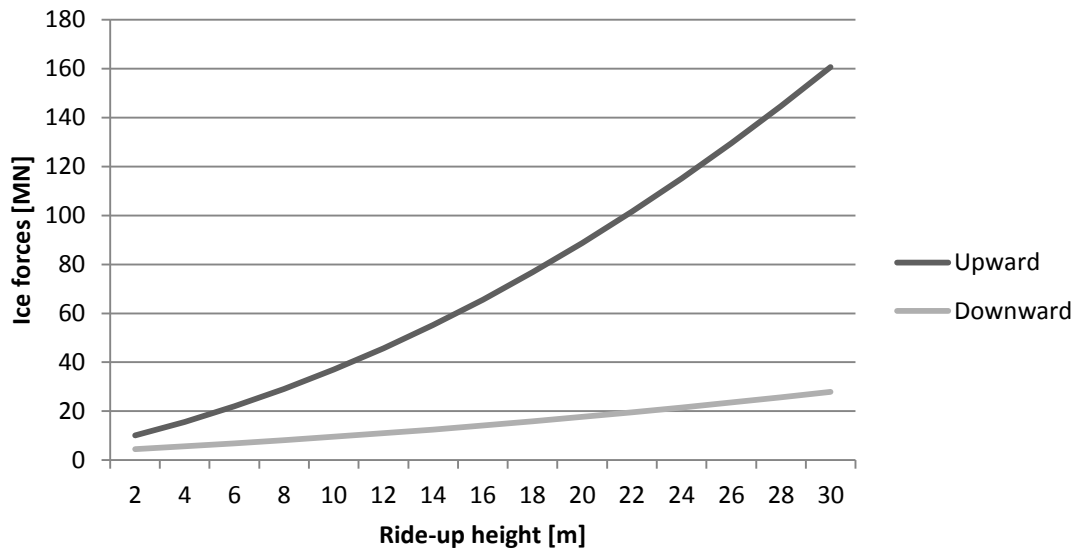
APPENDIX

F – Excel - Ridge

Input	
	Value
E_cl	5000000000,000
E_k	333333333,333
σ'_cl	640000,000
σ'_k	50000,000
σ'_k	25000,000
ρ_w	1025,000
g	9,814
μ	0,100
α	45,000
	0,785
W	70,000
h_cl	3,000
h_k	21,000
b	4,667
Parameters	
y_1	5,318
y_2	18,682
I_T	13380,818
L_c	139,624

F1 – Increasing consolidated layer thickness

				DOWNWARD SLOPING			
h_cl	y_1	y_2	I_T	L_c	V2_k (F_V)	F_H	N
0,5	8,171	13,329	6582,525	116,933	19,544	23,886617	30,7098
1	6,917	15,083	8548,167	124,827	21,009	25,678136	33,01306
1,5	6,181	16,319	10036,597	129,938	21,903	26,770306	34,41721
2	5,735	17,265	11271,990	133,764	22,586	27,605611	35,49112
2,5	5,468	18,032	12365,803	136,898	23,181	28,33203	36,42504
3	**5,318**	**18,682**	**13380,818**	**139,624**	**23,738**	**29,013422**	**37,30107**
3,5	5,250	19,250	14355,979	142,102	24,286	29,682466	38,16122
4	5,241	19,759	15317,426	144,423	24,838	30,358113	39,02987
4,5	5,275	20,225	16283,921	146,649	25,407	31,052452	39,92254
5	5,344	20,656	17269,729	148,820	25,997	31,773771	40,84991

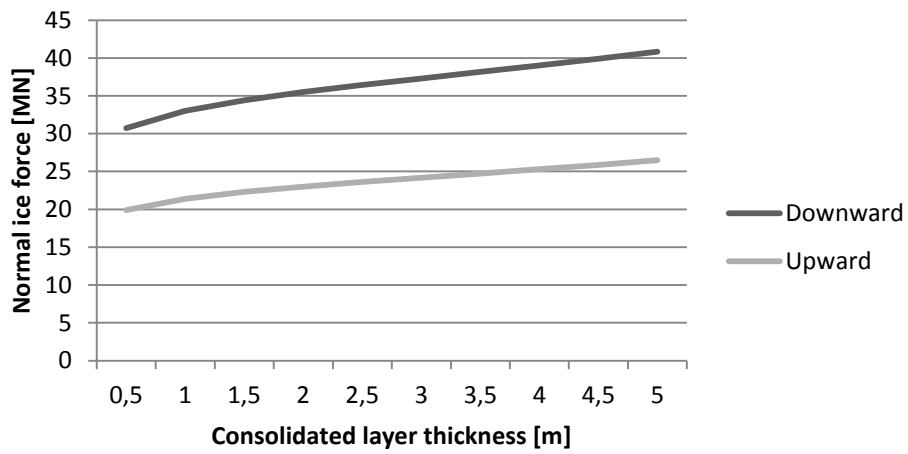|				UPWARD SLOPING			
h_cl	y_1	y_2	I_T	L_c	V2_k (F_V)	F_H	N
0,5	8,171	13,329	6582,525	116,933	12,670	15,48565	19,90911
1	6,917	15,083	8548,167	124,827	13,620	16,64709	21,40231
1,5	6,181	16,319	10036,597	129,938	14,200	17,35514	22,31262
2	5,735	17,265	11271,990	133,764	14,643	17,89667	23,00883
2,5	5,468	18,032	12365,803	136,898	15,028	18,3676	23,61429
3	**5,318**	**18,682**	**13380,818**	**139,624**	**15,389**	**18,80935**	**24,18222**
3,5	5,250	19,250	14355,979	142,102	15,744	19,24309	24,73985
4	5,241	19,759	15317,426	144,423	16,103	19,68111	25,30299
4,5	5,275	20,225	16283,921	146,649	16,471	20,13125	25,88171
5	5,344	20,656	17269,729	148,820	16,854	20,59888	26,48292

Downward: Ice forces versus consolidated layer thickness
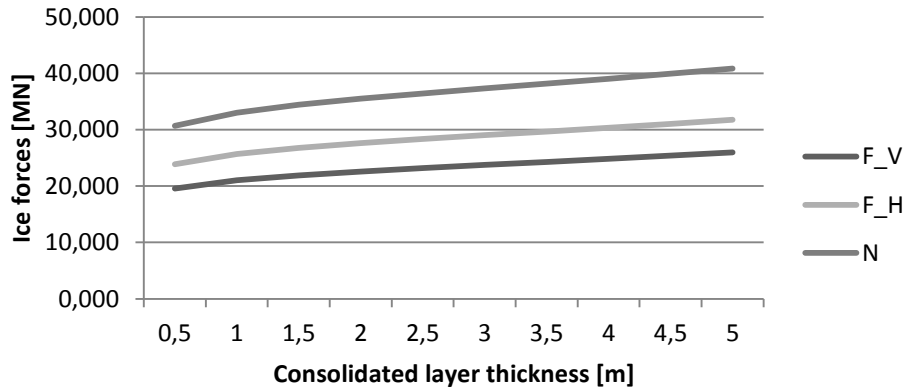
Upward: Ice forces versus consolidated layer thickness
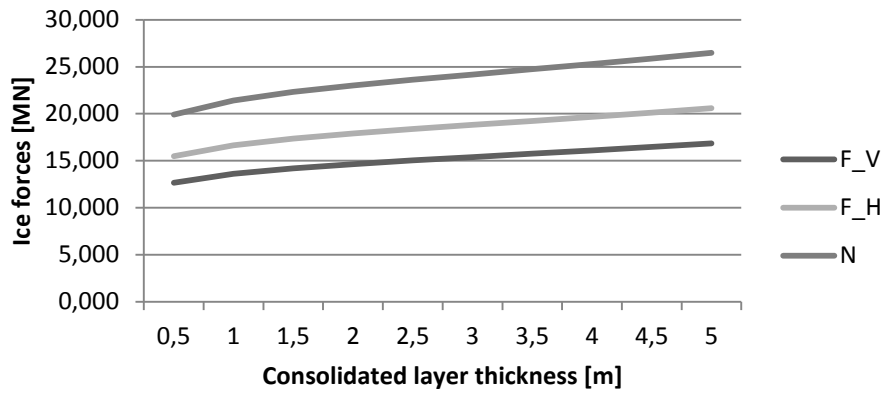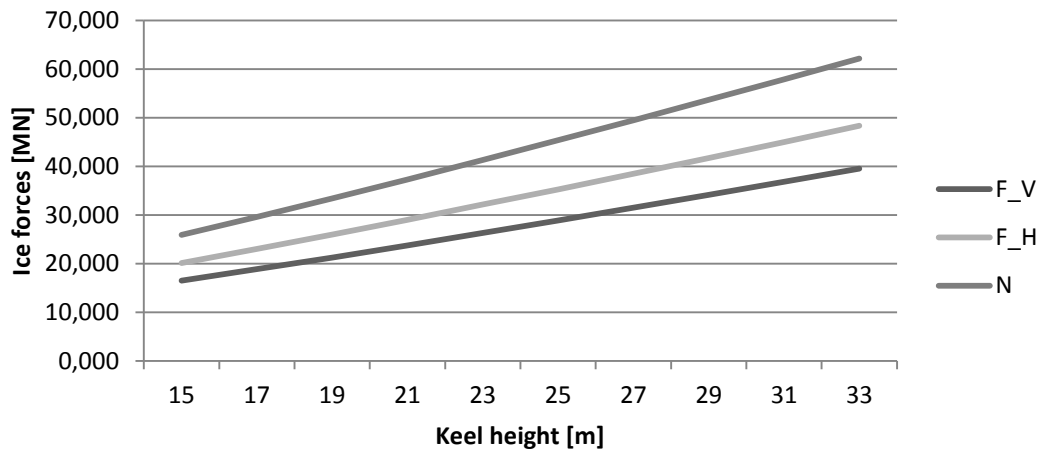

Upward versus downward breaking
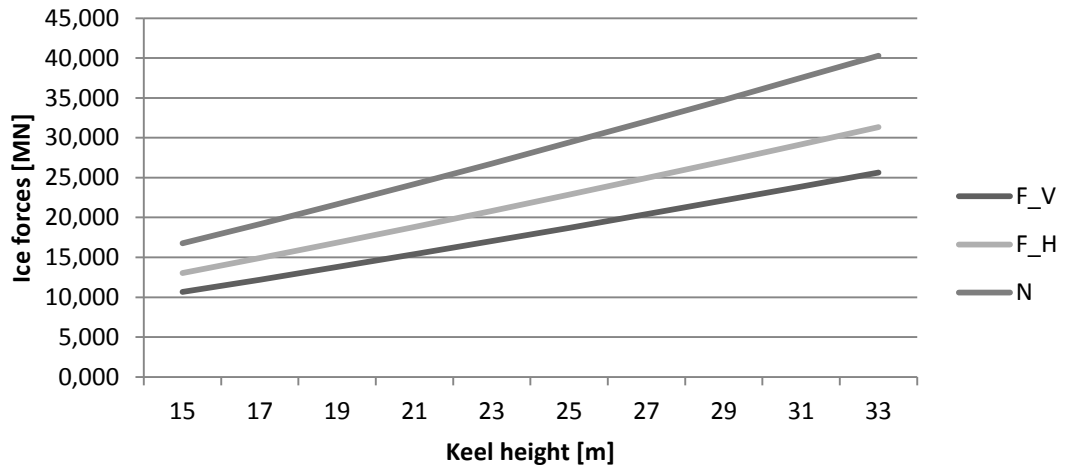
F2 – Increasing keel height

DOWNWARD SLOPING							
h_k	y_1	y_2	I_T	L_c	V2_k (F_V)	F_H	N
15	3,750	14,250	5722,500	112,911	16,458	20,115488	25,86145
17	4,242	15,758	7826,176	122,103	18,822	23,004638	29,57588
19	4,766	17,234	10368,483	130,999	21,252	25,974486	33,39406
21	**5,318**	**18,682**	**13380,818**	**139,624**	**23,738**	**29,013422**	**37,30107**
23	5,897	20,103	16893,082	148,002	26,274	32,112798	41,28578
25	6,500	21,500	20933,889	156,154	28,854	35,265908	45,33957
27	7,125	22,875	25530,750	164,099	31,473	38,467386	49,45554
29	7,770	24,230	30710,219	171,855	34,129	41,712835	53,62805
31	8,434	25,566	36498,020	179,435	36,817	44,998586	57,85237
33	9,115	26,885	42919,154	186,854	39,536	48,321525	62,12451

UPWARD SLOPING							
h_cl	y_1	y_2	I_T	L_c	V2_k (F_V)	F_H	N
15	3,750	14,250	5722,500	112,911	10,670	13,04084	16,76593
17	4,242	15,758	7826,176	122,103	12,202	14,91387	19,17399
19	4,766	17,234	10368,483	130,999	13,778	16,83921	21,64931
21	**5,318**	**18,682**	**13380,818**	**139,624**	**15,389**	**18,80935**	**24,18222**
23	5,897	20,103	16893,082	148,002	17,033	20,81867	26,7655
25	6,500	21,500	20933,889	156,154	18,706	22,86283	29,39356
27	7,125	22,875	25530,750	164,099	20,404	24,93834	32,06194
29	7,770	24,230	30710,219	171,855	22,126	27,04236	34,76697
31	8,434	25,566	36498,020	179,435	23,868	29,1725	37,50559
33	9,115	26,885	42919,154	186,854	25,631	31,32676	40,27521

Downward: Ice forces versus keel height

APPENDIX

Upward: Ice forces versus keel height

Upward versus downward breaking

XXVIII
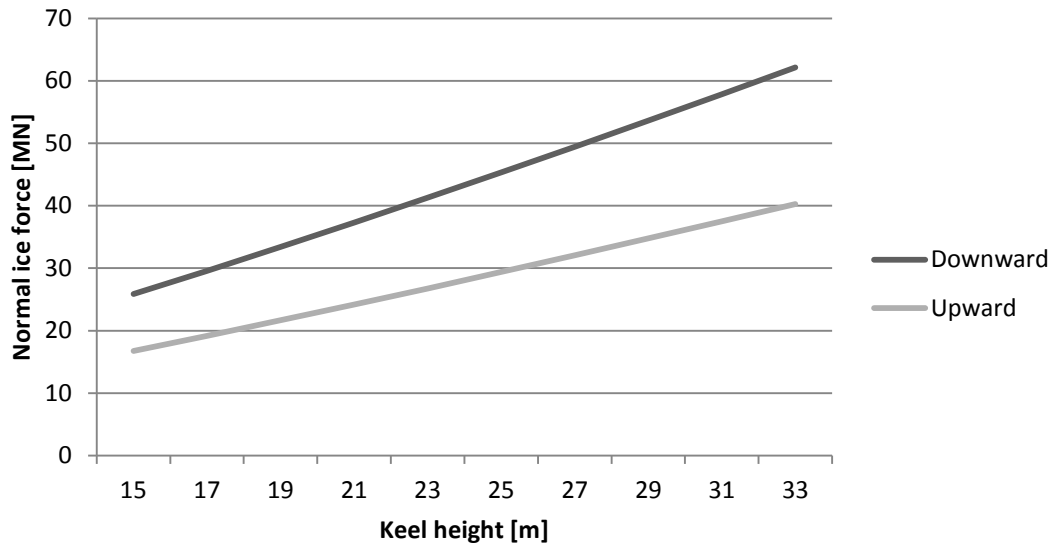
G – Local ice pressure

|			
a	1,2		loaded height
w_p	0,4		width plate
w_s	2		width stiffeners
w_m	8,6		width of model
A_p	0,48		loaded area plate
A_s	2,4		loaded area stiffeners
A_m	10,32		nominal loaded area for global load
Local pressure based on calculated global forces above:			
P_p	31,27086829	Mpa	local pressure plate
P_s	6,254173659	Mpa	local pressure stiffeners
P_m	1,45445899	Mpa	local pressure over nominal area of model
Local pressure based on ISO code for thick massive ice features (vertical structure)			
P_p	14,05366917		local pressure plate
P_s	4,555234329		local pressure stiffeners
Local pressure for first-year ice based on Artic offshore Engineering book (vertical structure)			
P_p	7,589466384		local pressure plate
P_s	3,39411255		local pressure stiffeners
Local pressure on sloping structure based in Artic offshore Engineering book			
p_L	1,5	MPa	no structural design significance in specifying ice pressure greater than this

PC4 -load patch

Dtk	73	kTon	Ship displacement
DF	15,6		
Coefficients			
CF_C	4,5		
CF_F	13,48		
CF_D	1,42		
CF_DIS	130		
CF_L	3,15		
x	distance from FP to location	0	m
Lwl	Length WL	81	m
Beta 1	Frame angle	45	deg
Alfa	Waterline angle	90	deg
fai1	Shape coefficient	1,10	
fai2	Shape coefficient	0,33	
fai3	Shape coefficient	0,60	
fai	Shape coefficient	0,33	
Ari	Load patch aspect ratio	5,28	
F_bow	Force	22,87631858	MN
P_bow	Pressure	6,61	Mpa

H – Convergence analysis

Mesh size [mm]	von Mises [Pa]	Displacement [m]
Element S4R		
200	2,28423E+08	0,00702
100	2,25456E+08	0,00670578
50	2,23671E+08	0,00667385
25	2,23633E+08	0,00667889
Element S8R		
200	2,21906E+08	0,00646502
100	2,22672E+08	0,00651835
50	2,23051E+08	0,00656473
25	2,23234E+08	0,00660836
Element S3		
200	1,85743E+08	0,00567906
100	2,19704E+08	0,00649504
50	2,22544E+08	0,00660939
25	2,23425E+08	0,00665806
Element STRI65		
200	2,23515E+08	0,00669592
100	2,23492E+08	0,00669092
50	2,23558E+08	0,00669239
25	2,23696E+08	0,00669349
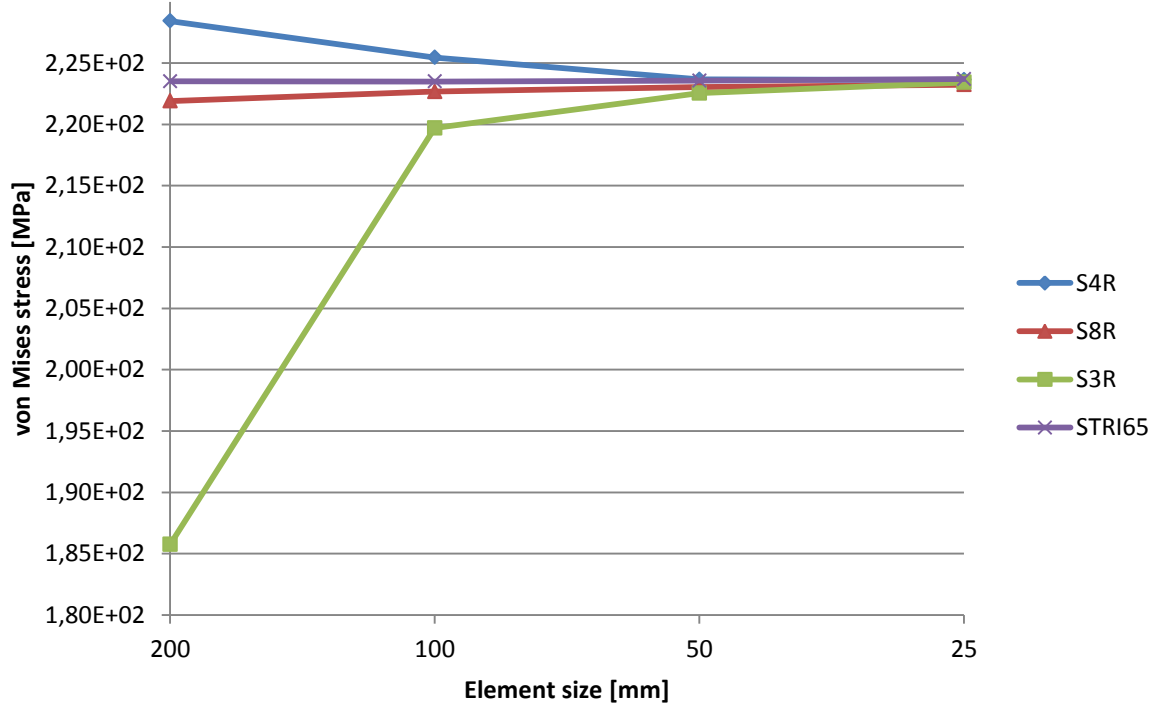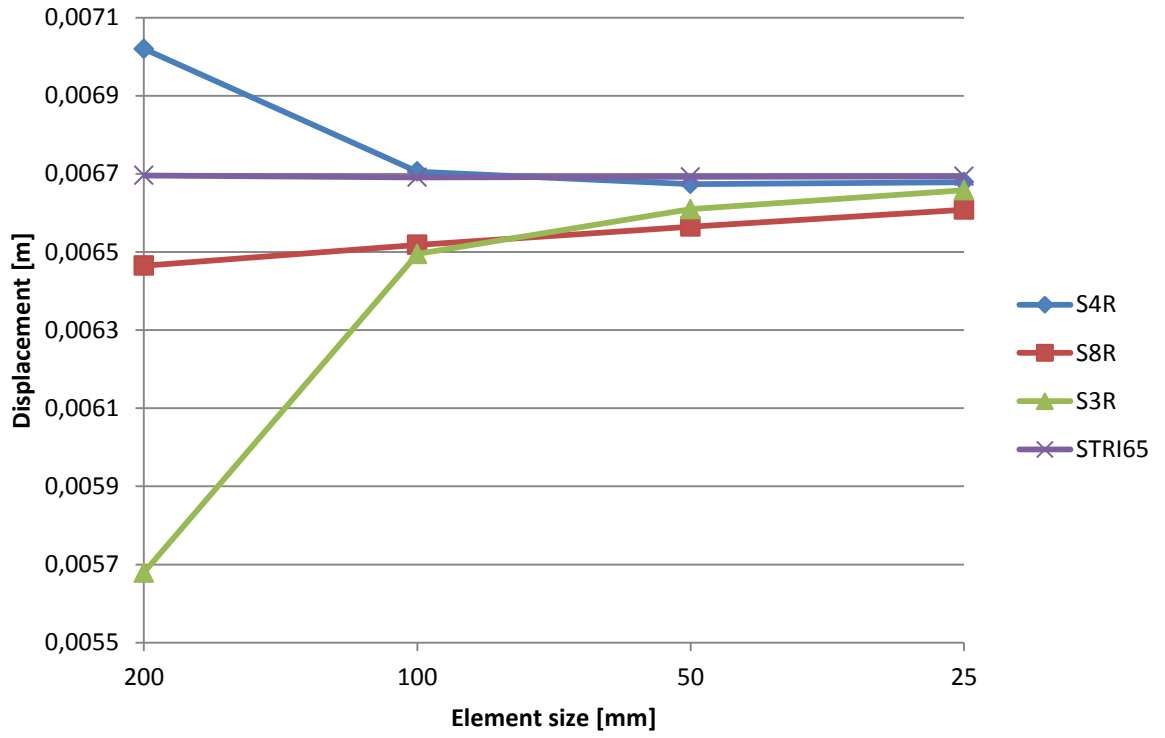
APPENDIX

I – Increasing ice pressure and mesh study

Plate

Pressure load [MPa]	von Mises in plate [MPa]		Comments:
	Refined mesh:	ABAQUS mesh:	
2	8,50E+07	8,45E+07	
4	1,70E+08	1,69E+08	
6	2,61E+08	2,12E+08	Yielding in stiffener
8	3,17E+08	3,17E+08	
10	3,39E+08	3,39E+08	
12	3,46E+08	3,46E+08	
14	3,47E+08	3,47E+08	
16	3,50E+08	3,50E+08	
18	3,57E+08	3,57E+08	
20	3,61E+08	3,62E+08	

Stiffener

Pressure load [MPa]	von Mises in plate [MPa]		
	Refined mesh:	ABAQUS mesh:	
1	1,55E+08	1,57E+08	
1,5	2,32E+08	2,35E+08	
2	3,10E+08	3,11E+08	
2,5	3,17E+08	3,16E+08	
3	3,30E+08	3,26E+08	Note: Between ice pressure from 3 MPa 4 Mpa there is a shift in where the maximum von Mises occur in the stiffener
3,5	3,45E+08	3,39E+08	.
4	3,46E+08	3,46E+08	
5	3,56E+08	3,54E+08	Yielding starts
6	3,71E+08	3,71E+08	